

**STUDY OF NICKELIFERROUS LATERITE  
REDUCTION**

# **STUDY OF NICKELIFEROUS LATERITE REDUCTION**

**BY**

**SHOUBAO LI, B.Eng., M.Eng.**

**A Thesis**

**Submitted to the School of Graduate Studies**

**in Partial Fulfilment of the Requirements**

**for the Degree**

**of Master Engineering**

**McMaster University**

**© Copyright by Shoubao Li, July 1999**



**MASTER OF ENGINEERING**  
**(Materials Science And Engineering)**

**McMaster University**  
**Hamilton, Ontario**

**TITLE: Study Of Nickeliferrous Laterite Reduction**

**AUTHOR: Shoubao Li, B.Eng. M.Eng. (University of Science and Technology,  
Beijing)**

**SUPERVISOR: Dr. K.S. Coley**

**NUMBER OF PAGES: xvii, 163.**

## ACKNOWLEDGEMENTS

I am particularly grateful to my supervisor, Dr. K. S. Coley, for his encouragement and guidance at all stages of this study. He has greatly contributed to my philosophy about scientific research.

I wish to express my gratitude to Professor W-K Lu for his discussion and beneficial advice on carrying out experiments. Grateful acknowledgements are also due to the faculty and staff of the Department of Materials Science and Engineering for their help and assistance in this work. Special thanks is given to: Mr. Martin Van Oosten, who helped me in chemical analysis and other experiment aspects; Mr. Ed McCaffery, who helped in the set-up of my apparatus; and, Ms. Connie Barry, who helped in BET surface area measurement.

I also would like to thank INCO and NSERC/CCPM for providing laterite samples and financial support.

Last, but not least, I wish to extend my great appreciation to my wife, Dawn Chen, and other family members for their inspiration and support throughout my study at McMaster University.

## ABSTRACT

Laterite is an important resource for the production of nickel. Pre-reduction of laterite is a critical step for all laterite based nickel production processes. The main kinds of laterite, limonitic and serpentinitic ore, behave differently upon reduction. In this study, general knowledge of laterites and nickel production were introduced. Research on laterite pre-reduction was reviewed. Using the compositions of two of laterite samples received from INCO Ltd, a thermodynamic study was carried out using F\*A\*C\*T (Facility for the Analysis of Chemical Thermodynamics, a thermodynamic software). Several graphs were plotted based on the theoretical calculation to predict nickel recovery and final nickel grade in the metallic phases for reduction at different temperatures with varied ratios of CO/CO<sub>2</sub>.

A series of reduction experiments was done using CO/CO<sub>2</sub> to examine reduction behaviour of Sample D, a serpentinitic laterite supplied by INCO. The effect of calcination time, temperature, reducing potential and other parameters were studied and discussed. The reduction mechanism and mineral phase change during reduction process were investigated using X-ray diffraction. This showed that with the serpentinitic laterite studied here there was a temperature range, 700~800 °C, where serpentine had decomposed but

not crystallised to form the high temperature phase. This resulted in a highly reducible ore. Optimum reducing conditions to maximise nickel recovery have been proposed for operation in this temperature range.

Partially reduced laterite pellets were chemically analysed. The data was subjected to kinetic study by using the Grain Model. This yielded detailed knowledge about gas diffusion through the solid matrix. Various reducing gas properties and other necessary parameters of the Grain Model were estimated. Some kinetic data were finally obtained.

# TABLE OF CONTENTS

<b>ACKNOWLEDGEMENTS .....</b>	<b>IV</b>
<b>ABSTRACT.....</b>	<b>V</b>
<b>TABLE OF CONTENTS .....</b>	<b>VII</b>
<b>LIST OF FIGURES.....</b>	<b>XI</b>
<b>LIST OF TABLES.....</b>	<b>XV</b>
<b>LIST OF PHOTOS.....</b>	<b>XVII</b>
<b>CHAPTER 1 INTRODUCTION .....</b>	<b>1</b>
1.1 LATERITES AS A SOURCE OF NICKEL .....	1
1.2 LATERITES .....	2
1.3 NICKEL EXTRACTION FROM LATERITES .....	6
<b>CHAPTER 2 LITERATURE REVIEW .....</b>	<b>12</b>
2.1 STUDIES BASED ON PURE INDIVIDUAL MATERIALS.....	12
2.2 STUDIES BASED ON ORES .....	13
2.2.1 <i>Reducing Potential and Temperature</i> .....	13
2.2.2 <i>Ore Composition and High Temperature Phase Crystallization</i> .....	15

# TABLE OF CONTENTS

<b>ACKNOWLEDGEMENTS .....</b>	<b>IV</b>
<b>ABSTRACT.....</b>	<b>V</b>
<b>TABLE OF CONTENTS .....</b>	<b>VII</b>
<b>LIST OF FIGURES .....</b>	<b>XI</b>
<b>LIST OF TABLES .....</b>	<b>XV</b>
<b>LIST OF PHOTOS .....</b>	<b>XVII</b>
<b>CHAPTER 1 INTRODUCTION .....</b>	<b>1</b>
1.1 LATERITES AS A SOURCE OF NICKEL .....	1
1.2 LATERITES .....	2
1.3 NICKEL EXTRACTION FROM LATERITES .....	6
<b>CHAPTER 2 LITERATURE REVIEW .....</b>	<b>12</b>
2.1 STUDIES BASED ON PURE INDIVIDUAL MATERIALS .....	12
2.2 STUDIES BASED ON ORES .....	13
2.2.1 <i>Reducing Potential and Temperature</i> .....	13
2.2.2 <i>Ore Composition and High Temperature Phase Crystallization</i> .....	15

2.2.3 Heating and Reducing Patterns.....	18
2.2.4 Additives.....	18
2.2.5 Reoxidation.....	19
2.2.6 Kinetics.....	20
<b>CHAPTER 3 APPARATUS AND EXPERIMENTAL PROCEDURE.....</b>	<b>22</b>
3.1 APPARATUS.....	22
3.2 SAMPLE PREPARATION AND EXPERIMENT PROCEDURE.....	25
<b>CHAPTER 4 THERMODYNAMIC STUDY.....</b>	<b>27</b>
4.1 THERMODYNAMIC STUDY METHOD.....	27
4.2 RESULTS AND DISCUSSION.....	30
4.3 SUMMARY OF THERMODYNAMIC STUDY.....	41
<b>CHAPTER 5 EXPERIMENTAL RESULTS.....</b>	<b>43</b>
5.1 SAMPLE CHARACTERIZATION.....	43
5.1.1 Sample Preparation and Size Distribution.....	43
5.1.2 X-Ray Diffraction.....	44
5.1.3 Chemical Composition.....	45
5.1.4 DTA/TGA Analysis.....	49
5.2 EFFECT OF CALCINATION.....	53
5.2.1 Calcination Effect On Reduction And BET Analysis.....	53
5.2.2 X-Ray Diffraction Study On Samples Calcined at Varied Conditions.....	57
5.3 EFFECT OF REDUCING GAS FLOW RATE.....	60
5.4 INVESTIGATION OF REDUCTION MECHANISM.....	63
5.4.1 Reduction Mode.....	63
5.4.2 Mineral Phase Change During the Reduction Process.....	70
5.5 REDUCTION TEMPERATURE AND GAS COMPOSITION.....	76

5.6 EXPERIMENTS USING GASES WITH COMPOSITION VARIED DURING REDUCTION .....	84
5.7 SUMMARY OF EXPERIMENTAL STUDY .....	88
<b>CHAPTER 6 KINETIC ANALYSIS.....</b>	<b>91</b>
6.1 INTRODUCTION .....	91
6.2 VERIFICATION OF EXPERIMENT PROCEDURE AND CHEMICAL ANALYSIS OF PARTIALLY REDUCED SAMPLES .....	100
6.3 THE GRAIN MODEL.....	107
6.4 ESTIMATION OF NECESSARY PARAMETERS.....	111
6.4.1 Porosity of Calcined Pellets .....	111
6.4.1.1 Apparent Density of The Pellet Before Reduction.....	111
6.4.1.2 True Density of The Pellet Before Reduction .....	111
6.4.1.3 Porosity of Calcined Pellets.....	112
6.4.2 Individual Grain Size of The Calcined Pellets .....	113
6.4.2.1 Specific Surface Area of Pellet Before Reduction .....	113
6.4.2.2 Individual Grain Size of Calcined Pellets .....	113
6.4.3 Effective Diffusivity of Gas Reactant Within Calcined Pellets .....	114
6.4.3.1 Gas Diffusion Within Fine Pores.....	115
6.4.3.2 Effective Diffusivity Within Calcined Pellets.....	121
6.4.4 Mass Transfer Coefficient .....	127
6.4.4.1 Viscosity Of Pure Gas.....	128
6.4.4.2 Viscosity Of Gas Mixture .....	129
6.4.4.3 Mass Transfer Coefficient.....	130
6.4.5 Equilibrium Constants For Different Reactions.....	132
6.4.6 Molar Concentration of Solid Reactant .....	132
6.4.7 Reaction Fraction of Nickel Oxide And Iron Oxide .....	133
6.5 KINETIC PARAMETER EXTRACTION .....	134
6.5.1 Reduction of Hematite To Magnetite.....	134

6.5.2 Reduction Of FeO And NiO.....	138
6.6 DISCUSSION .....	143
6.6 SUMMARY OF KINETIC ANALYSIS.....	145
6.7 NOMENCLATURE.....	145
<b>SUMMARY AND CONCLUSIONS .....</b>	<b>150</b>
<b>REFERENCE.....</b>	<b>154</b>

# LIST OF FIGURES

FIG. 1.1 GENERAL SUMMARY OF PROCESSES FOR NICKEL PRODUCTION FROM LATERITES .....	10
FIG. 3.1 SCHEMATIC DIAGRAM OF THE EXPERIMENT APPARATUS .....	22
FIG. 4.1 CALCULATED NICKEL RECOVERY WHEN LIMONITIC LATERITE (SAMPLE C IN TABLE 4.1) IS REDUCED BY CO/CO <sub>2</sub> .....	33
FIG. 4.2 CALCULATED NICKEL GRADE IN METALLIC PHASE WHEN LIMONITIC LATERITE (SAMPLE C IN TABLE 4.1) IS REDUCED BY CO/CO <sub>2</sub> .....	34
FIG. 4.3 CALCULATED NICKEL RECOVERY WHEN SERPENTINIC LATERITE (SAMPLE D IN TABLE 4.1) IS REDUCED BY CO/CO <sub>2</sub> .....	35
FIG. 4.4 CALCULATED NICKEL GRADE OF METALLIC PHASE WHEN SERPENTINIC LATERITE (SAMPLE D IN TABLE 4.1) IS REDUCED BY CO/CO <sub>2</sub> .....	36
FIG. 4.5 CALCULATED NICKEL RECOVERY AND TOTAL METALLIZATION PERCENTAGE WHEN SERPENTINIC ORE IS REDUCED USING CO/CO <sub>2</sub> MIXTURES WITH FIXED OXYGEN PARTIAL PRESSURE. ....	37
FIG. 4.6 CALCULATED NICKEL GRADE IN METALLIC PRODUCT WHEN SERPENTINIC ORE IS REDUCED USING CO/CO <sub>2</sub> MIXTURES WITH FIXED OXYGEN PARTIAL PRESSURE. ....	37
FIG. 4.7 CALCULATED NICKEL RECOVERY AND TOTAL METALLIZATION PERCENTAGE WHEN HIGH TEMPERATURE PHASES ARE CONSIDERED OR NOT (SERPENTINIC ORE, REDUCED USING CO/CO <sub>2</sub> MIXTURES WITH FIXED OXYGEN PARTIAL PRESSURE).....	40
FIG. 4.8 CALCULATED NICKEL GRADE IN METALLIC PRODUCT WHEN HIGH TEMPERATURE PHASES ARE CONSIDERED OR NOT (SERPENTINIC ORE, REDUCED USING CO/CO <sub>2</sub> MIXTURES WITH FIXED OXYGEN PARTIAL PRESSURE) .....	40

FIG. 5.1 SIZE DISTRIBUTION OF SAMPLE D AFTER GRINDING.....	44
FIG. 5.2 XRD PATTERNS OF SAMPLE D BEFORE CALCINATION.+ .....	47
FIG. 5.3 XRD PATTERNS OF SAMPLE D CALCINED IN ARGON AT 1000°C FOR 7 HOURS .....	48
FIG. 5.4 DTA/TGA CURVES OF SAMPLE D CALCINED IN AIR.....	51
FIG. 5.5 DTA/TGA CURVES OF SAMPLE D CALCINED IN ARGON, RETAINED AT 700°C FOR 4 HOURS .....	52
FIG. 5.6 EFFECT OF CALCINATION TIME ON REDUCTION RATE AND EXTENT AT 700°C FOR SERPENTINIC SAMPLE D.....	54
FIG. 5.7 EFFECT OF CALCINATION TIME ON REDUCTION RATE AND EXTENT AT 1000°C .....	56
FIG. 5.8 XRD PATTERNS OF SAMPLE D CALCINED IN ARGON UNDER THE CONDITIONS.....	59
FIG. 5.9 EFFECT OF REDUCING GAS FLOW RATE WITH CO/CO <sub>2</sub> =7.0.....	62
FIG. 5.10 EFFECT OF REDUCING GAS FLOW RATE WITH CO/CO <sub>2</sub> =1/3.....	62
FIG. 5.11 WHEN GAS FLOW RATE IS TOO SMALL, BOTH REDUCTION RATE AND REDUCTION EXTENT WILL BE AFFECTED .....	63
FIG. 5.12 SCHEMATIC FIGURE OF DIFFERENT REDUCTION MODES OF CYLINDRICAL PELLETS.....	65
FIG. 5.13 REDUCTION WITH DIFFERENT SIZE PELLETS .....	68
FIG. 5.14 RELATIONSHIP BETWEEN PELLET RADIUS (R <sub>p</sub> ) AND INITIAL SPECIFIC WEIGHT LOSS RATE (R) ....	70
FIG. 5.15 XRD PATTERNS OF SAMPLES PARTIALLY REDUCED FOR 2 MINUTES AND COMPLETELY REDUCED AT 1000°C WITH CO/CO <sub>2</sub> =7.0 .....	73
FIG. 5.16 XRD PATTERNS OF THE SHELL AND THE CORE PART OF SAMPLES PARTIALLY REDUCED AT 740°C WITH CO/CO <sub>2</sub> =3.0 FOR 10 SECONDS.....	74
FIG. 5.17 XRD PATTERNS OF THE SHELL AND THE CORE PART OF SAMPLES PARTIALLY REDUCED AT 1000°C WITH CO/CO <sub>2</sub> =7.0 FOR 10 SECONDS.....	75
FIG. 5.18 EFFECT OF REDUCING GAS COMPOSITION AT 740°C.....	80
FIG. 5.19 EFFECT OF REDUCING GAS COMPOSITION AT 1000°C.....	80
FIG. 5.20 REDUCTION AT DIFFERENT TEMPERATURES WITH CO/CO <sub>2</sub> =1/3 .....	81
FIG. 5.21 REDUCTION AT DIFFERENT TEMPERATURES WITH CO/CO <sub>2</sub> =1.0 .....	81
FIG. 5.22 REDUCTION AT DIFFERENT TEMPERATURES WITH CO/CO <sub>2</sub> =3.0 .....	82

FIG. 5.23 REDUCTION AT DIFFERENT TEMPERATURES USING CO/CO <sub>2</sub> MIXTURES WITH THE SAME OXYGEN PARTIAL PRESSURE.....	82
FIG. 5.24 REDUCTION UNDER THE SAME CONDITIONS (CO/CO <sub>2</sub> =3.0, 700°C) AFTER CALCINED AT DIFFERENT TEMPERATURES .....	83
FIG. 5.25 REDUCTION UNDER THE SAME CONDITIONS (CO/CO <sub>2</sub> =3.0, 740°C) AFTER CALCINED AT DIFFERENT TEMPERATURES .....	83
FIG. 5.26 WATER REMOVAL PATTERN OF SAMPLE D .....	84
FIG. 5.27 REDUCTION WITH WEAK REDUCING GAS AT EARLY STAGE GIVES LOW REDUCTION EXTENT.....	86
FIG. 5.28 IF MORE REDUCTION TAKES PLACE WHILE SOME LATERITE MINERALS ARE IN AMORPHOUS STATE, HIGHER FINAL REDUCTION EXTENT CAN BE ACHIEVED.....	88
FIG. 6.1 X-RAY ANALYSIS RESULTS OF SPOT A, B,C,D IN PHOTO 6.1 .....	94
FIG. 6.2 EXPERIMENTAL DATA (GAS FLOW RATE: 2200CC/MIN, TEMPERATURE:740°C, CO/CO <sub>2</sub> RATIO:3.0) SUBJECTED TO THE GRAIN MODEL .....	98
FIG. 6.3 EXPERIMENTAL DATA (GAS FLOW RATE: 2200CC/MIN, TEMPERATURE:740°C, CO/CO <sub>2</sub> RATIO:3.0) SUBJECTED TO THE UNIFORM INTERNAL REACTION MODEL .....	99
FIG. 6.4 XRD PATTERNS OF REDUCED CALCINE BEFORE AND AFTER LEACHING .....	105
FIG. 6.5 CHEMICALLY ANALYSED NICKEL GRADE OF METALLIC PRODUCT IN PARTIALLY REDUCED SAMPLE D .....	106
FIG. 6.6 CHEMICALLY ANALYSED NICKEL RECOVERY IN PARTIALLY REDUCED SAMPLE D .....	106
FIG. 6.7 SCHEMATIC PELLET CONSISTS OF CUBIC GRAINS .....	125
FIG. 6.8 COMPARISON OF PREDICTED AND EXPERIMENTAL WEIGHT LOSS AT 740°C WITH CO/CO <sub>2</sub> =3.0 WHEN HEMATITE REDUCTION IS CONSIDERED.....	137
FIG. 6.9 COMPARISON OF PREDICTED AND EXPERIMENTAL WEIGHT LOSS AT 850°C WITH CO/CO <sub>2</sub> =3.0 WHEN HEMATITE REDUCTION IS CONSIDERED.....	137
FIG. 6.10 COMPARISON OF PREDICTED AND EXPERIMENTAL IRON RECOVERY WHEN SAMPLE D WAS REDUCED AT 850°C WITH CO/CO <sub>2</sub> =3.0 FOR DIFFERENT TIME.....	141

FIG. 6.11 COMPARISON OF PREDICTED AND EXPERIMENTAL IRON RECOVERY WHEN SAMPLE D WAS REDUCED AT 1000°C WITH CO/CO <sub>2</sub> =3.0 FOR DIFFERENT TIME.....	141
FIG. 6.12 COMPARISON OF PREDICTED AND EXPERIMENTAL NICKEL RECOVERY WHEN SAMPLE D WAS REDUCED AT 770°C WITH CO/CO <sub>2</sub> =3.0 FOR DIFFERENT TIME.....	142
FIG. 6.13 COMPARISON OF PREDICTED AND EXPERIMENTAL NICKEL RECOVERY WHEN SAMPLE D WAS REDUCED AT 1000°C WITH CO/CO <sub>2</sub> =3.0 FOR DIFFERENT TIME .....	142
FIG. 6.14 ARRHENIUS PLOT FOR REDUCTION OF NiO .....	143
FIG. 6.15 ARRHENIUS PLOT FOR REDUCTION OF FeO.....	144
FIG. 6.16 ARRHENIUS PLOT FOR REDUCTION OF HEMATITE.....	144

# LIST OF TABLES

TABLE 1.1 SIGNIFICANT MINERAL IN NICKEL LATERITE <sup>[2]</sup> .....	5
TABLE 1.2 TYPICAL CHEMICAL COMPOSITIONS OF LIMONITIC AND SERPENTINIC LATERITES .....	5
TABLE 1.3 MAJOR PROCESS FOR PROCESSING LATERITE .....	6
TABLE 2.1 THE HIGH TEMPERATURE BEHAVIOUR OF CERRO MATOSO NICKEL BEARING MINERALS <sup>[36]</sup> ....	17
TABLE 4.1 X-RAY FLUORESCENT ANALYSIS RESULTS OF SAMPLE C AND SAMPLE D (WT%) .....	28
TABLE 4.2 SOLUTIONS CONSIDERED IN CALCULATION USING F*A*C*T .....	28
TABLE 4.3 MAJOR SPECIES CONSIDERED IN CALCULATION USING F*A*C*T .....	29
TABLE 4.1 X-RAY FLUORESCENT ANALYSIS RESULTS OF SAMPLE C AND SAMPLE D (WT%) .....	43
TABLE 5.1 BET RESULTS OF CALCINED PELLETS OF SAMPLE D. ....	55
TABLE 5.2 INITIAL SPECIFIC WEIGHT LOSS RATE WHEN DIFFERENT SIZES OF PELLETS ARE REDUCED AT DIFFERENT TEMPERATURES .....	69
TABLE 5.3 MINERAL PHASE COMPOSITION OF LATERITE AT DIFFERENT REDUCTION STAGES.....	72
TABLE 6.1 NICKEL GRADE IN METALLICS PRODUCED FROM GOETHITE AND SERPENTINE DERIVATIVE MINERALS MEASURED BY SEM/EDX (FOR SAMPLE PARTIALLY REDUCED AT 740°C WITH CO/CO <sub>2</sub> =3.0 FOR 9.9 MINUTES).....	96
TABLE 6.2 CHEMICAL ANALYSIS OF PARTIALLY REDUCED SAMPLES .....	103
TABLE 6.3 TRUE DENSITY OF CALCINED PELLET. ....	113
TABLE 6.4 BET SURFACE AREA AND GRAIN SIZE .....	114
TABLE 6.5 EFFECTIVE DIFFUSIVITY OF CO WITHIN CALCINED PELLET .....	127
TABLE 6.6 ESTIMATED MASS TRANSFER COEFFICIENTS .....	132
TABLE 6.7 EQUILIBRIUM CONSTANTS FOR OXIDE REDUCTIONS .....	132

TABLE 6.8 MOLAR CONCENTRATION OF SOLID REACTANTS .....	133
TABLE 6.9 RATE CONSTANT FOR HEMATITE REDUCTION TO MAGNETITE IN LATERITE.....	135
TABLE 6.10 RATE CONSTANT FOR FeO REDUCTION TO Fe.....	140
TABLE 6.11 RATE CONSTANT FOR NiO REDUCTION TO Ni .....	140

# LIST OF PHOTOS

PHOTO 5.1 PARTIALLY REDUCED SAMPLE DEMONSTRATES A SHRINKING CORE MODE .....	64
PHOTO 6.1 LATERITE COMPRISES OF DIFFERENT MINERALS .....	93
PHOTO 6.2 METALLIC PHASE IS FINELY DISTRIBUTED IN THE REDUCED PELLET .....	95
PHOTO 6.3 PARTIALLY REDUCED CYLINDRICAL PELLET SECTIONED ALONG CYLINDER AXIS .....	102

# CHAPTER 1

## INTRODUCTION

### 1.1 Laterites As A Source Of Nickel

Nickel is an important element and is widely used in this modern world<sup>[1]</sup>. Natural processes have concentrated it to an exploitable grade producing three kinds of deposits: sulphides, laterites and deep-sea manganese nodules. Although deep-sea nodules are of huge quantity<sup>[2]</sup>, they can not be used economically nowadays, so the primary resources used now in nickel industry are the other two, and because of the relative ease of recovery of nickel from sulphide, the bulk of the total nickel produced in the world has been from sulphide deposits. However, in studying the situation as it exists today, we may draw the conclusion that laterites will dominate nickel production in the not too distant future. The reasons are:

- 1) RESERVES: land-based nickel reserves in the Market Economic Countries are of 36% sulphides and 64% laterites<sup>[3]</sup>. The amount of laterite reserves is greater than that of sulphides.
- 2) GRADE: after many years of extraction, the sulphide reserves are growing leaner.
- 3) MINING COST: since sulphide ores occur in hard rock, they are characterized by high mining cost, moreover, as the exploration continues, sulphide reserves will get

# CHAPTER 1

## INTRODUCTION

### 1.1 Laterites As A Source Of Nickel

Nickel is an important element and is widely used in this modern world<sup>[1]</sup>. Natural processes have concentrated it to an exploitable grade producing three kinds of deposits: sulphides, laterites and deep-sea manganese nodules. Although deep-sea nodules are of huge quantity<sup>[2]</sup>, they can not be used economically nowadays, so the primary resources used now in nickel industry are the other two, and because of the relative ease of recovery of nickel from sulphide, the bulk of the total nickel produced in the world has been from sulphide deposits. However, in studying the situation as it exists today, we may draw the conclusion that laterites will dominate nickel production in the not too distant future. The reasons are:

- 1) RESERVES: land-based nickel reserves in the Market Economic Countries are of 36% sulphides and 64% laterites<sup>[3]</sup>. The amount of laterite reserves is greater than that of sulphides.
- 2) GRADE: after many years of extraction, the sulphide reserves are growing leaner.
- 3) MINING COST: since sulphide ores occur in hard rock, they are characterized by high mining cost, moreover, as the exploration continues, sulphide reserves will get

deeper and therefore mining cost will be higher. The mining of laterites, however, is essentially an earth moving operation and therefore the mining cost is relatively low.

- 4) ENVIRONMENT PROTECTION PRESSURE: the regulations on sulphur dioxide emissions will put more pressure on the production of nickel from sulphides. Laterite based nickel production has fewer environmental concerns.
- 5) NEW TECHNOLOGY FACTOR: there are ways which can make the treatment of laterites more profitable through reducing operating costs and increasing by-product revenue, thus making laterites economic and competitive.

Actually, laterites are becoming more and more important. In the 1950's, about 10% of the Western World's nickel production came from laterites, during the 1970's, this had increased to nearly 1/3<sup>[4]</sup>, and since 1988, the percentage of the world's nickel produced from laterites has risen from 38% to almost 50%.<sup>[2]</sup>

## 1.2 Laterites

Laterites originated from mafic and ultramafic igneous rock, which have high contents of iron and magnesium. Due to the similar ionic radii of  $Mg^{2+}$  (0.78Å),  $Ni^{2+}$  (0.78Å) and  $Fe^{2+}$  (0.83Å)<sup>[5]</sup> ( $Mg^{2+}$ :0.65Å,  $Ni^{2+}$ :0.69Å and  $Fe^{2+}$ :0.75Å in Reference[10],  $Mg^{2+}$ :0.66Å,  $Ni^{2+}$ :0.69Å and  $Fe^{2+}$ :0.74Å in Reference[6] ), nickel has a tendency to replace magnesium in the mineral structure and thereto become enriched in the early crystallised magnesium and ferromagnesium minerals, among which, olivine and hypersthene are the most important<sup>[2]</sup>.

In the course of time, the mafic or ultramafic rocks were attacked by natural agencies such as water containing CO<sub>2</sub>, and during this weathering process, nickel and magnesium were leached from the solid and were carried downwards by the acid ground water. Under some conditions, nickel was precipitated as hydrous silicate, whereas magnesium was carried off by water, as magnesium is more soluble than nickel. In this way, nickel was concentrated<sup>[7]</sup>. As the ground surface is lower during the natural process, the fresh acid ground water again attacked the precipitate which was already enriched in nickel, and in a similar way, nickel was re-concentrated. The eventual insoluble residue has an abnormally high nickel content. That natural product is referred to as laterite<sup>[7]</sup>. So in general, the nickel laterite formation process involves the following steps: dissolution of original minerals, movement of elements in solution and precipitation of some elements in another location.

According to mineral composition, nickel laterite deposits can usually be divided into five zones. The relative thickness of each zone can vary from site to site, the summary of the five zones is<sup>[2][12]</sup>:

#### 1) IRON CAPPING ZONE

This zone is at the top of the laterite deposit and is also referred to as ferricrete<sup>[2]</sup>. It has undergone the greatest amount of weathering and much of the nickel from the original parent rock has been leached away. The main mineral in this zone is goethite which has been recrystallised as a result of repeated attacks by natural agencies. Since the mineral value is not very high, this zone is usually discarded during mining.

#### 2) LIMONITE ZONE

This zone is below the iron capping zone, and has also undergone extensive weathering. This zone characteristically has a fine grain size, low nickel content and uniform chemical and mineralogical composition. The primary mineral phase containing the bulk of the nickel is goethite. This zone represents the upper part of a laterite ore deposit.

### 3) TRANSITION OR INTERMEDIATE ZONE

The zone falls between the limonite and saprolite ore zones. The existence of this zone is due to the difficulty of separating the limonite and saprolite zones during mining. Actually, any sharp classification of laterites is arbitrary because the difference among them is only one of degree.

### 4) SAPROLITE ZONE

This zone is at the lower part of the laterite ore deposit and just above the bed rock, it represents an intermediate stage of weathering. Nickel-rich mineral phases, such as serpentine, are found in this zone. Both chemical and mineralogical compositions in this zone are extremely heterogeneous.

### 5) BED ROCK

This is the original rock prior to the start of the laterization process. The main minerals in the parent rock are serpentine and olivine. Minor minerals are orthopyroxene and clinopyroxene.

The significant minerals in nickel laterites are shown as Table 1.1:

**Table 1.1 Significant Mineral In Nickel Laterite<sup>[2]</sup>**

name	Formula	Ni%
<b><u>Limonite Zone:</u></b>		
Goethite	(Fe,Al,Ni)OOH	0.5~1.5
"Asbolite" lithiophorite cryptomelane	Mn,Fe,Co, Ni oxide	1~10
<b><u>Intermediate zone :</u></b>		
Nontronite	(Ca,Na,K) <sub>0.5</sub> (Fe <sup>3+</sup> ,Ni,Mg,Al) <sub>4</sub> (Si,Al) <sub>8</sub> O <sub>20</sub> (OH) <sub>4</sub>	0~5
Quartz	SiO <sub>2</sub>	0
<b><u>Saprolite zone:</u></b>		
Nickeliferous serpentine	(Mg,Fe,Ni) <sub>3</sub> Si <sub>2</sub> O <sub>5</sub> (OH) <sub>4</sub>	1~10
"garnierite"	(Ni,Mg) <sub>3</sub> Si <sub>4</sub> O <sub>10</sub> (OH) <sub>2</sub>	10~24
<b><u>Peridotite bedrock:</u></b>		
Olivine	(Mg,Fe,Ni) <sub>2</sub> SiO <sub>4</sub>	0.25
Orthopyroxene	(Mg,Fe)SiO <sub>3</sub>	0.05
Serpentine	Mg <sub>3</sub> Si <sub>2</sub> O <sub>5</sub> (OH) <sub>4</sub>	0.25

The chemical composition and grade of laterites may show great variations due to different climatic histories, different leaching rate and bedrock properties, but it is usual to classify them into two groups according to the principle mineralogical composition of which they consist: limonitic type and serpentinic type.

The primary minerals contained in limonitic ore are hydrated ferric oxide (goethite) and also free quartz, whereas the dominant mineral species of serpentinic ore is hydrated magnesium silicate, in which magnesium is commonly replaced by iron and nickel. While the composition of limonite and serpentine vary considerably, the following analysis of a dried sample was given by Crawford<sup>[8]</sup>:

**Table 1.2 Typical Chemical Compositions Of Limonitic And Serpentinic Laterites**

	Ni(%)	Fe(%)	MgO(%)	SiO <sub>2</sub> (%)
Limonite type	1.37	35.6	7.8	16.5
Serpentine type	1.64	8.3	30.8	39.6

## 1.3 Nickel Extraction From Laterites

Laterites can either be processed to produce nickel metal by hydrometallurgy or pyrometallurgy, or can be used to produce ferronickel by pyrometallurgy. The major processes that have been put into industrial service for processing laterites are listed in Table 1.3 [9][12].

**Table 1.3 Major Process For Processing Laterite**

Year	basic process
1889	matte smelting of silicate.
1943	Reduction roast-ammonia leach of laterite ore
1958	Electric furnace smelting to ferronickel
1959	Pressure leaching of oxide ores with sulphuric acid
1974	Reduction roast and electric furnace smelt

### 1) MATTE SMELTING PROCESS

This process consists of several main steps. First the ore is put into a rotary kiln or vertical shaft reduction furnaces and subjected to high temperature heating under a reducing atmosphere. During this process step, bound crystalline water is driven off followed by reduction of nickel and some iron to the metallic state. Then, the reduced calcine reacted with sulphur in an electric furnace. Sulphur can added either in the elemental form in the form of gypsum or pyrite. As a result, a slag containing the oxide components of the ore and a matte of iron and nickel sulphides are formed. This crude matte, which contains 30~35% of nickel, is then transferred to a converter, in to which air is blown into, and by preferentially oxidizing iron, a final matte containing 75~78% Ni is produced. This matte is roasted, reduced, and finally by refining,

commercial nickel is produced.<sup>[10]</sup>

## 2) REDUCTION ROAST-AMMONIA LEACH PROCESS

This process is also referred to as Caron process and four main steps are involved in it, they are: ore drying and grinding, reduction roasting, leaching with ammoniacal ammonium carbonate solution, and metal recovery, among these reduction roasting is a critical step. Reducing potential and temperature pattern must be controlled to achieve maximum nickel and cobalt recovery as well as the best selective reduction of nickel and cobalt over iron. Drying will remove the moisture contained in the ore, while leaching will dissolve metallic iron, nickel and cobalt. The ferrous iron in the solution is then oxidized to ferric state and precipitated as leach residue. Nickel and cobalt can be recovered from the solution as the final stage. The Caron process can recover 75~80% of nickel and only 40~50% of cobalt. It is mainly used to treat limonitic type ore. When this process is used to treat serpentinitic ore or laterites containing low iron and high magnesium contents, nickel recovery will be significantly decreased<sup>[11]</sup> because the strongly basic magnesia tends to combine with silica and NiO making NiO largely unreducible during reduction roasting stage.

## 3) ELECTRIC FURNACE SMELTING TO FERRONICKEL

In this process, the ore is first heated and calcined to remove moisture and chemically bound water, it is then charged directly into electric furnace and subjected to reduction and melting at about 1550°C. Nearly all the nickel and a large percentage of iron is reduced at this stage and a crude ferronickel alloy is produced, which usually contains about 25% Ni. The final processing step involves the refining of this

crude ferronickel into a saleable product. Refining is achieved by tapping the electric furnace ferronickel into ladles where additives such as soda ash, lime, and/or calcium carbide are added for impurity removal<sup>[10]</sup>.

#### 4) PRESSURE LEACHING OF OXIDE ORES WITH SULPHURIC ACID

In this process, the ore is directly treated at high pressure and at 240~260°C. Because at high temperatures ferric iron has the propensity to hydrolyse and form goethite, hematite and, in sulphate solutions, jarosites, separation of Ni and Co from Fe in the ore is enabled. Compared with the Caron process, pressure leaching of oxide ores with sulphuric acid has two advantages. Besides the elimination of the energy-intensive drying and reduction steps, it has high recoveries of nickel and cobalt (both are over 90%). This process is used to treat limonitic ores with lower magnesium content<sup>[10]</sup>.

#### 5) REDUCTION ROAST AND ELECTRIC FURNACE SMELT

This process is very similar to the process of electric furnace smelting to ferronickel except that at the end of the heating and calcination stage, emphasis is given to the selective reduction of nickel in order to increase the utilization of fuel in this stage and to reduce the electric power requirement in the subsequent smelting stage. Here again attention should be paid to the reducing potential and temperature patterns, since the pre-reduction stage will affect the nickel recovery and product grade.

Which process should be selected will depend on the nature of the ores. Generally for limonitic laterites because of they tend to produce corrosive slag on smelting, a

hydrometallurgy process is employed. For serpentinitic ores, because they are not so amenable to leaching, a pyrometallurgy method is usually used.

Process selection also depends on the composition of laterites, particularly with respect to Fe/Ni and SiO<sub>2</sub>/MgO ratios. For serpentinitic ores where on smelting the SiO<sub>2</sub>/MgO ratio in the slag falls into 1.5~1.6, processes to produce ferronickel are adopted because the melting point of the slag corresponds to the melting point of ferronickel. For serpentinitic ores which on smelting the SiO<sub>2</sub>/MgO ratio in the slag is about 2, a matte smelting process is used, because the low melting point of the slag allows the production of sulphide matte, which also has a lower melting point. For limonitic ores, if Mg content is less than 5%, a high pressure sulphuric acid leaching process is used. If the Mg content is larger than 5%, a reduction-roast-ammonia leach process is used<sup>[12]</sup>, because magnesium oxide is acid soluble. Therefore the higher Mg content will increase the consumption of solvent if treated by the high pressure sulphuric acid process.

Based on the above, a range of processes now exist around world, and many new methods to extract nickel from laterites have been demonstrated experimentally at different scales, Some of these seem to be promising in the future.<sup>[10][13][14][15][16][17]</sup>, but generally nickel production from laterites can be summarised by Figure 1.1:

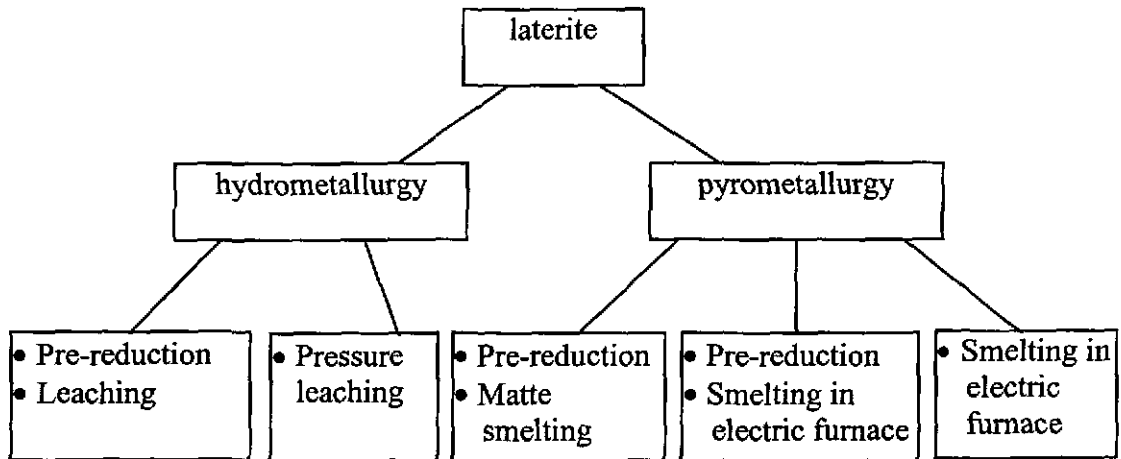


**Fig. 1.1 General Summary Of Processes For Nickel Production From Laterites**

Laterite based nickel production is energy intensive, it requires 3 times as much energy as sulphide based production<sup>[18]</sup>, thus energy saving in nickel production from laterites is critical.

In pyrometallurgy, the processes which involve pre-reduction will yield a high grade ferronickel, which requires less refining work and thus can reduce the energy requirement.

In hydrometallurgy, most laterite based plants also employ a pre-reduction step in the early stages. It is found that pre-reduction affects the final production grade and nickel recovery.

To make laterite based nickel production more profitable, it is desired in the pre-reduction stage, to reduce as much nickel as possible in order to get a maximum nickel recovery. On the other hand, it is also desired to reduce as little iron as possible to get a more valuable high grade product. Furthermore, a high reduction rate is always desired.

These, however, require conflicting reducing conditions, and in order to optimize them, it is desirable to have a knowledge about the mechanism and kinetics of laterite reduction.

## CHAPTER 2

# LITERATURE REVIEW

### 2.1 Studies Based on Pure Individual Materials

Extraction of nickel from laterites has received a lot of attention since 1867 when the rich nickel silicates of New Caledonia were discovered<sup>[9]</sup>. Consequently a number of studies on selective reduction of mixtures of the individual nickel and iron oxides have been carried out. Though these mixtures are not entirely representative of real ores, some kinetic and thermodynamic information has been provided. Szekely<sup>[19]</sup> studied the reduction of NiO-Fe<sub>2</sub>O<sub>3</sub> mixture in H<sub>2</sub> and found that the best selectivity was obtained at lower temperatures where the reduction was controlled by chemical reaction. Nasr's<sup>[20]</sup> study showed that the reduction of NiO-Fe<sub>2</sub>O<sub>3</sub> mixture led to a product of series Ni-Fe solid solutions. This conclusion was shared by Ajarov<sup>[21]</sup> and Core<sup>[22]</sup> *et al.* Core also observed that the reduction of NiO-Fe<sub>3</sub>O<sub>4</sub> mixture consists of two stages, the first is the reduction of NiO and of nickel ferrite, the second corresponds to the reduction of iron oxides, and as the result of mutual influence of the metallic nickel and metallic iron, the reduction process became faster. This is quite reasonable, because as the metallic iron and nickel alloy formed, both of their activities are lowered, increasing the driving force for the reduction of their oxides.

In some cases, different conclusions were drawn regarding the reduction of mixtures of individual iron and nickel oxides. When Konchakovskaya<sup>[23]</sup> studied the reduction of NiO-Fe<sub>2</sub>O<sub>3</sub> mixture by H<sub>2</sub>, it was found the product was pure nickel and pure iron, no solid solution was formed. In non-isothermal reduction of a mechanical mixture of NiO and Fe<sub>2</sub>O<sub>3</sub> using coal, Sarkisyan<sup>[24]</sup> found NiO and Fe<sub>2</sub>O<sub>3</sub> were reduced separately without a significant interaction. These results can be attributed to insufficient mixing between reactants, which greatly limits the relevance of the work to laterite reduction.

Shirane<sup>[25]</sup> studied the activity of NiO in the MgO-NiO solid solution and the Mg<sub>2</sub>SiO<sub>4</sub>-Ni<sub>2</sub>SiO<sub>4</sub> solid solution, and found in these systems the activity of NiO deviates negatively from ideality, causing the reducibility of NiO to decrease greatly. Hallett<sup>[26]</sup> incorporated solid solution behaviour of nickel in the oxide and silicate phase in his thermodynamic study of laterite minerals, and produced several stability diagrams for the Fe-Ni-O and Ni-Mg-Si-O systems. Both Shirane's and Hallett's work indicated that the reduction of laterite ore can be far more complicated than that of simple mixtures of iron and nickel oxides.

## **2.2 Studies Based on Ores.**

### **2.2.1 Reducing Potential and Temperature**

Maybe the most important factors in laterite reduction are temperature and reducing gas composition. Many studies have shown the dependency of laterite reduction on temperature and gas composition. Caron<sup>[27]</sup> found that for normal laterite ores at

900°C, reducing gas mixture containing 90% H<sub>2</sub>O and 10% H<sub>2</sub> or 75% CO<sub>2</sub> plus 25% CO will result in desired high extraction of nickel. In the further study of the Caron process, De Graaf<sup>[28]</sup> found that for different types of ores, when reduced with different gaseous reductants, there are optimum temperature and reducing potential ranges. When H<sub>2</sub> is used, optimum reduction temperature range for limonitic ore is 550~850°C, whereas for serpentinitic ore it is 550~650°C (for the sample of Gag I) or about 850°C (for the sample of Gag II). When CO is used, the optimum temperature range for reducing limonitic ore is 850°C, but for serpentinitic ores, Gag I and Gag II, are 600~650°C and 900~950°C respectively. As for reduction potential, when H<sub>2</sub> is used as the reductant, the best effect can be achieved when the reducing power is in the “Fe” zone, while for CO, the best reducing power is in the “magnetite/wustite” zone. Here the zone is based on the pure oxide stability diagram. It should be pointed out that in both Caron and De Graaf’s work, the extraction (recovery) is obtained after an ammoniacal leaching process, and because the ferric hydroxide, which is generated from metallic iron on leaching, tends to scavenge or absorb nickel, the presence of too much metallic iron will cause nickel loss into the leachresidue, therefore, the optimum conditions found by Caron and De Graaf are actually the best conditions for the combination of nickel recovery and selectivity of pre-reduction stage.

Utigard and co-workers<sup>[29]</sup> studied the reduction of laterites in H<sub>2</sub>-CO<sub>2</sub> mixture and found that the degree of metallization increased with increasing temperature and /or H<sub>2</sub>/CO<sub>2</sub> ratio, but the tendency with which the metallization degree increases is different at different temperatures and /or different H<sub>2</sub>/CO<sub>2</sub> ratios. When H<sub>2</sub>/CO<sub>2</sub> is 0.5 to 2, the

degree of metallization increases linearly with increasing temperature. For  $H_2/CO_2$  ratio between 2.5 to 5.0, the degree of metallization increases significantly from 500°C to 600°C, but then changes only marginally with further increase in temperature. For  $H_2/CO_2$  ratio above 7, the degree of metallization increases rapidly with increasing temperature.

As for the reduction mechanism, Utigard *et al.* considered 600°C to be the minimum temperature required for the formation of metallics, and once metallic nickel has formed, FeO reduction is feasible if metallic iron forms an alloy with metallic nickel. Kawahara *et al.*<sup>[30]</sup> showed that the nickel reducibility was changed at different temperatures.

### **2.2.2 Ore Composition and High Temperature Phase Crystallization**

The dependency of laterite reduction behaviour upon chemical and mineral compositions has also been well documented. As mentioned above, De Graaf found for different ores, the optimum reduction to get the best leaching results are different. For high iron ores, reduction should be carried out in the “magnetite” zone, while for low iron ores should be just within the “metallic iron” zone. In studying Sukinda laterite, Mohanty<sup>[31]</sup> observed that the nickel reduction rate is higher for samples with a high iron, high nickel and low silica content. Since in this type of ore, nickel is associated with goethite, which, on heating, will undergo a phase transformation to hematite, and in this process, nickel will be liberated and available for reduction. The situation is different

with the samples which contain more silica and less iron. Kawahara<sup>[30]</sup> studied a range of laterites and observed that nickel reducibility increases with increasing iron content in the ore. This is, however, similar to the findings of Utigard *et al.*, who showed that the ore with the highest concentration of Ni and Fe was most readily metallized. Kawahara *et al.* indicated that this tendency increases dramatically with an increase in reduction temperature. The reducibility of nickel decreases with increasing MgO/SiO<sub>2</sub> ratio and with increasing magnesia and silica content in the ore.

Since the ionic radii of Ni<sup>2+</sup> and Mg<sup>2+</sup> are close, Ni<sup>2+</sup> readily replaces Mg<sup>2+</sup> in high MgO laterites, and once nickel is tied up in this form, it is difficult to reduce. Although it is still unclear whether this is entirely related to the decreased NiO activity, or the kinetics of reduction.

Caron<sup>[27]</sup> noticed that when magnesia was present, NiO, MgO and SiO<sub>2</sub> would become strongly combined at elevated temperatures making NiO largely unreducible. Later researchers<sup>[32][33][34][35][36]</sup> attributed this phenomenon to the formation of olivine, and it was found that nickel is most readily reduced after serpentine is decomposed to the amorphous state prior to olivine crystallization. So it is suggested that if the heating rate can be controlled so that reduction can be completed prior to olivine formation, much higher levels of nickel recovery can be achieved.

Using X-ray diffraction and differential thermal analysis, Hayashi<sup>[33]</sup> studied three kinds of serpentine mineral found in Ocuhal-San Juan deposits of Cuba: lizardite, clinochrysotile and antigorite. On heating, they behaved differently. Lizardite transformed to the amorphous state between 500~550°C, and formed forsterite and enstatite between

800~850°C. Clino-chrysotile transformed to amorphous state between 550~600°C and formed forsterite and enstatite between 750~800°C. Antigorite, however, decomposed to the amorphous state and transformed to forsterite and enstatite simultaneously. When nickel is largely associated with antigorite, its extraction will be greatly decreased.

Lopez-Rendon<sup>[36]</sup> identified and characterized different nickel bearing minerals in the Cerro Matoso deposits and the temperature ranges for these minerals to decompose and recrystallise determined by his DTA testwork are shown in Table 2.1.

In Table 2.1, MO stands for divalent metal oxides in the minerals. It is found minerals with higher MO/SiO<sub>2</sub> ratios tend to form olivine if heated at high temperature, thus decreasing the nickel reducibility.

**Table 2.1 The High Temperature Behaviour Of Cerro Matoso Nickel Bearing Minerals<sup>[36]</sup>**

Ni bearing minerals	MO/SiO <sub>2</sub> (molar ratio)	Temperature of decomposition (°C)	Temperature of crystallization (°C)	High Temperature phase
Lizardite	1.5	595~615	815	Olivine and minor Pyroxene
Smectite	0.5	>835	855~890	
Pimelite	0.8	Completed by 800~850	(800)	Enstatite /Pyroxene
Sepiolite	0.6	510~810	825	Enstatite (Pyroxene)
Chlorite	1.5	600~800	850	Olivine and/or spinel

Due to the variation in mineral composition and heating rate used to carry out TGA/DTA, the temperatures determined by different researchers for laterite ores to dehydrate or to crystallise will inevitably show some discrepancy.

### 2.2.3 Heating and Reducing Patterns

When studying garnierite samples, Caron<sup>[27]</sup> found that when heated in a reducing gas, the samples were readily reduced. Otherwise, if the samples were reduced after heating in inert gas, the extraction of nickel became difficult, even when the reduction was carried out at 950°C with pure hydrogen. More over, the higher the preheating temperature prior to reduction, the greater the decrease in nickel extraction. However, with “Rothsiet”, a hydrated nickel silicate mineral which is almost free from magnesia, preheating had virtually no detrimental effect. What Caron observed may now be easily understood with a knowledge of phase transformations of hydrated silicate minerals in laterite at elevated temperature.

Using the laterite from Ocuja-San Juan, Hayashi<sup>[33]</sup> found that oxidizing roast before reduction was harmful to nickel extraction, and a higher oxidizing roasting temperature prior to reduction will further decrease the nickel extraction.

### 2.2.4 Additives

A number of studies showed that the reduction of laterite would be enhanced by additives such as NaCl, FeS, sulphur or jarosite. Caron<sup>[27]</sup> stated that the beneficial effect of pyrite(FeS) addition is the most pronounced for hydrated nickel silicate and the effect decreases with the increase in iron concentration. In the UOP and the USBM processes, which are modified forms of the Caron process, sodium chloride and/or sulphur containing materials are added at roasting reduction stage, as a result, higher nickel

extraction is achieved at lower maximum reduction temperatures, and faster heating rates can be tolerated. In the Caron process, nickel recovery is 75~80%, maximum reduction temperature is 750~800°C, heating rate is less than 5°C/min. in the UOP process, 86~88% nickel extraction can be achieved at 650°C, whereas in the USBM process, the effective reduction temperature is only 525°C. In the UOP process, the heating rate can be up to 15°C/min<sup>[10][37]</sup>. De Graaf<sup>[38]</sup> concluded through the experimental works that the addition of pyrite during the reduction of laterite increased nickel extraction and lowered the sensitivity to reduction conditions. Saha<sup>[35]</sup> thought the addition of NaCl had a catalytic effect that considerably increased the kinetics of reduction of nickel oxide, while the addition of FeS allowed dehydration to occur at a lower temperature and thus gave a longer time where nickel oxides were available for reduction. Crawford<sup>[8]</sup>, however, considered that the addition of FeS helped to catalyze the rate of reduction. Jha *et al.*<sup>[39],[40]</sup> studied the carbothermic reduction of sulphide ore, and found that the reaction rate is increased by the formation of oxysulphide liquid. It is likely that when FeS or jarosite is added, the increase of the laterite reduction rate may also arise from the formation of this kind of liquid. The mechanism by which additives increase the reduction rate remains unclear.

### 2.2.5 Reoxidation

In laterite reduction, newly produced metallic phases have a fine particle size and large fresh surface area, therefore they are quite active to oxygen. Caron<sup>[27]</sup> noticed that

the Ni-Fe alloy in reduced ores will adsorb oxygen and raise the ore's temperature. The increased temperature in turn will promote the oxygen adsorption. If the ore is reduced at low temperature and exposed to moist air thereafter, the reduced calcine may even become pyrophoric. Some researchers have already paid attention to this problem. In a laboratory study, De Graaf<sup>[28]</sup> reduced laterite samples and then let them cool under nitrogen to 50°C prior to transferring them to a leach liquor. When Anderson<sup>[12]</sup> transferred the cooled reduced laterite from his furnace tube to a vial, a "glove bag" was used to prevent metallics from reoxidation.

## 2.2.6 Kinetics

Studies on pure materials or their mixtures comprise most of the kinetic investigation of laterite reduction<sup>[19]-[24]</sup>. Very few studies has been carried out systematically with real laterite. Saha<sup>[35]</sup> reduced an Indian low grade siliceous nickel ore at 750°C using fuel oil. After leaching with aqueous ammoniacal solution in air, it was found that nickel extraction increased with longer reduction times up to 120 minutes, but after that nickel recovery declined. Saha proposed that longer reduction times produced more iron and more iron-nickel alloy, which are deleterious to the leaching of nickel. Using serpentine ore and reducing it with H<sub>2</sub>/CO<sub>2</sub> mixture, Utigard<sup>[29]</sup> found that the amount of metallic product increased with increasing reduction time up to 4 hours. Kawahara<sup>[30]</sup> studied several types of laterite and showed that for both serpentinitic and limonitic ores, the reduction degree for nickel and iron tended to remain constant after

about 40 minute reduction, and for limonitic ore the temperature effect on nickel and iron reducibility was greater than for serpentinitic ore.

Nath<sup>[41]</sup> *et al.* reduced Indian Sukinda laterite for different times. By assuming nickel and iron exist as pure oxides in laterite, experimental data were fitted to the grain model proposed by Szekely *et al.*<sup>[44]</sup> and the two layer model. Various kinetic parameters were estimated by these means. A generalized model was developed to predict the reduction rate of laterite pellets. They concluded that the established model for analyzing pure oxide reduction can be easily extended for studying low grade laterite ores.

# CHAPTER 3

## APPARATUS AND EXPERIMENTAL PROCEDURE

### 3.1 Apparatus

The schematic diagram of the apparatus used in this study is shown in Fig.3.1.

The principal components of which are described in the following.

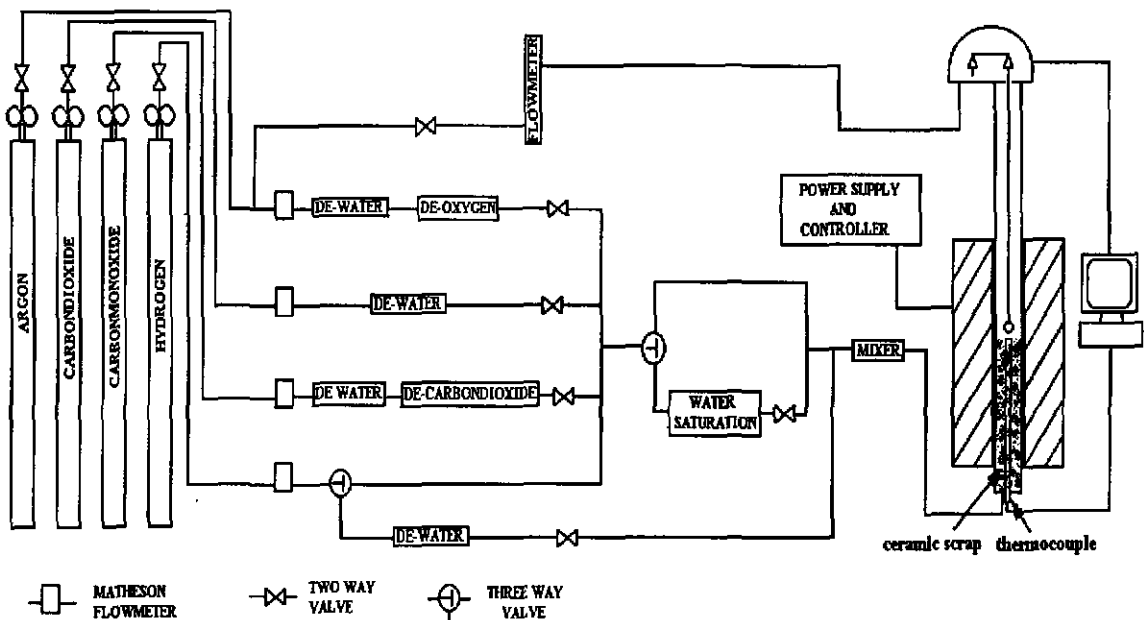


Fig. 3.1 Schematic Diagram of The Experiment Apparatus

### Furnace:

The Rapid Temp Furnace is heated by Mo-disilicide heating elements which are about 300 mm long. It has a uniformly heated zone of more than 100 mm in length, within which the temperature changes no more than 5 °C. The specimen is placed put in the center of the zone. The furnace is controlled and power supplied by a Eurotherm Controller. Heating patterns can be programmed and adjusted.

### Reaction Tube:

A mulite tube of 62.5 mm inside diameter is used. The top end of it is connected with the tube hang down from the microbalance and sealed with O rings, the lower end has two narrow inlets of which one is used for reaction gases and the other for a thermocouple. The lower part of the reaction tube is packed with ceramic scraps, this serves two purposes: one is to distribute the reaction gas evenly, the other is to provide adequate surface area to preheat the gas so that when it reaches the uniform temperature zone, it will have the same temperature as the specimen.

### Gas Purification Train:

Before being introduced to the furnace, the gases were purified by removing moisture from H<sub>2</sub>, Ar, CO<sub>2</sub> and CO, removing CO<sub>2</sub> from CO and removing O<sub>2</sub> from Ar. Moisture was removed by using silica gel and Drierite, where silica gel removed most of moisture, Drierite (chemical composition is mainly CaSO<sub>4</sub>) ensured a low level. CO<sub>2</sub> was removed by NaOH. O<sub>2</sub> was removed by hot copper turnings.

### Microbalance:

The specimen weight was continuously monitored during the reduction process by a Cahn 1000 microbalance, designed for weight and forces up to 100 grams with a sensitivity of 0.5 micrograms. During the reduction, an Ar flow of nearly 20 cc/min was blown through the balance head to prevent the reaction off-gases going into the balance chamber.

### Data recording:

Experimental data were recorded by a computer using Labview software. A program has been developed to record time, time of calcination, temperature, weight, total weight loss, and the rate of weight loss in a certain time interval. The rate of weight loss was obtained by regressing seven data points into a third order polynomial which was subsequently differentiated. Then by dividing this rate by the sample weight, the specific weight loss rate can be obtained. The program is quite flexible, the data recording procedure can be adjusted easily by the user. The data recording procedure used in this study was: every half second 20 digital signals for weight and temperature were read by the computer, among them the two largest and the two smallest were discarded and the average of the others was shown graphically on the screen. The weight was checked and compared with the previously recorded data at 0.5 second intervals. If the weight change was more than the given critical value (1mg), a new set of data was recorded, otherwise, new data was collected every 30 seconds (or more).

### Experiment Errors

Because of electrical noise, the uncertainty in the weight is  $\pm 1$  mg, the sample weight is around 1500 mg, so the error should be less 0.1%. The gas flow meters' accuracy is 1.5% of their full scales, the temperature, as stated above, within the uniform heat zone, varies less than 5°C.

## **3.2 Sample Preparation and Experiment Procedure**

Representative samples were pressed under 3000 psi (20.67 kPa) of ram pressure into a cylinder of 6.35 mm in diameter and approximately 30 mm in height with a weight about 1.5 gram. For other sizes of samples, diameter in 3.15 mm or 9.45 mm, the pressure was adjusted according to the base area of the cylinder so as to the samples would have the same density. The pellets were dried in air for several days and then stored in desiccator for at least 72 hours before use. After the cylindrical sample was placed in the reaction tube, the system was flushed with argon then heated to the predetermined temperature following a pre-programmed heating pattern. The sample remained at that temperature and was calcined for a given time prior to reduction. In most of this study, the calcination time was 60 minutes. Thereafter, argon was turned off and reducing gases were introduced. The moment that a weight change was detected is defined as the start point of the experimental run. Complete reduction usually took more than one hour, but most of the reduction took place within the first 15 minutes. After reduction the sample was cooled to below 50°C in argon then stored in a desiccator or transferred quickly to a

sealed plastic bag filled with argon, where the sample was ground and then subjected to chemical analysis.

Metallic nickel and iron in the reduced calcine were mostly analysed by a bromine-methanol leaching method. The bromine-methanol leaching procedure was provided by INCO Ltd. A titration method was used for comparison purpose. The iron and nickel content in the bromine-meleaching filtrate was finally determined by ICP (Inductively Coupled Plasma Spectrophotometry).

# CHAPTER 4

## THERMODYNAMIC STUDY

### 4.1 Thermodynamic Study Method.

To investigate how the temperature and the gas reducing potential will affect the nickel recovery and the nickel grade of the metallic product and to identify the optimum reduction conditions, a thermodynamic analysis was undertaken using Equilib program of F\*A\*C\*T, a thermodynamic software package.

Two kinds of laterite samples, Sample C and Sample D which were received from INCO, were studied. As will be seen in Table 4.1, X-Ray Fluorescent analysis showed that Sample C is mostly a limonitic ore but contained some magnesium silicate minerals, whereas Sample D is mainly a serpentinic laterite which may contain minor quantities of goethite. Due to the limitations of the software package and the available data, only four major chemical components of laterite,  $\text{Fe}_2\text{O}_3$ , NiO, MgO, and  $\text{SiO}_2$ , as well as gas reactants were considered. The products considered included gases, pure metals, pure oxides, spinels, an ideal nickel-iron solid solution and non-ideal solutions such as monoxide solution and olivine solution. Details of species selection are listed in Table 4.2 and Table 4.3 Although the reaction system employed here is still simple compared with

the complicated real situation, according to other similar work<sup>[42]</sup>, it is sufficient for preliminary investigation.

**Table 4.1 X-Ray Fluorescent Analysis Results of Sample C and Sample D (wt%)**

Sample	MgO	SiO <sub>2</sub>	Al <sub>2</sub> O <sub>3</sub>	CaO	Cr <sub>2</sub> O <sub>3</sub>	MnO	Co <sub>3</sub> O <sub>4</sub>	Fe <sub>2</sub> O <sub>3</sub>	NiO
C	2.70	8.20	7.60	0.15	1.70	0.51	0.20	76.8	1.1
D	20.0	47.9	2.7	0.12	0.94	0.50	---	24.1	3.4

**Table 4.2 Solutions Considered In Calculation Using F\*A\*C\*T**

Ideal Ni-Fe Solution	Spinel Solution	Olivine Solution	Glass oxide solution	Monoxide solution
Fe	Mg <sub>3</sub> O <sub>4</sub>	Mg <sub>2</sub> SiO <sub>4</sub>	MgO	MgO
Ni	FeMg <sub>2</sub> O <sub>4</sub>	Fe <sub>2</sub> SiO <sub>4</sub>	FeO	FeO
	MgFe <sub>2</sub> O <sub>4</sub>	Ni <sub>2</sub> SiO <sub>4</sub>	SiO <sub>2</sub>	NiO
	Fe <sub>3</sub> O <sub>4</sub>		NiO	

Table 4.3 Major Species Considered In Calculation Using F\*A\*C\*T

Chemical symbol	Phase	Name
O <sub>2</sub>	G1	Gas
CO	G1	Gas-1
CO <sub>2</sub>	G1	Gas
C	S1	Graphite
MgO	S1	Periclase
SiO <sub>2</sub>	S2	Quartz
SiO <sub>2</sub>	S4	Tridymite
SiO <sub>2</sub>	S6	Cristobalite
SiO <sub>2</sub>	S7	Coesite
SiO <sub>2</sub>	S8	Stishovite
MgSiO <sub>3</sub>	S1	Low-clinoenstatite
MgSiO <sub>3</sub>	S3	Orthoenstatite
MgSiO <sub>3</sub>	S4	Protoenstatite
MgSiO <sub>3</sub>	S6	Mg-ilmenite
MgSiO <sub>3</sub>	S7	Mg-garnet
MgSiO <sub>3</sub>	S8	Mg-perovskite
Mg <sub>2</sub> SiO <sub>4</sub>	S1	Forsterite
Mg <sub>2</sub> SiO <sub>4</sub>	S2	beta-forsterite
Mg <sub>2</sub> SiO <sub>4</sub>	S3	gamma-forsterite
Fe	S1	BCC
Fe	S2	FCC
Fe <sub>3</sub> C	S2	Solid-B, Triiron carbide
FeO	S1	Wustite
Fe <sub>2</sub> O <sub>3</sub>	S2	Hematite
Fe <sub>3</sub> O <sub>4</sub>	S2	Magnetite
FeSiO <sub>3</sub>	S1	Orthoferrosilicate
FeSiO <sub>3</sub>	S2	Fe-Perovskite
(FeO) <sub>2</sub> (SiO <sub>2</sub> )	S1	Fayalite
(FeO) <sub>2</sub> (SiO <sub>2</sub> )	S2	beta-fayalite
(FeO) <sub>2</sub> (SiO <sub>2</sub> )	S3	gamma-fayalite
Ni	S1	Solid-FCC
NiO	S3	Solid-C
Ni <sub>2</sub> SiO <sub>4</sub>	S1	Solid, Nickel orthosilicate

## 4.2 Results and Discussion

Preliminary experiments showed that it is difficult to remove chemically bound water for both Sample C and Sample D under 700°C. According to De Graaf<sup>[28]</sup> and Kukura<sup>[37]</sup>, the presence of water vapor in reducing gas will have a deleterious effect on nickel extraction. Moreover, unremoved water, upon reducing, will continue to be released and this will hamper the interpretation of reduction weight loss data. Therefore in this investigation, the studied temperature range was selected as 700~1000°C. Considering the carbon precipitation problem, the range of studied CO/CO<sub>2</sub> ratio was set as 0.5 to 3.0.

The calculated nickel recovery and nickel grade of metallic phases when limonitic ore is reduced by CO/CO<sub>2</sub> mixtures are shown in Fig.4.1 and Fig.4.2 respectively. Generally, when the CO/CO<sub>2</sub> ratio increases and temperature decreases, i.e. when reducing power is increased, nickel recovery will increase. However, when temperature is in the range of 700~810°C and CO/CO<sub>2</sub> ratio is around 1.0, non-ideal MgO-FeO-NiO solution is formed, this causes a trough in Fig.4.1. A similar calculation result has been obtained by Hallet<sup>[26]</sup>. In his stability diagram for goethite reduction, he showed that the nickel metallization percentage drops when the reduction condition moves from the spinel/alloy phase field to wustite/alloy phase field, although the reduction condition for this change to take place is different from that found in the present case. In Hallet's diagram, the change takes place abruptly. For limonite

reduction, nickel grade in the metallic product almost always increases as the reducing power of gas reactants decreases.

When serpentinitic ore is reduced, nickel recovery increases as reducing power increases under most reduction conditions, see Fig.4.3, but when the temperature is around 740°C and the CO/CO<sub>2</sub> ratio is 2.0~3.0, nickel recovery has a maximum value. This is because in this region the amount of olivine solution formed is minimized, therefore less nickel oxide is held in this solution. Fig.4.4 shows that when the CO/CO<sub>2</sub> ratio is decreased, nickel grade of the metallic phase is increased. In the region where the temperature is low and the CO/CO<sub>2</sub> ratio is high, carbon is precipitated and the reducing power does not change further with CO/CO<sub>2</sub> ratio, thus nickel grade can not be changed by varying reducing gas composition. When reducing power is lowered by increasing temperature, the nickel grade decreases. This somehow contradicts with the reduction behavior of limonitic ore, in which case the high temperatures and low reducing powers give better nickel reduction selectivity. By examining the calculation results, it is found for serpentinitic laterite, higher reduction temperatures results in more olivine solution, and relatively more nickel is associated with this phase and become unreducible.

On average, reduction of limonitic laterite will give a higher nickel recovery and a lower nickel grade in the metallic phase than reduction of serpentinitic ore. In limonitic ore, the SiO<sub>2</sub> content is low and at high temperature most of iron exists in the form of oxide, which is relatively easily reduced. As reduced iron and nickel will form an alloy, decrease the activity of metallic nickel and hence promote the reduction of nickel oxides, ease of reduction of iron will lead to a high recovery of nickel. Since the iron content in

limonitic ore is higher, the grade of metallic product is lower. In serpentinitic ore, more silicate minerals are formed at high temperature. Compared with pure oxides, the reduction condition required for reducing the silicate is more severe. In the case of nickel silicate, only a slight increase in the reducing power of the gas reactant is required compared with that for nickel oxide reduction. Whereas in the case of iron silicate, quite a substantial increase in the reducing power of the gas is needed compared with the requirement for the pure iron oxide<sup>[26]</sup>. This may partially account for the higher nickel grade of the metallic product when serpentinitic ore is reduced. For serpentinitic ore, more olivine solution will be formed at high temperatures when reduced, therefore more nickel will be tied up and nickel recovery will be lower.

Care must be taken here. In Fig.4.1 ~ Fig.4.4, when we talk about the temperature effect, the CO/CO<sub>2</sub> ratio is fixed. In this case, if temperature increases, the equilibrium oxygen partial pressure, pO<sub>2</sub>, in gas phase will increase substantially, therefore the actual reducing power will decrease greatly. When the equilibrium oxygen partial pressure, i.e. reducing power of gas mixture is fixed, temperature will affect the nickel recovery and the nickel grade of the metallic product in a different way. Fig.4.5 and Fig.4.6 show the calculation results using sample D's composition. For serpentinitic ore, when gas reducing power is the same, increasing temperature will give a higher nickel recovery and total metallization percentage. Whilst the nickel grade in the metallic phase still decreases with increasing temperature.

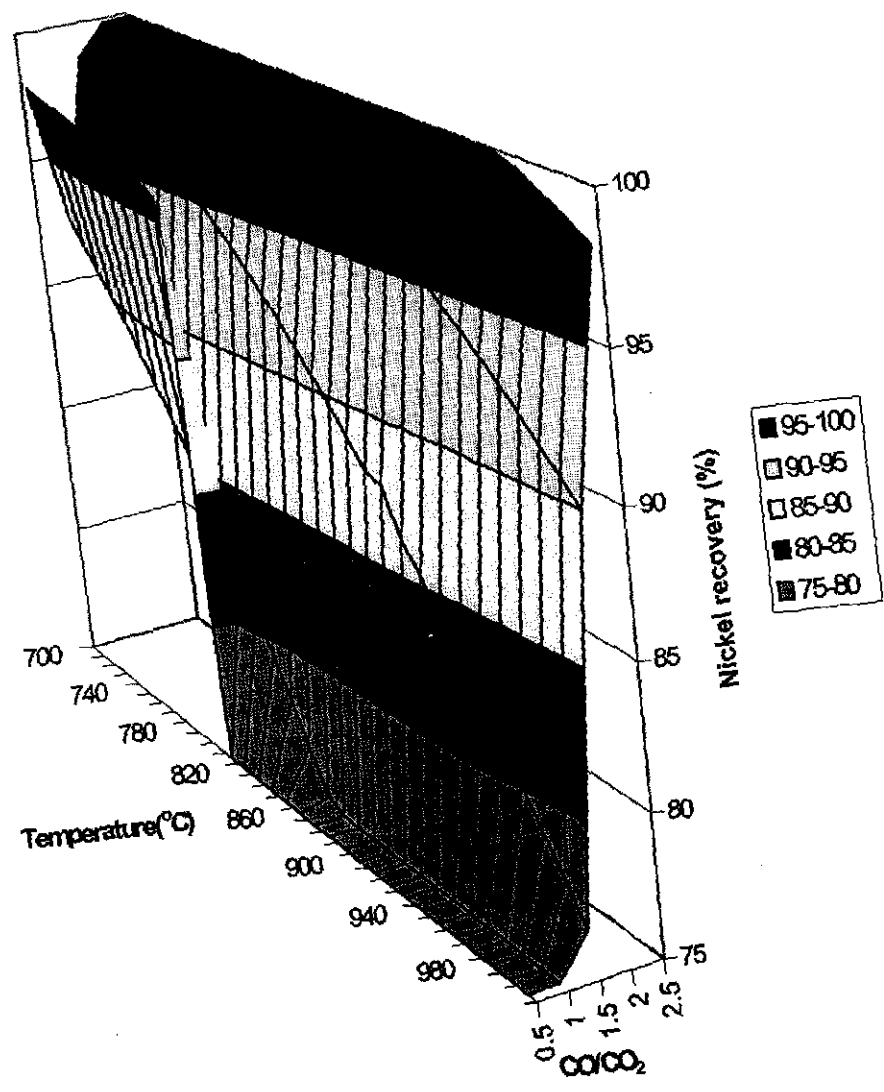
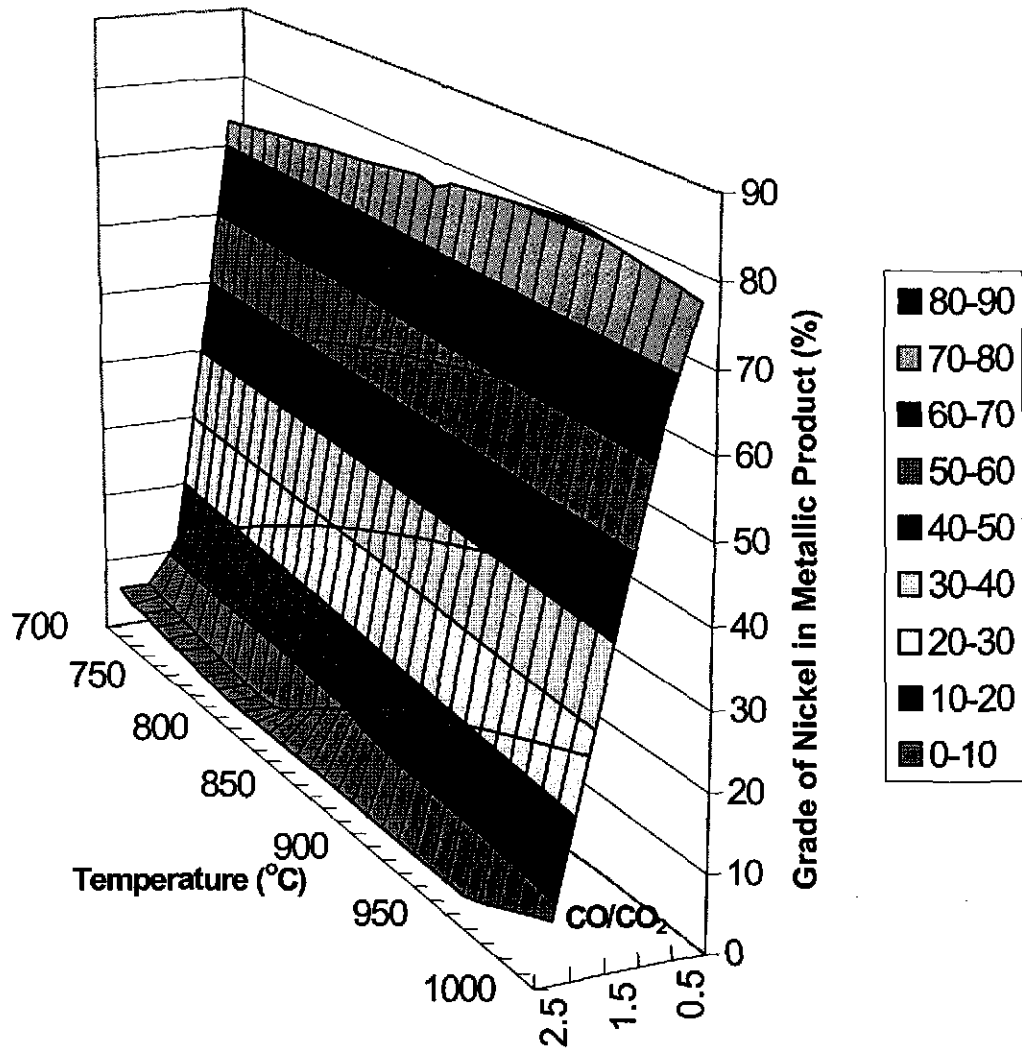
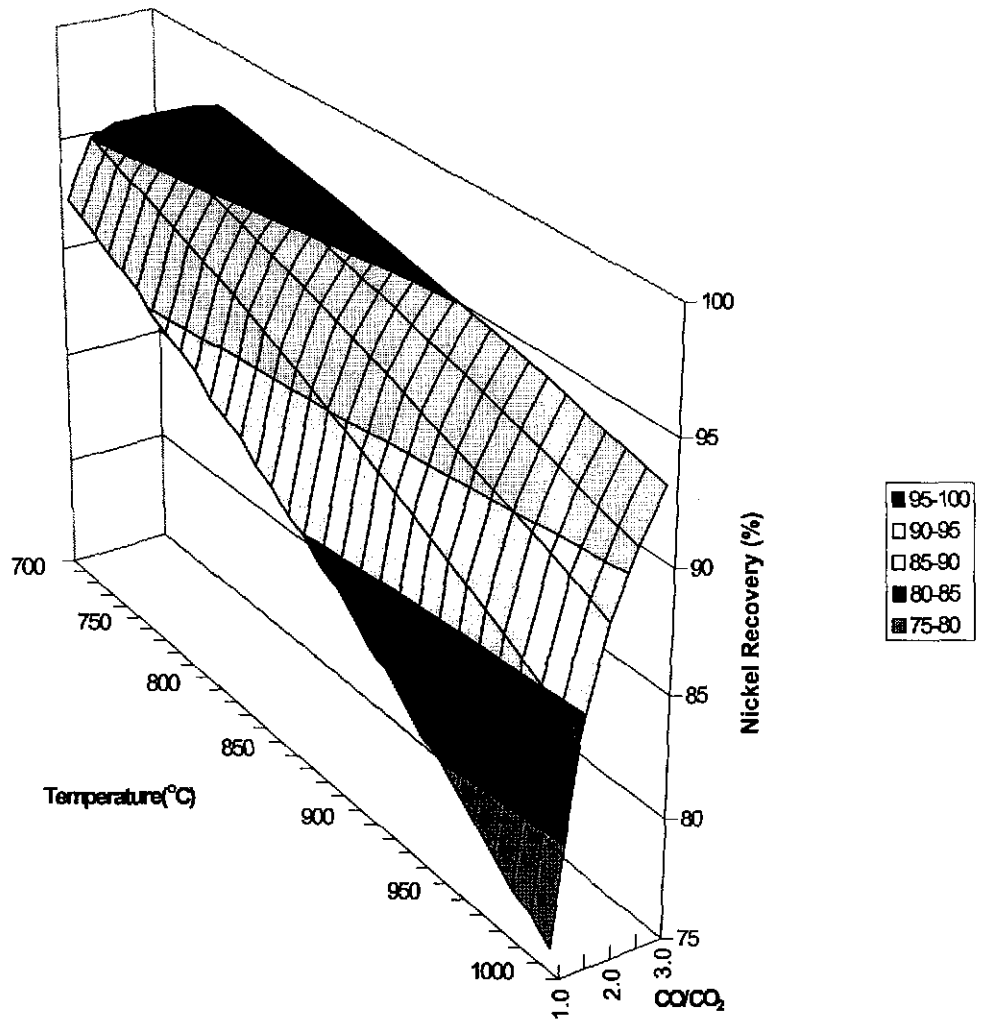


Fig. 4.1 Calculated Nickel Recovery When Limonitic Laterite (Sample C In Table 4.1) Is Reduced By CO/CO<sub>2</sub>



**Fig. 4.2** Calculated Nickel Grade in Metallic Phase When Limonitic Laterite (Sample C In Table 4.1) Is Reduced By CO/CO<sub>2</sub>



**Fig. 4.3** Calculated Nickel Recovery When Serpentinic Laterite (Sample D In Table 4.1) Is Reduced By CO/CO<sub>2</sub>

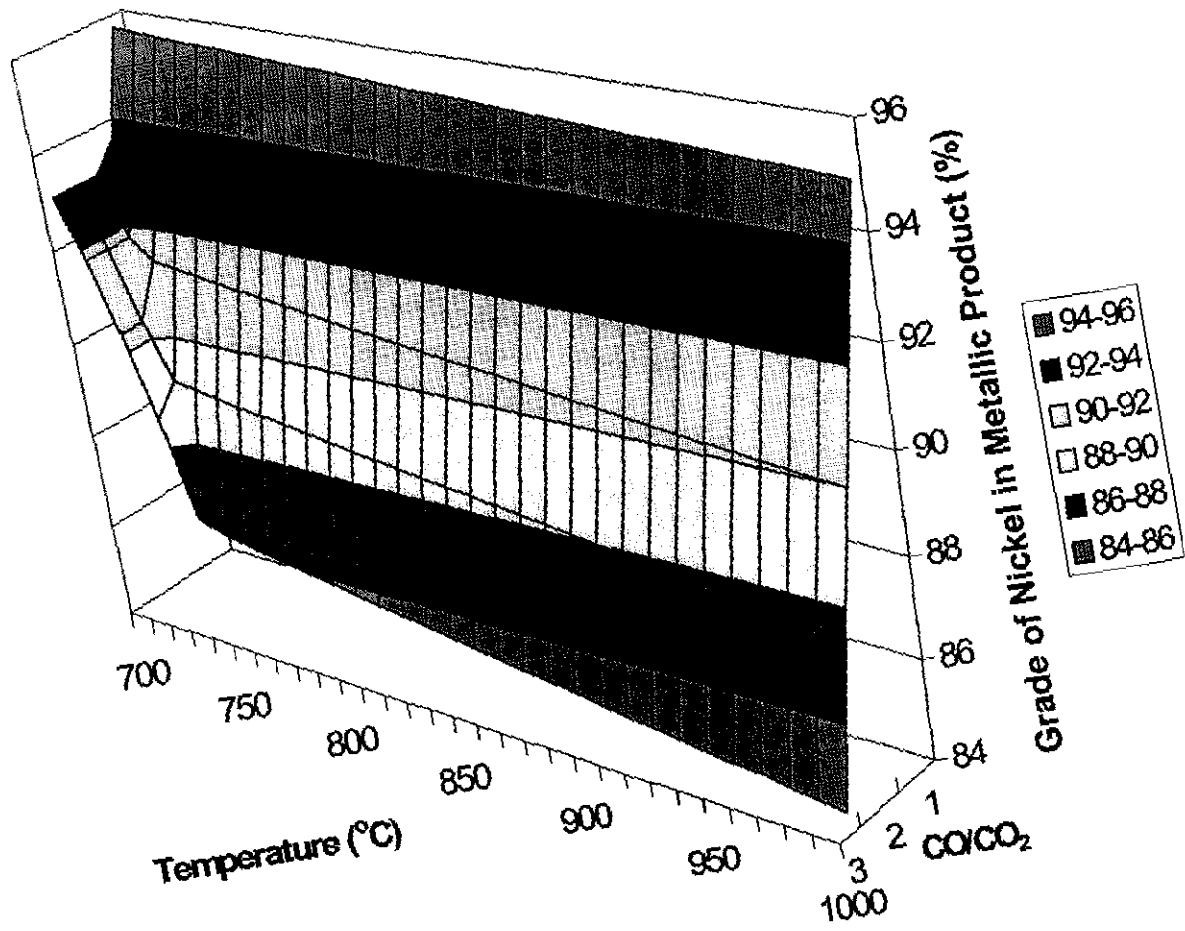
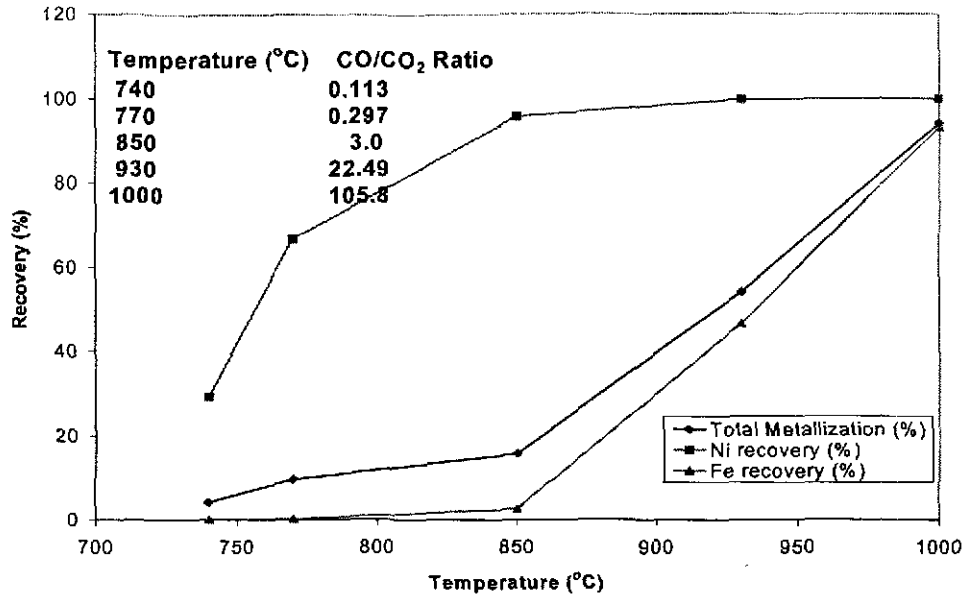
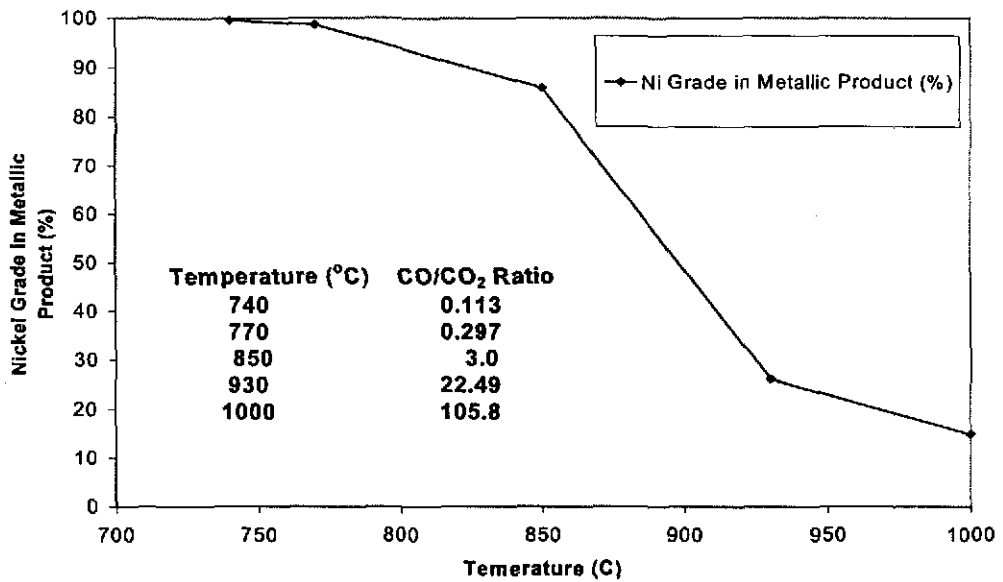


Fig. 4.4 Calculated Nickel Grade Of Metallic Phase When Serpentinic Laterite (Sample D In Table 4.1) Is Reduced By CO/CO<sub>2</sub>



**Fig. 4.5** Calculated Nickel Recovery and Total Metallization Percentage When Serpentinic Ore Is Reduced Using CO/CO<sub>2</sub> Mixtures with Fixed Oxygen Partial Pressure.



**Fig. 4.6** Calculated Nickel Grade in Metallic Product When Serpentinic Ore Is Reduced Using CO/CO<sub>2</sub> Mixtures with Fixed Oxygen Partial Pressure.

As noted in Section 2.2.2, it is found that laterite is most readily reduced after serpentine is decomposed to the amorphous state but before high temperature phases are crystallised. Thermodynamic calculations were also undertaken to investigate the effect of high temperature phase crystallization on metallization and nickel grade in the metallic product for serpentinic laterite. Since the thermodynamic properties of the amorphous phases are not available in F\*A\*C\*T, the olivine and enstatite solution and their components were not selected when the calculation was carried out. In such a manner we assume serpentine remains stable at elevated temperature. This is clearly not the case but the thermodynamic properties of the amorphous phase must fall between those of serpentine and olivine. Therefore calculation with the assumption that the high temperature phases do not form, provides an “upper bound” condition for the activities of the reducible oxides in the amorphous material. The “lower bound” condition is that for which the high temperature phases are assumed to form. The real case, where there is a kinetic impediment to formation of the high temperature phase from the decomposed serpentine, will lie somewhere between the two conditions. The calculation results are shown in Fig.4.7 and Fig.4.8.

It can be seen that when high temperature phases are present, nickel recovery, iron recovery and total metallization percentage are all lower, since high temperature phases tie up nickel and iron and make them unreducible. Because when high temperature phases formed, relatively more iron would be combined with them, the nickel grade in the metallic phase would be higher. Therefore, from the view point of thermodynamics we may say that when in amorphous state, laterite is the most reducible,

but would give a poor selectivity. This poorer selectivity is not entirely supported by experimental results presented in the subsequent chapters of this thesis. Therefore it is suspected that our current thermodynamic data is insufficient to predict the behaviour of serpentinitic ores.

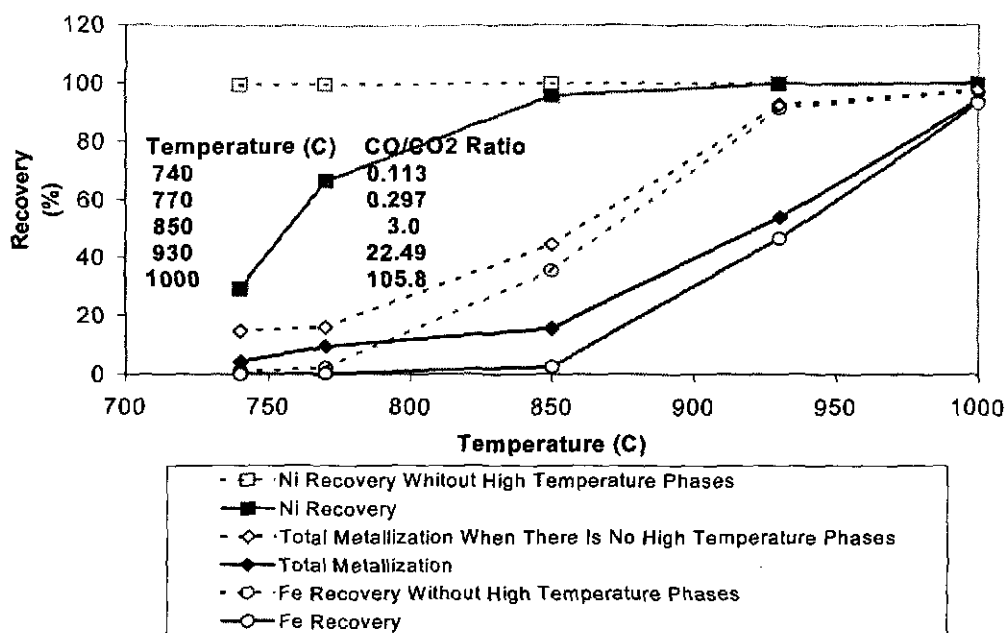


**Fig. 4.7** Calculated Nickel Recovery and Total Metallization Percentage When High Temperature Phases Are Considered Or Not (Serpentinic Ore, Reduced Using CO/CO<sub>2</sub> Mixtures with Fixed Oxygen Partial Pressure)

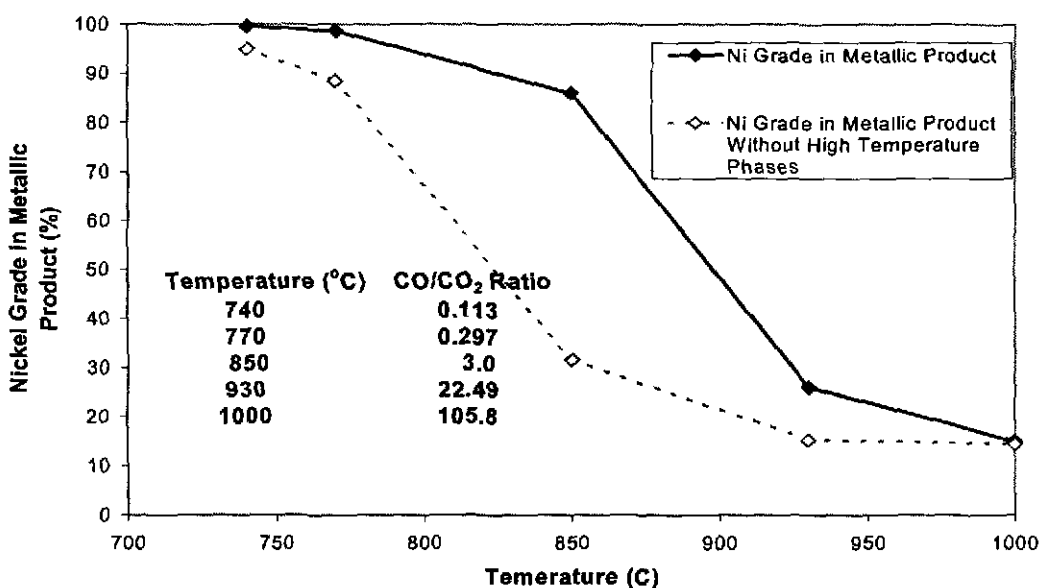


**Fig. 4.8** Calculated Nickel Grade in Metallic Product When High Temperature Phases Are Considered Or Not (Serpentinic Ore, Reduced Using CO/CO<sub>2</sub> Mixtures with Fixed Oxygen Partial Pressure)

### 4.3 Summary of Thermodynamic Study

In this thermodynamic study, the four major components of laterite, i.e.  $\text{Fe}_2\text{O}_3$ ,  $\text{NiO}$ ,  $\text{MgO}$  and  $\text{SiO}_2$  were taken into consideration. The open process, the case for industry reactor such as rotary kiln and shaft furnace in which the gas reactants react with the solid and then pass through the reactor, was simulated. Although the situation considered is less complicated than the real case, some conclusions may still useful to predicting the results of laterite reduction.

- 1) Metallic phase is in form of Ni-Fe alloy, no pure metal will be produced after laterite reduction.
- 2) By comparison, limonitic ore reduction will give higher nickel recovery and lower nickel grade in metallic product than serpentinitic ore reduction.
- 3) For limonitic ore, if the reducing power of gas mixture is lowered by temperature increase, the nickel recovery will be lowered. If the reducing power is lowered by changing  $\text{CO}/\text{CO}_2$  ratio, nickel recovery will also decrease, but not in a simple way. Instead, within some range ( $\text{CO}/\text{CO}_2$  ratio is around 1.0) the nickel recovery will be the lowest.
- 4) For limonitic ore, decrease in the reducing power of gas mixture will result in increase of nickel grade in metallic product.
- 5) For serpentinitic ore reduction, when the reducing power is lowered by decreasing  $\text{CO}/\text{CO}_2$  ratio, nickel grade in metallic product will be increased. However, when the

reducing power is lowered by temperature increase, nickel grade will decrease, because of the effect of temperature on the relative stability of the oxide and metal phase. As for recovery, stronger reducing conditions will generally give a higher nickel recovery, but at 710~740°C when CO/CO<sub>2</sub> ratio is 2.0~3.0, nickel recovery has maximum values.

- 6) Higher temperature will result in more olivine formation, therefore more nickel will be tied into it and become difficult to be reduced.
- 7) For serpentinitic ore, if the equilibrium oxygen partial pressure in gas phase is fixed, both nickel and iron recovery will increase with increase in temperature. Since the amount of metallic iron increase faster, nickel grade in metallic phase will decrease when temperature is higher.
- 8) With the assumption that the reduction of the amorphous material falls between the reductions when high temperature phases are considered and not considered, thermodynamic calculations showed that after serpentine decomposition and before high temperature phase formation, laterite is the most reducible, but the equilibrium metallic product would have a poor nickel grade.

# CHAPTER 5

## EXPERIMENTAL RESULTS

### 5.1 Sample Characterization

Five batches of samples were received from INCO Ltd for use in this study. They have been designated as A,B,C,D and E. Preliminary work was carried out with sample C using pure H<sub>2</sub> as a reducing gas. However, most of the work presented here was done with the sample D and the reducing gas was a CO/CO<sub>2</sub> mixture.

The compositions of the sample D have been listed in Chapter 4. For convenience, the table is shown again in the following.

**Table 4.1 X-Ray Fluorescent Analysis Results of Sample C and Sample D (wt%)**

	MgO	SiO <sub>2</sub>	Al <sub>2</sub> O <sub>3</sub>	CaO	Cr <sub>2</sub> O <sub>3</sub>	MnO	Co <sub>3</sub> O <sub>4</sub>	Fe <sub>2</sub> O <sub>3</sub>	NiO
Sample D	20.0	47.9	2.7	0.12	0.94	0.50	---	24.1	3.4

#### 5.1.1 Sample Preparation and Size Distribution

As received samples contained coarse particles, the largest being more than 10 mm. Since in this study the mass of laterite used for each experiment is limited, to ensure that every pellet was representative, the ore was ground. The size distribution after crushing is shown in Fig.5.1.

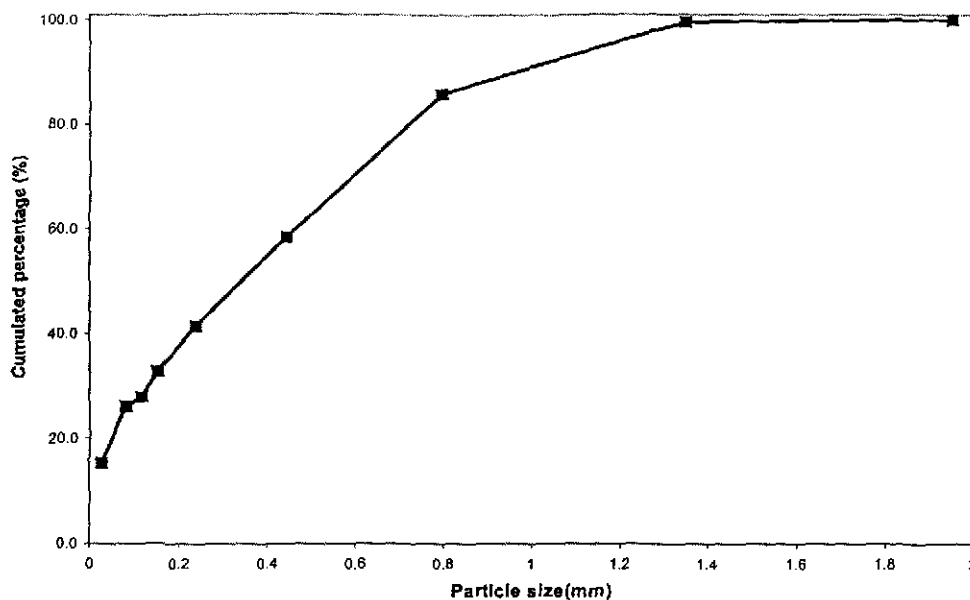


**Fig. 5.1 Size Distribution Of Sample D After Grinding**

The result in Fig.5.1 was obtained by screening. It must be pointed out that the measured grain size of the laterite varied considerably depending on the methods used for measurement. When the sieving method was used, parts of small particles would adhere to each other or to bigger particles, thus the result tended to be erroneously high. When the Coulter Counter method was used, it was noticed that particles were segregated by their size and density even with a strong stir, therefore bigger particles tended to be missed, and the measured value was unrepresentatively small.

### **5.1.2 X-Ray Diffraction**

X-ray diffraction analysis was first done with the original sample D. As there was a noticeable amount of amorphous material in the sample, calcination, which was aimed to provide a suitable condition for crystallization, was performed in order to have a full

knowledge of the sample composition. Calcination was carried out in argon at 1000°C for 7 hours. The XRD patterns are shown in Fig.5.2 and Fig.5.3.

From the XRD patterns, it is found that:

- 1) In original sample, serpentine/chrysotile and enstatite/pyroxene were present as the major phases, goethite and hematite as minor phases, and forsterite/olivine was present as a trace phase.
- 2) After calcination in Ar at 1000°C for 7 hours, serpentine/chrysotile was no longer detectable. As the result of phase transformation, forsterite/olivine was noticeable and hematite became a major phase. Enstatite/pyroxene remained a major phase and appeared to increase.

### 5.1.3 Chemical Composition

The chemical composition obtained by X-Ray Fluorescence analysis has been given in Table 4.1. Chemical analysis was done using two methods to determine nickel and iron content. Samples were dissolved in a heated hydrochloric/nitric acid mixture, the filtrate was then analysed using titration or ICP (Inductively Coupled Plasma Spectrophotometry) method.

According to XRF analysis,  $\text{Fe}_2\text{O}_3$  and NiO contents in sample D are 24.1% and 3.4% respectively, the corresponding Fe and Ni contents are 16.87% and 2.67%. While Fe content determined by the titration method is 16.83%, Fe and Ni contents determined by ICP are 16.26% and 2.34%. The different methods are in good agreement. Thus,

combined with XRD results, it is confirmed that Sample D is mostly a serpentinic laterite. It contains high content of MgO and SiO<sub>2</sub> and its major mineral phase is serpentine/chrysotile. The Fe content in goethite and in serpentine are 49% and 8% respectively<sup>[42A]</sup>. Therefore the estimated proportions of serpentine and goethite, assuming all Fe in Sample D comes from these two minerals, are about 80% and 20% respectively.

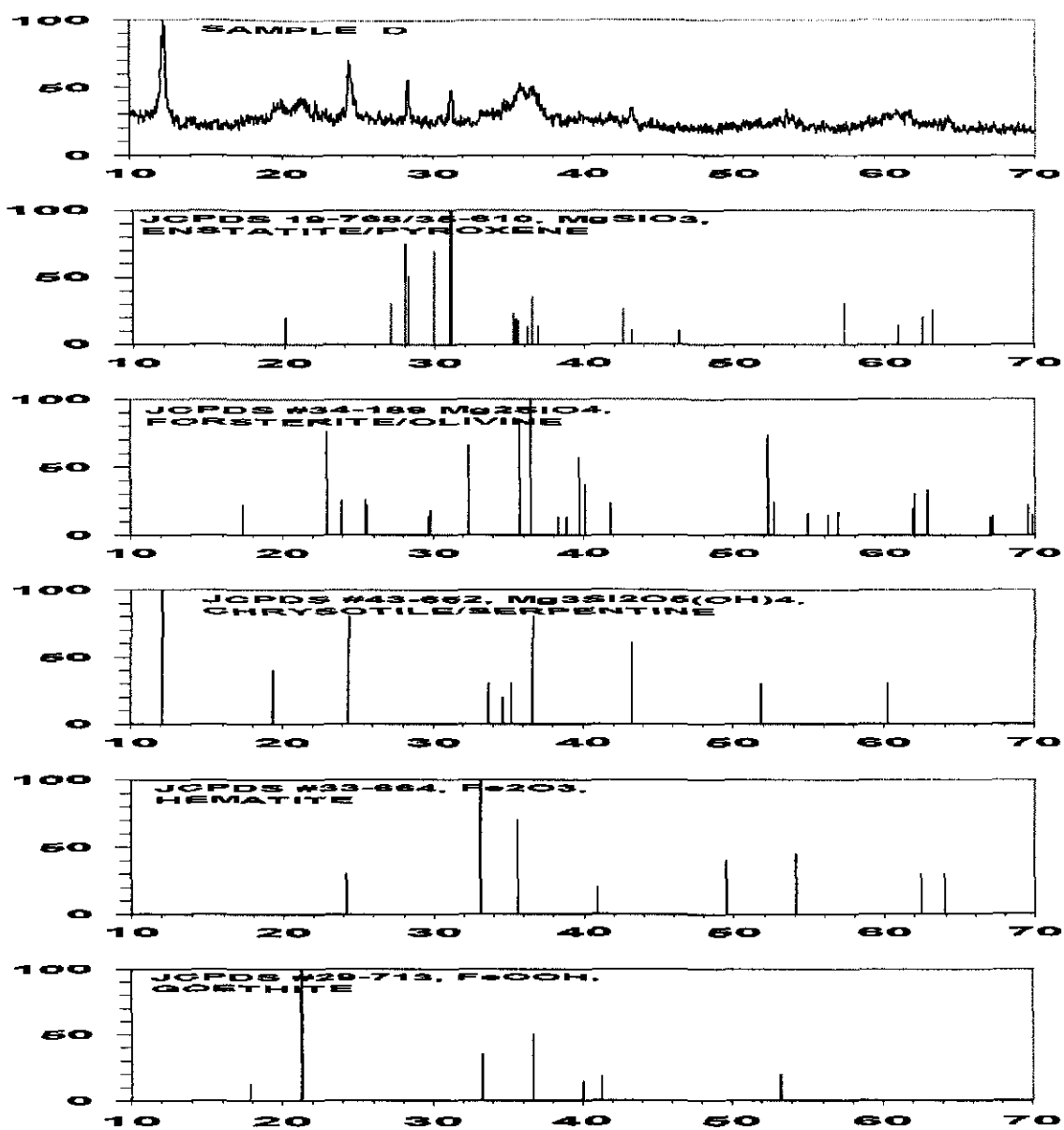


Fig. 5.2 XRD Patterns Of Sample D Before Calcination.+

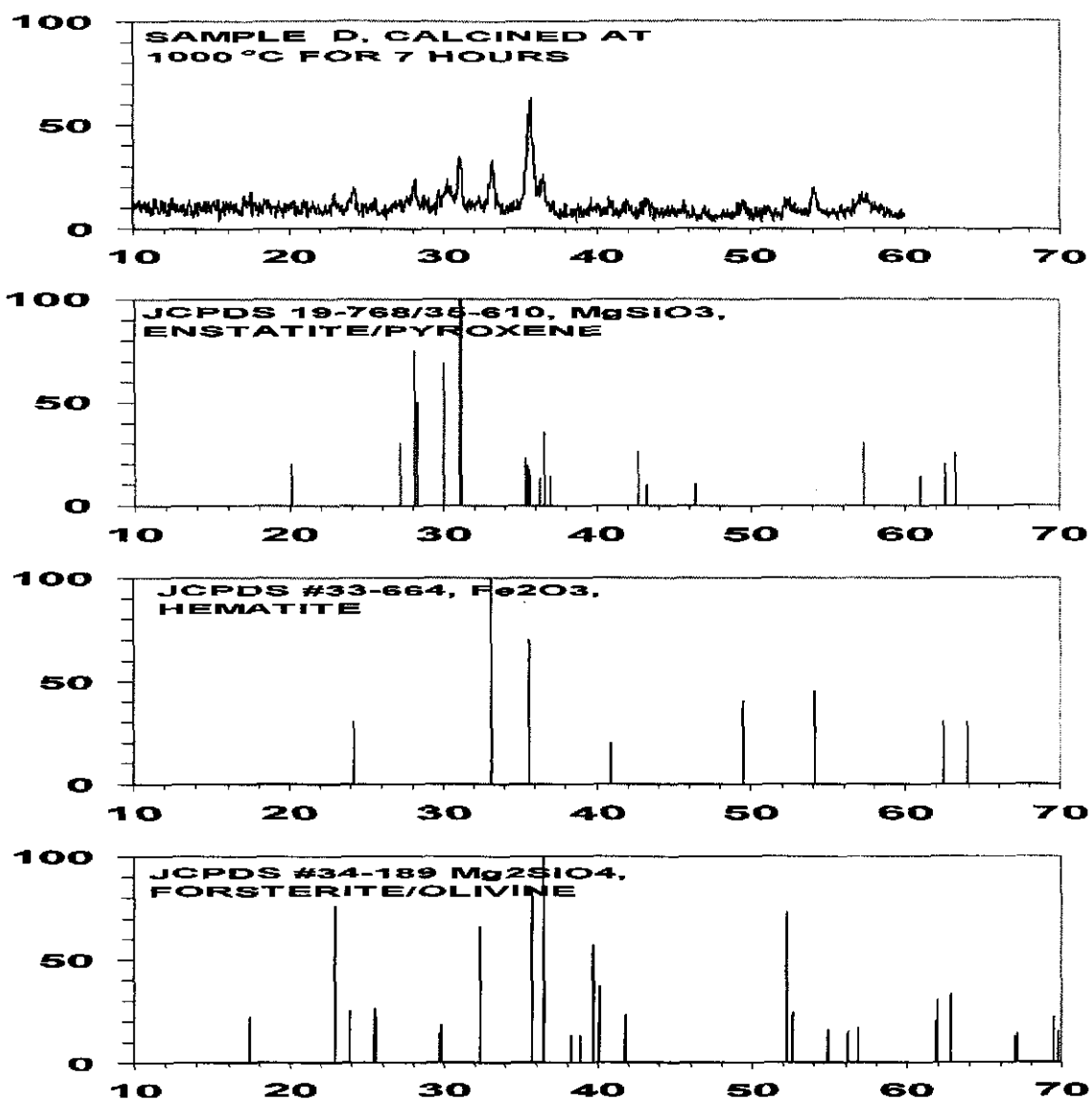
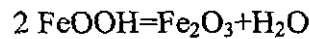


Fig. 5.3 XRD Patterns Of Sample D Calcined In Argon At 1000°C For 7 Hours

### 5.1.4 DTA/TGA Analysis

DTA(Differential thermal Analysis)/TGA(Thermogravimetric Analysis) conducted in air and in argon with Sample D were very similar. In Fig.5.4, three endothermic peaks, which correspond to three steps of dehydration, and one exothermic peak were detected. The first endotherm occurs at  $\sim 100^{\circ}\text{C}$ , which is due to moisture removal. The second endotherm at  $\sim 250^{\circ}\text{C}$  is ascribed to goethite decomposition<sup>[41][43]</sup>:



During this process, nickel which has been in solid solution with iron oxide in goethite structure  $[(\text{FeNi})\text{O}.\text{OH}.\text{nH}_2\text{O}]$  will be released and become reducible. Since this peak is not high, it can be inferred that there is not much goethite contained in the sample. This is consistent with XRD results.

The third endotherm at  $\sim 600^{\circ}\text{C}$  is due to removal of crystalline bound water from serpentine:



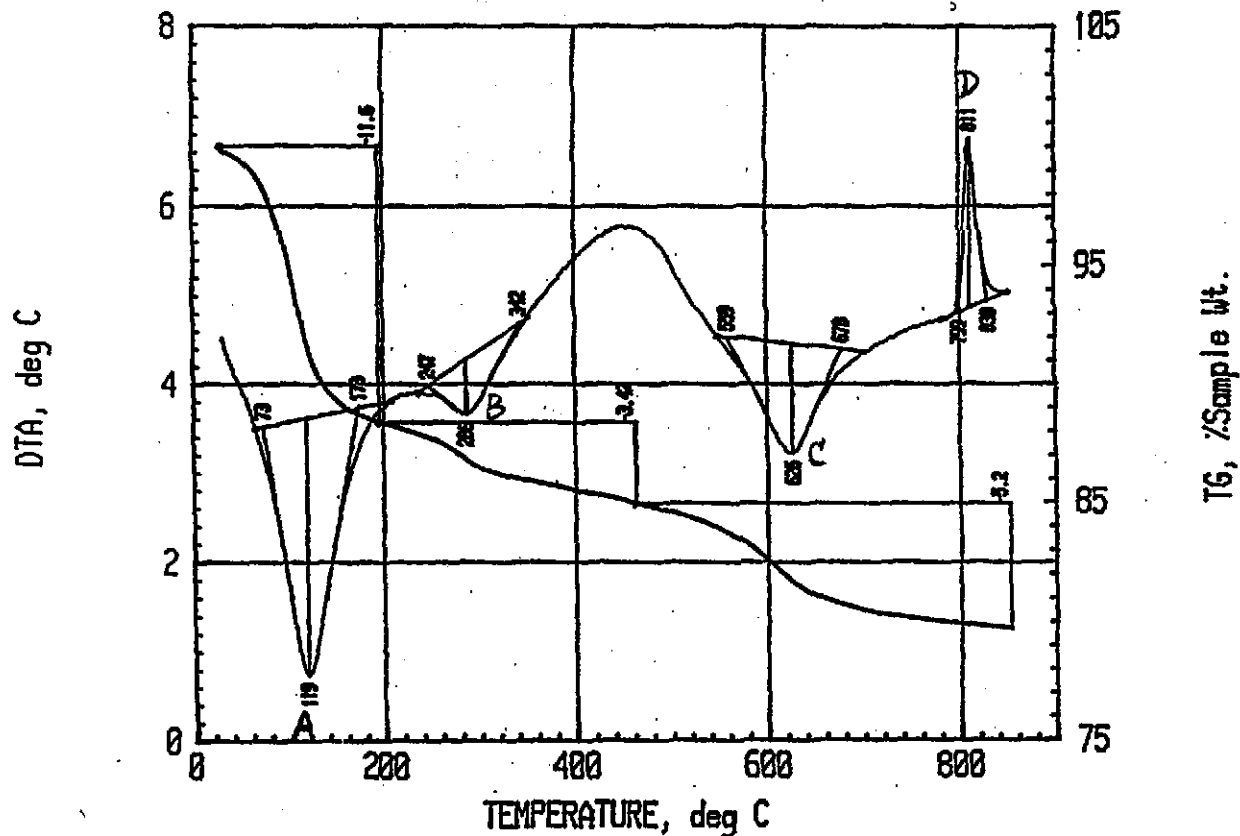
At this stage, the serpentine/chrysotile lattice is broken down and becomes an amorphous material. NiO is active and relatively easily reduced<sup>[26]</sup>. Although the third endothermic peak on the DTA curve is at  $626^{\circ}\text{C}$ , experiments showed that it is hard to expel all the water from laterite at temperatures below  $700^{\circ}\text{C}$ .

The exothermic peak is considered to be due to olivine or enstatite formation from the amorphous products of serpentine decomposition. At a temperature of about  $810^{\circ}\text{C}$ ,

the amorphous material will crystallise and NiO will be locked up in the enstatite or olivine. After this temperature, reduction of nickel will become difficult<sup>[27][32]-[36]</sup>.

Another DTA/TGA analysis was carried out in argon to look in depth at the serpentine component. In this analysis the sample was first heated up to 700°C, held there for 4 hours, and then the temperature was increased to 900°C, see Fig.5.5. Experiment showed that the exothermic peak was still prominent. This means that after serpentine dehydration, when temperature is below the critical value for olivine or enstatite formation, there was no significant amorphous material crystallised. According to Hayashi<sup>[33]</sup>, the serpentine material in this sample must be mainly composed of lizardite or chrysotile or a mixture of the two. Because if antigorite comprised the bulk of the serpentine in the ore, the dehydration and crystallization would take place simultaneously. In that case, after heating at 700°C for long time, the exothermic peak in the DTA curve would diminish considerably when temperature was subsequently increased to higher level.

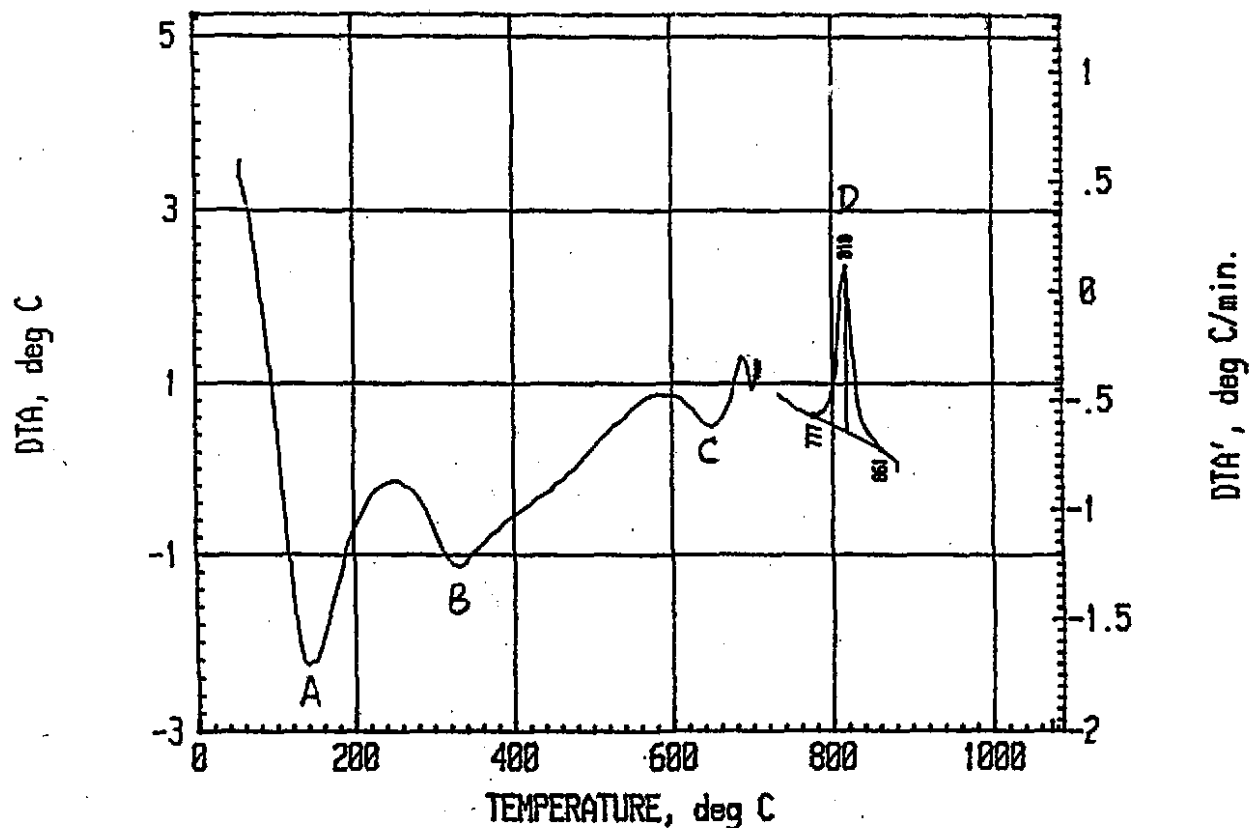
OPERATOR:	HFG	## NETZSCH STA ANALYSIS ##	ATMOSPHERE	AIR	
DATE:	31 Jan 1998	REFERENCE:	AI203	FLOW RATE, cc/min:	38
RUN No.	2	CRUCIBLE:	AL203	HEAT RATE, deg C/min:	18.8
SAMPLE No.	1	FILE NAME:	8-LI-D	SAMPLE Wt., mg:	133.4
SAMPLE NAME:	D	LOT No.	1	REFERENCE Wt., mg:	138.7



A: moisture removal; B: goethite decomposition; C: removal of crystalline bound water in serpentine; D: crystallization of enstatite or olivine

Fig. 5.4 DTA/TGA Curves Of Sample D Calcined In Air

OPERATOR:	HFG	** NETZSCH STA ANALYSIS **	ATMOSPHERE	ARGON	
DATE:	6 Mar 1998	REFERENCE:	AI203	FLOW RATE, cc/min:	100
RUN No.	1	CRUCIBLE:	AL203	HEAT RATE, deg C/min:	25.0
SAMPLE No.	0	FILE NAME:	0:LI-06	SAMPLE Wt., mg:	107.3
SAMPLE NAME:	D	LOT No.	1	REFERENCE Wt., mg:	105.4



A: moisture removal; B: goethite decomposition; C: removal of crystalline bound water in serpentine;  
D: crystallization of enstatite or olivine

Fig. 5.5 DTA/TGA Curves Of Sample D Calcined In Argon, Retained At 700°C For 4 Hours

## 5.2 Effect Of Calcination

### 5.2.1 Calcination Effect On Reduction And BET Analysis

On calcination at high temperature, porous solids may undergo sintering, swelling, softening or even cracking. These processes will change the pore size distribution, specific surface area and other physical characteristics of the pellet, therefore diffusion processes and the overall reduction rate can be affected considerably.

From the results shown in Fig.5.6, it can be seen that the calcination time, during which the sample was held at constant temperature before the reducing gas was introduced, can affect the reduction behavior of the serpentinic laterite samples(Sample D). The longer the calcination time, the slower the overall reduction rate, and the lower the final reduction extent.

To examine how calcination affects the structure parameters of the solid reactant, a series of BET (Brunauer-Emmett-Teller) analyses was carried out. The BET results are shown in Table 5.1.

BET analysis shows that when calcination time is longer and/or calcination temperature is higher, the specific surface area is smaller, the average pore radius for small pores(less than  $\sim 200 \text{ \AA}$ ) is larger, the total pore volume for small pores at  $P/P_0=0.95$  decreased at the same time. This is indicative of pore-sintering. Since measurement showed that for Sample D, when calcination time is longer or calcination temperature is higher, the pellet porosity is larger (see Section 6.4.1.3), it can be inferred that the macropore volume in the sample increased, although the overall surface area decreased.

However, the effect of calcination time is not as significant as calcination temperature. For instance, at 740°C, calcination for 90 minutes decreased BET surface area from 153.56 m<sup>2</sup>/g to 97.71 m<sup>2</sup>/g, while at 1000°C, calcination for 60 minutes reduced BET surface area from its original value to 24.09 m<sup>2</sup>/g.

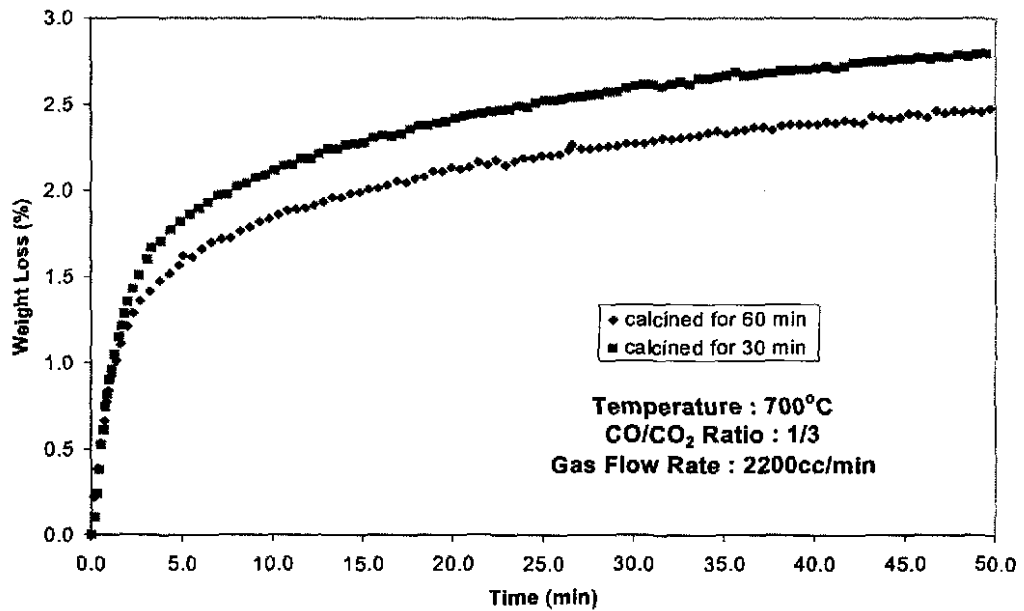


**Fig. 5.6 Effect of Calcination Time on Reduction Rate and Extent at 700°C for Serpentinic Sample D**

At a given temperature, calcination time for more than 60 minutes does not make much difference in the BET surface area and other structural parameters. This is especially true at higher temperatures. One example is calcination at 1000°C. At this temperature, calcination for 60 minutes and for 130 minutes resulted in a similar BET surface area. In fact, after water removal, BET surface area has already dropped to as small as 34.22 m<sup>2</sup>/g. So we can assume that after calcination for 1 hour, prior to

isothermal reduction, changes in the solid reactant structure will not affect the overall reduction rate. This assumption can greatly simplify the kinetic analysis and has been shown to be reasonable by experimental data (see Fig.5.7).

**Table 5.1 BET Results Of Calcined Pellets Of Sample D.**

Calcination temperature (°C)	Calcination time (min)	Multi-point BET surface area (m <sup>2</sup> /g)	For Pores Radius Less Than R(Å) at P/P <sub>0</sub>			
			R(Å)	P/P <sub>0</sub>	Total pore volume V (cm <sup>3</sup> /g)	Average pore radius (Å)
Origin		153.56	188	0.95	0.1786	23.26
700	60	113.44	-----	-----	-----	-----
740	60	103.16	-----	-----	-----	-----
740	90	97.71	-----	-----	-----	-----
770	30	89.77	-----	-----	-----	-----
770	60	86.38	-----	-----	-----	-----
770	90	75.35	-----	-----	-----	-----
850	30	49.87	-----	-----	-----	-----
850	60	42.21	-----	-----	-----	-----
850	90	42.15	-----	-----	-----	-----
930	60	32.15	-----	-----	-----	-----
1000	Just remove H <sub>2</sub> O	34.22	190	0.95	0.0976	57.047
1000	60	24.09	201	0.95	0.0705	58.85
1000	130	21.767	196	0.95	0.0635	58.38

Since at high temperature, after all moisture is removed, further calcination time does not appreciably affect the surface area of pellets of Sample D, the calcination time has little influence on reduction rate. As shown in Fig.5.7, at 1000°C for two samples calcined for 25 minutes and 60 minutes respectively, reduction behaviour is almost the same.

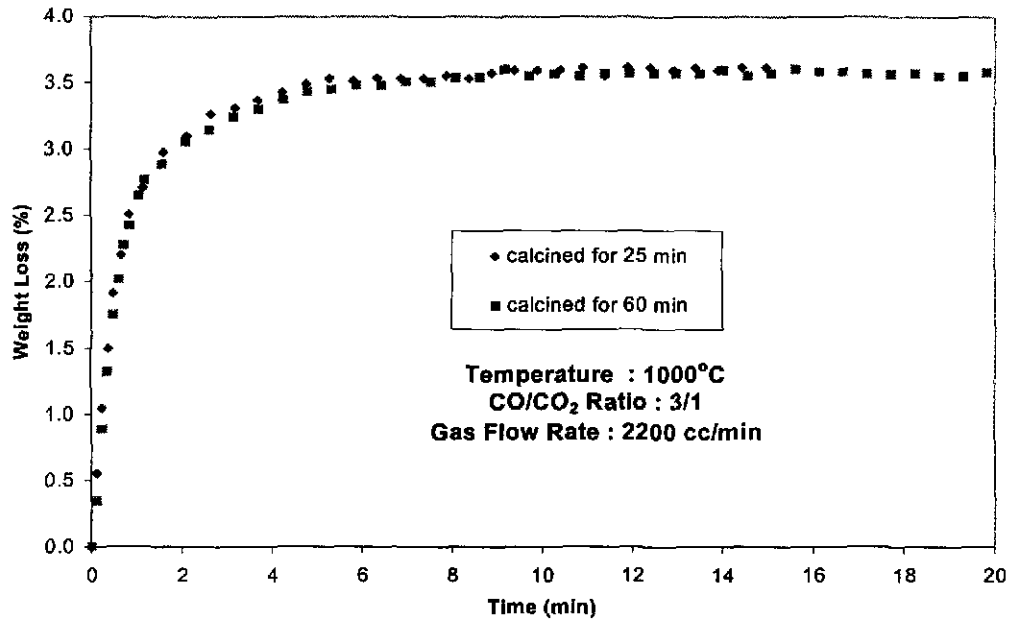


**Fig. 5.7 Effect of Calcination Time on Reduction Rate and Extent at 1000°C**

BET results showed that at lower temperatures, the calcination time has a relatively stronger effect on specific surface area of the solid reactant. Longer calcination times will give a smaller surface area and fewer sites for gas-solid reactions. This may result in the decrease in overall reduction rate shown in Fig.5.6. The difference in reduction extent, however, is believed to be caused by a phase change after calcination. This is discussed in detail in Section 5.5 and Section 5.6. It was suspected here that there may be some antigorite in this laterite, and at temperatures below 810°C, longer calcination time allows more antigorite to crystallise and hence more nickel/iron is tied up giving a lower reduction extent. At higher temperatures, antigorite and other

serpentine minerals decompose and crystallise more rapidly, the decomposition and crystallization process appears to be finished after calcination for more than 30 minutes, hence calcination time longer than 30 minutes makes little difference in solid mineral composition. Therefore reduction extent is nearly the same in Fig.5.7. However, as antigorite is not a significant part of the bulk of the serpentine, this explanation does not seem to be convincing.

Further study showed that the major reason for the difference in reduction extent in Fig.5.6 may be that the reducing atmosphere favours olivine and enstatite formation. Details will be discussed in Section 5.4.2. If reduction proceeds at a lower rate, there will be more time for olivine and enstatite to form, this will give a lower final reduction extent. In Fig.5.6, since the sample calcined for 60 minutes had a smaller BET surface area, it was reduced at slower rate, therefore more olivine and enstatite was formed during the reduction process, more  $\text{Ni}^{2+}$  and  $\text{Fe}^{2+}$  were tied up and became unreducible, therefore it gave a lower reduction extent.

### **5.2.2 X-Ray Diffraction Study On Samples Calcined at Varied Conditions**

Samples calcined at different temperatures for different times were subjected to XRD analysis. The calcination conditions were: 700°C for 4 hours, 740°C for 1 hour, 740°C for 4 hours and 1000°C for 1 hour. XRD patterns are shown in Fig.5.8. Combined with the XRD patterns of the original sample and the sample calcined at 1000°C for 7 hours (Fig.5.1 and Fig.5.2), the following observations may be made:

- 1) After calcination at above 700°C, the serpentine/chrysotile in Sample D was diminished, while the content of forsterite/olivine and enstatite/pyroxene were increased. This indicates that calcination resulted in the decomposition of serpentine/chrysotile and the formation of forsterite/olivine and enstatite/pyroxene.
- 2) After calcination, goethite was decomposed to form hematite.
- 3) Even when samples were calcined below 810°C, which is the critical temperature obtained by DTA for crystallization of lizardite and chrysotile, formation of olivine/forsterite and enstatite/pyroxene occurred. This may be evidence of antigorite existence in sample D.
- 4) The amount of crystallized olivine/forsterite and enstatite/pyroxene increased with increasing calcination temperature and calcination time.

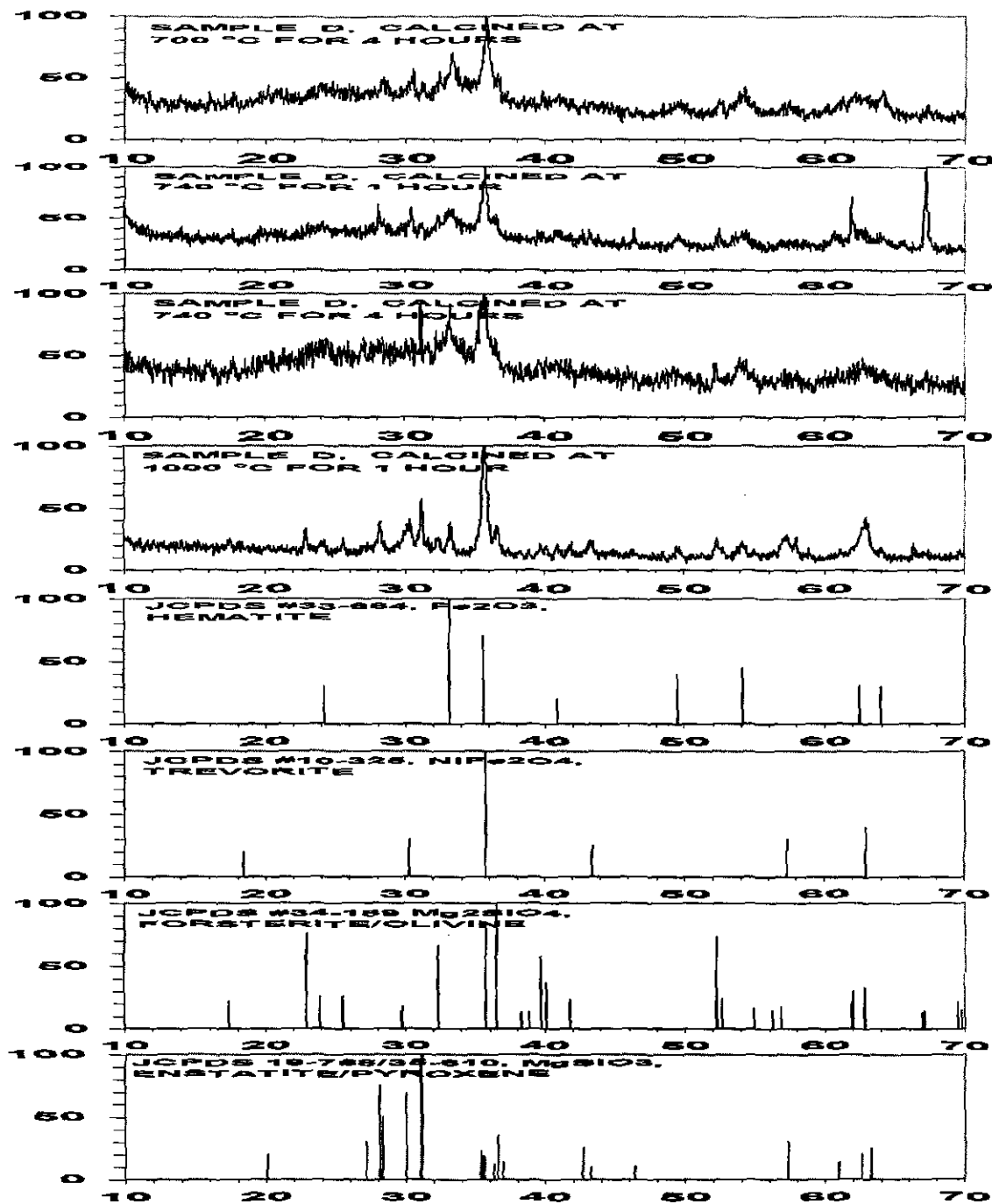


Fig. 5.8 XRD Patterns Of Sample D Calcined In Argon Under the Conditions

### 5.3 Effect of Reducing Gas Flow Rate

This series of experiments was done to determine the appropriate gas flow rate that can be used to avoid mass transfer control in kinetic experiments.

In the case of solid-gas reactions, if the gas flow rate is too low at a given temperature, the resistance to mass transfer from the bulk gas phase to the solid pellet through the boundary layer will be too large. The reduction process will then be controlled by gas phase mass transfer. When the gas flow rate is increased, the boundary layer will become thinner, so the overall reduction will become faster and, eventually, when the gas flow rate is large enough, the rate will be controlled by gas diffusion within the pellet or by chemical reaction at the gas/solid interface, hence the overall reduction rate will not change with further increase in the gas flow rate. This trend can be seen in Fig.5.9. The experimental data obtained with sufficiently large gas flow rates can then be subjected to appropriate kinetic analysis to determine kinetic parameters, which is one of the major long term goals of this study.

Because mass transfer control is usually maximized at high temperature, this series of experiments were carried out at 1000°C, the highest temperature to be used in this study. To compare the reduction rates more accurately, only the reduction data in the first a few minutes were shown in Fig.5.9 and Fig.5.10. The specific weight loss rate  $R$  was also included. The method used to determine specific weight loss rate  $R$  has been described in Chapter 3.

The experiments with  $\text{CO}/\text{CO}_2=7.0$  showed a flow rate of 1700 cc/min is large enough to eliminate mass transfer control effect (Fig.5.9). Whereas the experiments using gas mixture of  $\text{CO}/\text{CO}_2=1/3$  (Fig.5.10) showed gas flow rate of 2200 cc/min may be necessary. Therefore 2200 cc/min was selected as the required flow rate to proceed with the subsequent series of experiments.

In the range of flow rates used in Fig.5.9 and Fig.5.10, the reducing gas flow rate did not affect reduction extent (this can not be seen in the figures, because of the time-axis scales). This can be simply attributed to the same reducing power. However, in additional experiments when gas flow rate was much lower than the critical value to avoid mass transfer control, both reduction rate and reduction extent were affected. The lower gas flow rate resulted in not only a lower reduction rate, but also a lower reduction extent, see Fig.5.11. This is believed to be because of the faster and further crystallization of olivine and/or enstatite under reducing conditions, as was found in the case of decreased reacting surface (Fig.5.6). A detailed discussion of this phenomenon will be given in the next section.

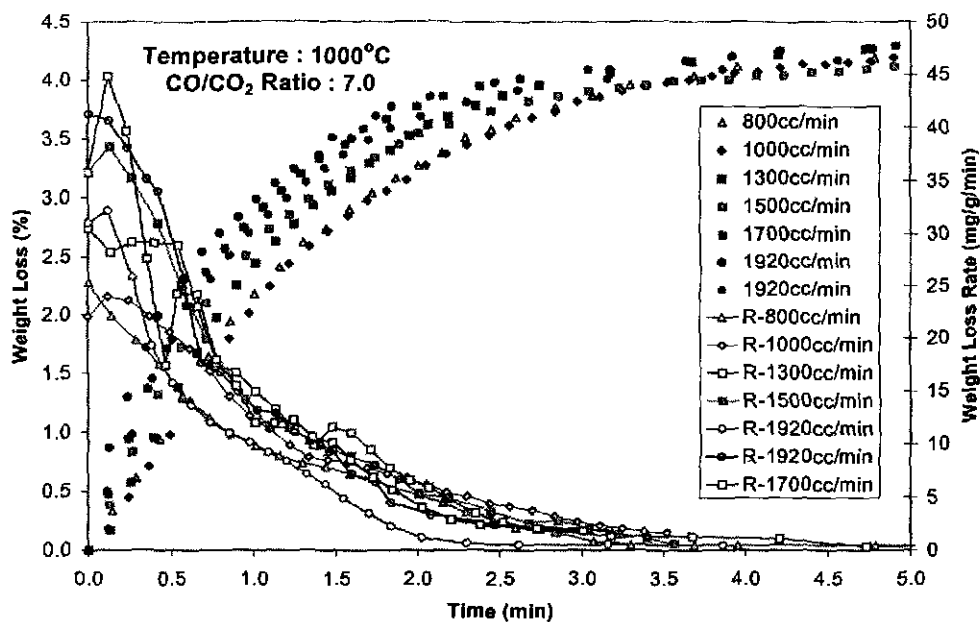


Fig. 5.9 Effect of Reducing Gas Flow Rate With  $\text{CO}/\text{CO}_2=7.0$

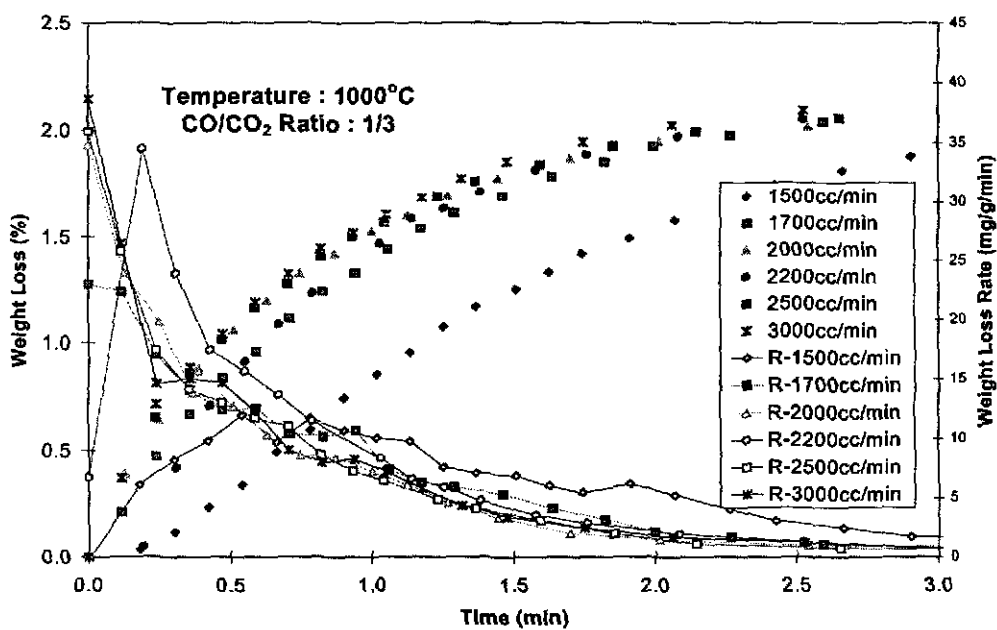
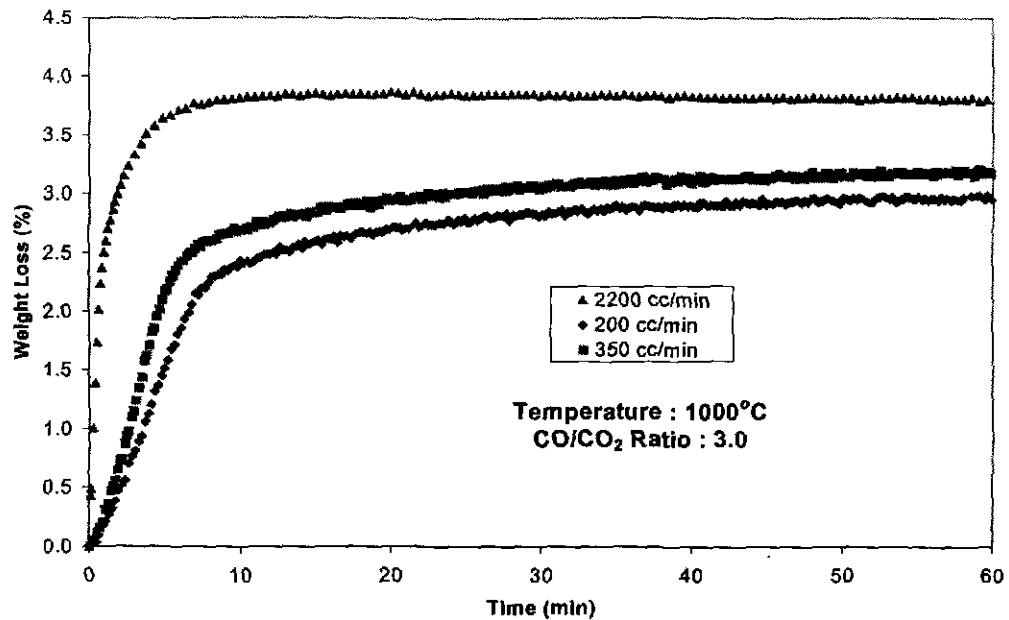


Fig. 5.10 Effect of Reducing Gas Flow Rate With  $\text{CO}/\text{CO}_2=1/3$



**Fig. 5.11 When Gas Flow Rate Is Too Small, Both Reduction Rate and Reduction Extent Will Be Affected**

## 5.4 Investigation of Reduction Mechanism

### 5.4.1 Reduction Mode

Partially reduced samples were sectioned radially and photographed under an optical microscope. Even with the naked eye, the different appearance between the reduced shell and unreduced core could be observed clearly. See Photo 5.1. This indicates that the reduction process follows a shrinking core mode during the early stages of reduction. This conclusion has been confirmed later (Section 5.4.2) by XRD analysis of the outer shell and the core of a pellet reduced for less than half a minute.

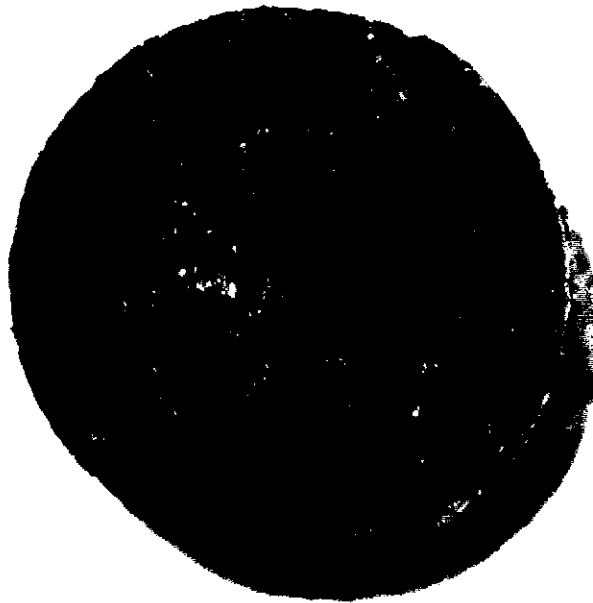


**Photo 5.1 Partially Reduced Sample Demonstrates a Shrinking Core Mode**  
(Reduced for 10 seconds at 740°C with  $\text{CO}/\text{CO}_2=1.0$ )

To determine how long the first reduction stage lasts, and to see how the reduction proceeds subsequently, experiments were carried out with different sized pellets.

The basic idea underlying this experiment is, if reduction takes place only at the interface between unreacted core and reacted shell, type I in Fig.5.12, then for a cylindrical pellet the specific weight loss rate,  $R$ , which is defined as weight loss per unit of pellet mass and per unit of time, is inversely proportional to the pellet radius. This

situation would happen if gas diffusion through unreacted solid is extremely slow, or if chemical reaction was very much faster than diffusion through the reacted shell.

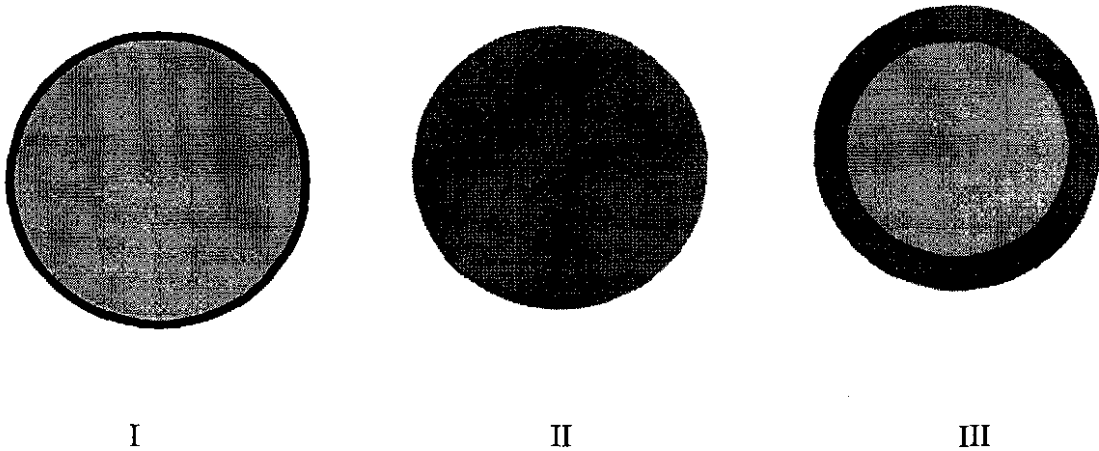


**Fig. 5.12 Schematic Figure of Different Reduction Modes of Cylindrical Pellets**

In the situation I:

$$R = \frac{k \cdot 2\pi r_p L \cdot C_{int} M_o}{r_p^2 \pi L \cdot \rho_{app}} = \frac{2k C_{int} M_o}{\rho_{app}} \cdot \frac{1}{r_p}$$

That is:

$$R \propto \frac{1}{r_p}$$

Where:

R: the specific weight loss rate of pellet sample, (g/g /sec).

k: reaction rate constant, (cm/s).

$r_p$ : the initial radius of the pellet, (cm).

L: the length of the pellet, (cm).

$C_{\text{intf}}$ : the gas reactant concentration at gas-solid reaction interface,(mole/cm<sup>3</sup>).

$M_o$ : the mole mass of [O], (=15.999g/mole).

$\rho_{\text{app}}$ : the apparent density of the pellet, (g/cm<sup>3</sup>).

In the situation II, if gas diffusion through the pellet provides negligible resistance, and chemical reaction or diffusion in the individual grains is relatively slow, the reaction will proceed uniformly through the pellet, then the specific weight loss is independent of pellet radius:

$$R = \frac{k \cdot \pi r_p^2 L \cdot S \cdot C_{\text{unif}} M_o}{r_p^2 \pi L \cdot \rho_{\text{app}}} = \frac{k \cdot S \cdot C_{\text{unif}} M_o}{\rho_{\text{app}}}$$

Where:

$S$ : surface area measured by BET, (cm<sup>2</sup>/g).

$C_{\text{unif}}$ : the uniform concentration of gas reactant within the solid pellet,(mole/cm<sup>3</sup>).

In the situation III, if gas diffusion through solid reactant and chemical reaction jointly controls the reduction process, the reaction will be confined within a certain width of pellet and a reaction band will be formed. In this case, if the pellet size is large compared with the reaction band width, the band width can be taken as the same for different size pellets under same reaction condition, then the relationship between the specific weight loss rate and the width of the reaction band  $\delta$  is as below:

$$R = \frac{\left[ r_p^2 \cdot \pi - (r_p - \delta)^2 \cdot \pi \right] L \cdot \rho_{\text{app}} \cdot S \cdot k \cdot C_{\text{av}} \cdot M_o}{r_p^2 \cdot \pi \cdot L \cdot \rho_{\text{app}}} = \frac{(2 \cdot r_p \cdot \delta - \delta^2) \cdot S \cdot k \cdot C_{\text{av}} \cdot M_o}{r_p^2}$$

Where:

$\delta$ : the width of the reaction band, (cm).

$C_{av}$ : the average concentration of gas reactant within the reaction area,(mole/cm<sup>3</sup>).

The above equation is equivalent to:

$$R.r_p^2 = 2.M_o.S.k.C_{av}.\delta.r_p - M_o.S.k.C_{av}.\delta^2$$

Then it can be seen there is a linear relationship between  $R.r_p^2$  and  $r_p$ .

The experiment results for different sizes of pellets at 770°C are shown in Fig.5.13. Again the specific weight loss rates are included. It can be observed here that the larger the pellet radius, the slower the initial specific weight loss rate. The difference in the initial specific weight loss rate means the reduction at the first stage did not proceed uniformly within the pellet. This situation lasts for about one minute, after which, the specific weight loss rates follow approximately the same curve and the reduction can then be assumed to proceed roughly uniformly within the pellets used in this experiment. This is consistent with the relatively uniform appearance of the pellet cross-section when observed after 1 minute reduction.

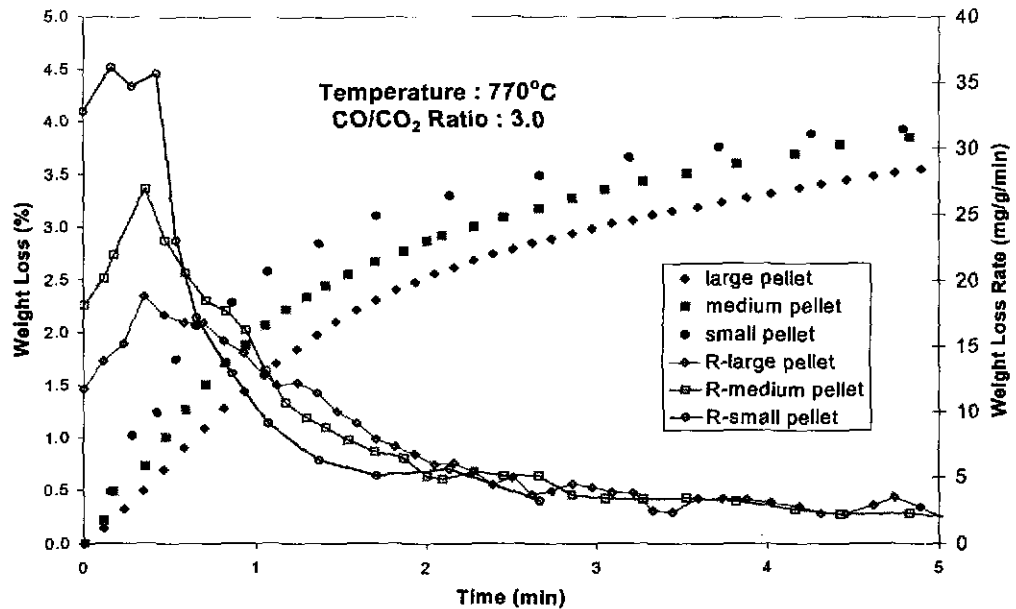


**Fig. 5.13 Reduction With Different Size Pellets**

However, at the second stage, the reduction does not proceed in a way that can be described by the generally accepted model for uniform internal reduction, in which, for the first order reaction<sup>[43]</sup>:

$$-\ln(1-X)=kt$$

Where:

X: reaction fraction of solid.

k: reaction constant, cm/s.

t: time, sec.

On attempting to apply the above model, we did not get good agreement with the experimental data for the second reduction stage. It is perhaps not surprising that this model did not fit the experimental data, as one of the fundamental assumptions of the

model is that reacting surface area decreases in proportion to the fraction reacted. In the present case the reacting surface should remain relatively constant throughout the reaction.

At other temperatures, similar experiments were carried out. The results are shown in Table 5.2. By examining the relationship between the initial specific weight loss rate and pellet radius at different temperatures, it is found that they are not inversely proportional, instead,  $R.r_p^2$  is an approximately linear function of  $r_p$ , see Fig.5.14. Therefore, we can say that in this study, the first stage of laterite pellet reduction was under mixed control of gas diffusion through the porous solid matrix and chemical reaction. While at later stages, reduction proceeded almost uniformly within the pellet.

**Table 5.2 Initial Specific Weight Loss Rate When Different Sizes Of Pellets Are Reduced At Different Temperatures**

Radius of small pellet=1.575mm, medium pellet=3.125mm, large pellet=4.725mm (CO/CO <sub>2</sub> =3.0)						
Temperature (°C)	700	740	770	850	930	1000
R of Small pellet (mg/g/min)	30.37	32.14	36.15	52.80	62.99	72.65
R of medium pellet (mg/g/min)	21.07	24.53	27.06	37.21	46.73	52.70
R of large pellet (mg/g/min)	13.17	15.62	19.10	24.85	27.50	31.22

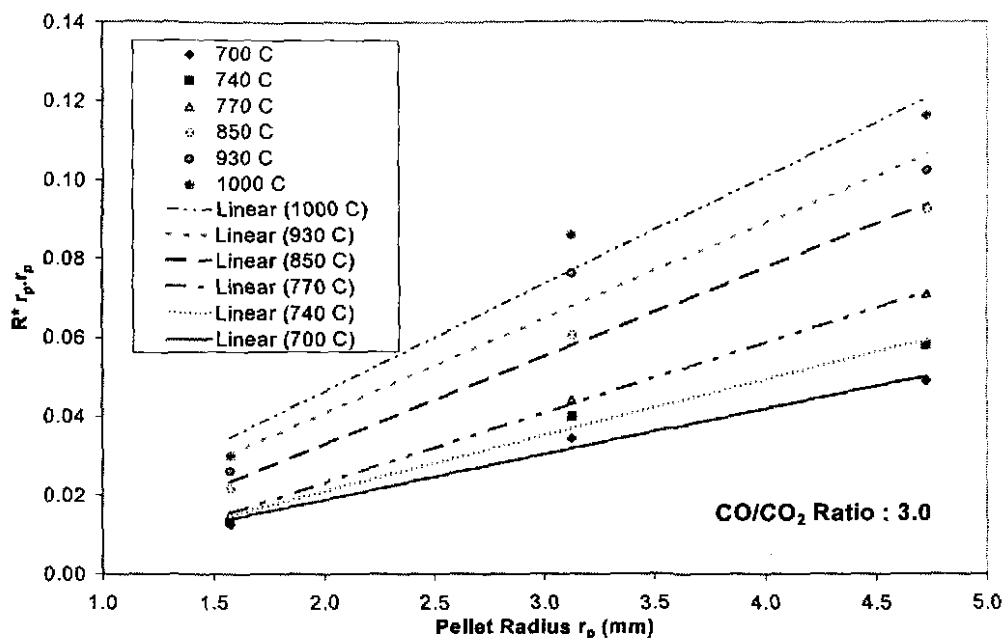


**Fig. 5.14 Relationship Between Pellet Radius ( $r_p$ ) and Initial Specific Weight Loss Rate ( $R$ )**

## 5.4.2 Mineral Phase Change During the Reduction Process

Samples reduced under a range of conditions, including some that were partially reduced and taken from both the outer shell and the core of the individual pellets, were analysed by X-Ray Diffraction. The XRD patterns are shown in Fig.5.15 to Fig.5.17.

By comparing partially and completely reduced samples with calcined samples, (Fig.5.8, Fig.5.15), it is found:

- 1) Since magnetite or spinel was present as the major phase in partially reduced samples, it then can be inferred that when calcined, goethite decomposed into

hematite and when reduced, it yielded magnetite or spinel first, then produced metallic phases thereafter.

- 2) Compared with calcination, reducing samples for a few minutes gave a considerable increase in the amount of olivine/forsterite and enstatite/pyroxene. This increase is larger than the increase when the same ore, Sample D, was subjected to calcination for several hours. About one hour reduction process (complete reduction) also resulted in a considerable increase in the amount of high temperature phases compared with partial reduction. This increase was not found in the calcination experiments. Therefore it appears that reducing conditions favour the formation of olivine/forsterite and enstatite/pyroxene in two ways. First, reducing conditions accelerate the formation of the high temperature phases. Second, reducing conditions cause the crystallization to proceed to a greater extent.
- 3) In completely reduced samples, metallic phases were present either as kamacite, or as taenite(both are Ni-Fe alloy). Magnetite or spinel may still remain. Unlike the results of chemical analysis, which showed there is a noticeable content of metallic product in partially reduced samples, no noticeable metallic phase was detected by XRD in partially reduced pellets. This may be because the metallic content is too small for XRD analysis, or be due to the easy reoxidation of the newly produced metallic phase.

By comparing XRD patterns of the shell and the core of partially reduced samples in Fig.5.16 and Fig.5.17, the following are observed:

- 1) In both parts no metallic phase was detected. For the shell, this, again, may be because of the reoxidation of newly produced metal alloy when XRD was carried out, or because metallic content was below the lower detectable limitation for XRD analysis. For the core, there may have been no reduction to metal.
- 2) The XRD patterns of the core are similar to unreduced calcined pellet, while the shell shows the characteristics of partially reduced material. This supports the conclusion of microscopic study that in the initial reduction stages, the reduction follows a shrinking core mode.
- 3) Even after about 10 seconds reduction, XRD showed that there was more olivine/forsterite and enstatite/pyroxene in the shell. Therefore the reducing atmosphere appears to help the crystallisation of olivine and enstatite.

The XRD study of Sample D at different stages of the reduction process is summarised in Table 5.3.

**Table 5.3 Mineral Phase Composition Of Laterite At Different Reduction Stages**

Reduction Stage	Identified Phase (in decreasing order of abundance)
Original ore	Serpentine/chrysotile + enstatite/pyroxene + goethite + hematite +forsterite/olivine
Calcined (700°C~1000 °C)	Hematite+ enstatite /pyroxene +forsterite/olivine + magnetite/spinel
Partially reduced (700°C~1000 °C)	Olivine/forsterite + magnetite/spinel+ enstatite/pyroxene
Completely reduced (700°C~1000 °C)	Olivine/forsterite+ enstatite/pyroxene + metallics + magnetite/spinel

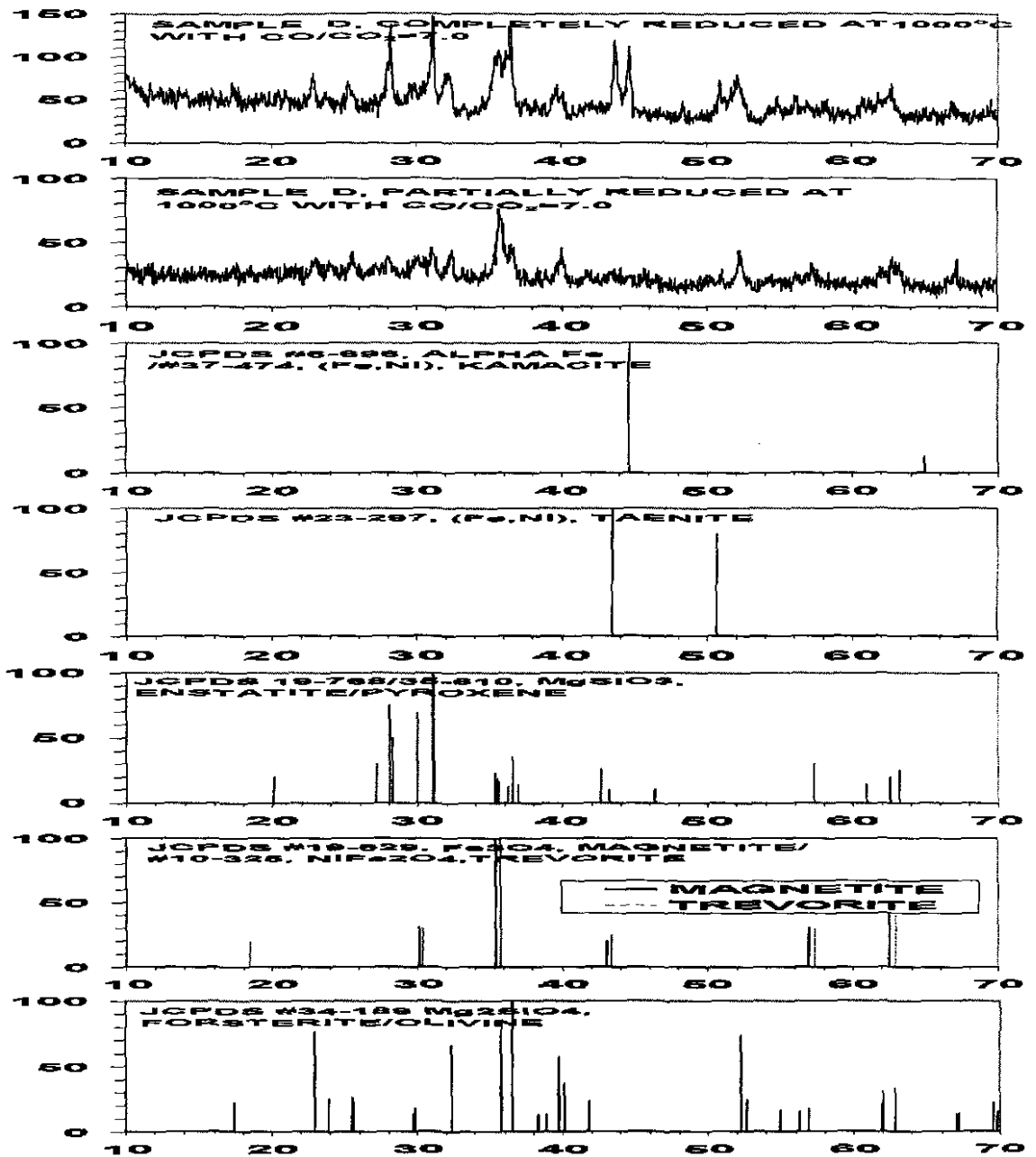


Fig. 5.15 XRD Patterns Of Samples Partially Reduced For 2 Minutes And Completely Reduced At 1000°C With CO/CO<sub>2</sub>=7.0

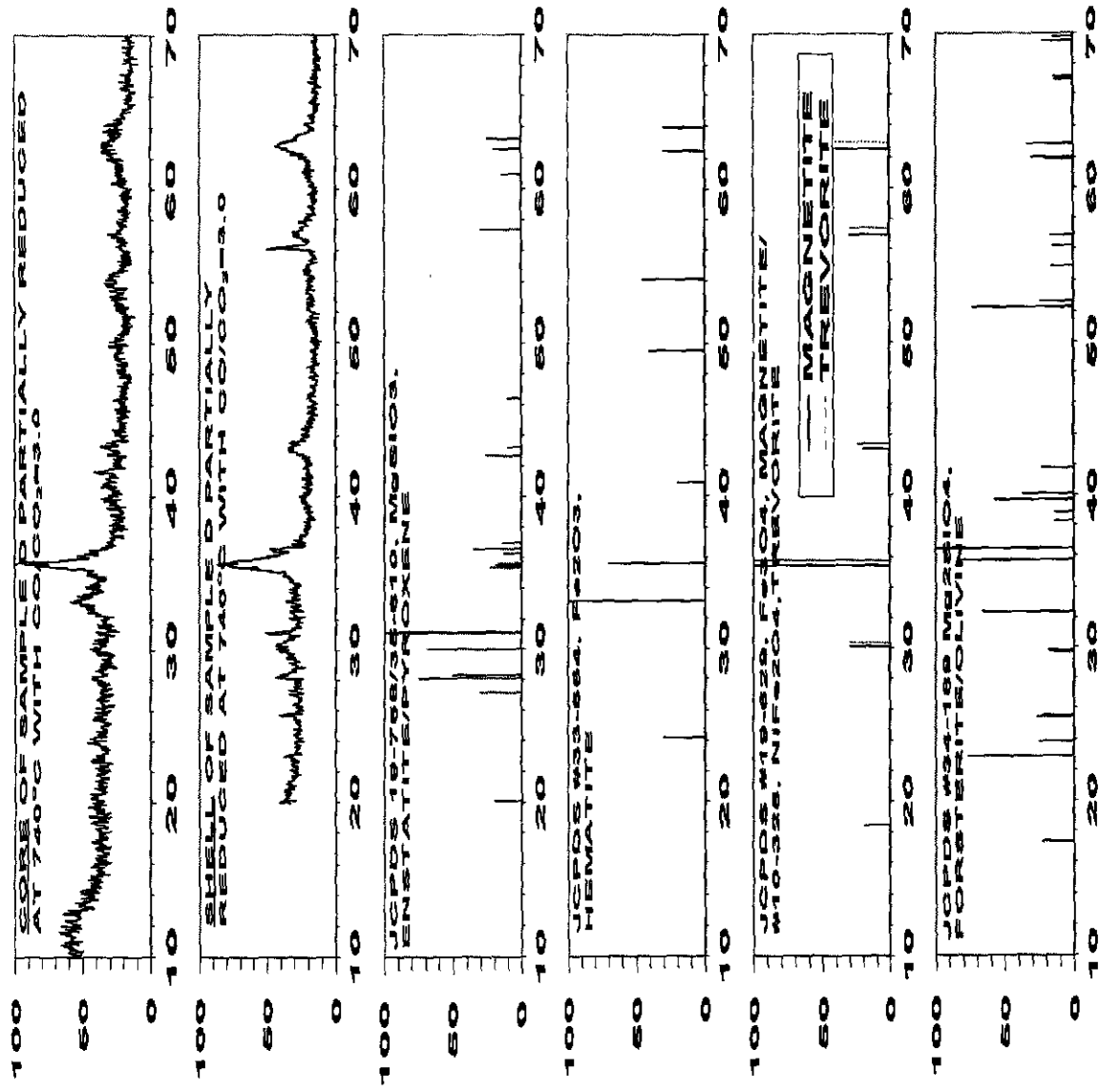


Fig. 5.16 XRD Patterns Of The Shell And The Core Part Of Samples Partially Reduced At 740°C With  $\text{CO}/\text{CO}_2=3.0$  For 10 Seconds

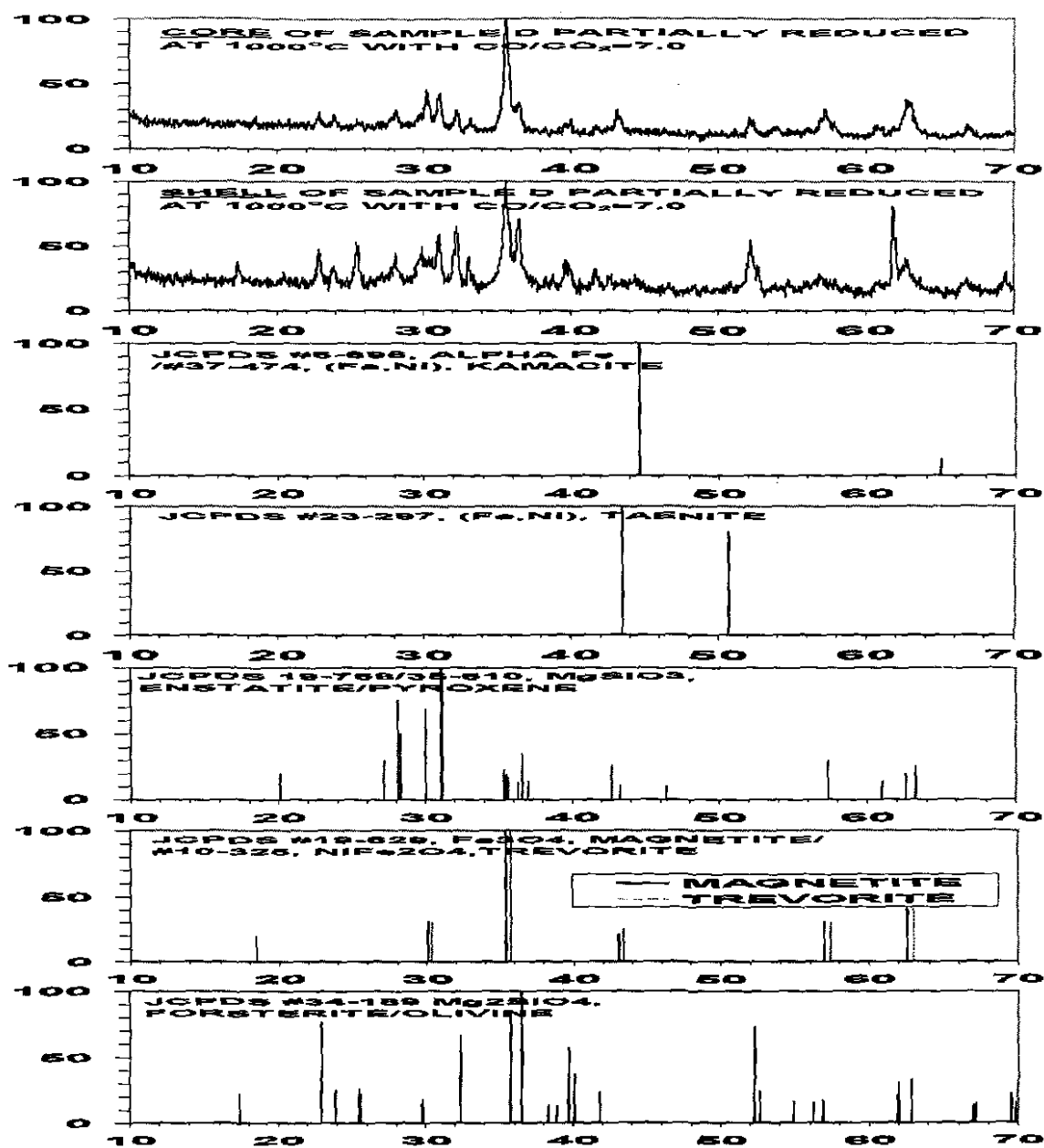


Fig. 5.17 XRD Patterns Of The Shell And The Core Part Of Samples Partially Reduced At 1000°C With CO/CO<sub>2</sub>=7.0 For 10 Seconds

## 5.5 Reduction Temperature and Gas Composition

For a given temperature, an increase in the CO/CO<sub>2</sub> ratio will give a stronger reducing force, this will increase the equilibrium reduction extent. At the same time, increase in the CO/CO<sub>2</sub> ratio will give a higher partial pressure of carbon monoxide in the reducing gas, therefore, assuming that the reaction rate is proportional to  $(P_{CO})^n$ , (here  $P_{CO}$  is partial pressure of carbon monoxide,  $n$  is the reaction order with respect to CO), the overall reduction rate will increase. Experimental results at 740°C and 1000°C with varied reducing gas composition are shown in Fig.5.18 and Fig.5.19.

Fig.5.20~Fig.5.22 show the results of reduction at different temperatures with three fixed gas compositions, i.e. CO/CO<sub>2</sub> ratios of 1/3, 1.0, and 3.0 respectively. At a given CO/CO<sub>2</sub> ratio, when temperature is higher, the overall reduction rate is faster. At higher temperatures there is a mineral phase change which is believed to hamper laterite reduction, higher temperature calcination also gives lower BET specific surface area, however the exponential effect of temperature on the reaction rate constant seems to be dominant.

When temperature increases with fixed CO/CO<sub>2</sub> ratios, the reduction extent generally decreases, but when the temperature is below 700°C, for example at 600°C in Fig.5.20, the reduction extent is also low. Two reasons may account for this phenomenon. One is that at low temperature serpentine does not completely decompose after 60 minutes calcination. In this case, serpentine will not be so easy to reduce, because the remaining crystalline water will affect deleteriously the laterite reduction. The need to

remove chemically bound water in order to improve nickel extraction was documented by Kukura<sup>[37]</sup>.

From Fig.5.20 to Fig.5.22, it is shown that reduction extent is maximized at 720°C ~740°C, which is the temperature between serpentine/chrysotile decomposition and olivine or enstatite crystallization. A superficial analysis may lead to the conclusion that it is the high reducibility of solid materials in this temperature range gives the high reduction extent, but at lower temperatures the reducing power of a gas with fixed CO/CO<sub>2</sub> ratio is higher than at elevated temperatures, and based on another series of experiments (Fig.5.23), it is found that higher reducing power also contributed to the high reduction extent at 720°C ~740°C.

In the series of experiments mentioned above, samples were reduced at different temperatures using gas mixtures of different CO/CO<sub>2</sub> ratios but with the same equilibrium oxygen partial pressure. The results, see Fig.5.23, showed that the reduction extent increased with increase in temperature in this situation. DTA and other studies<sup>[32]</sup>-<sup>[36]</sup> have shown that at high temperature olivine or enstatite have already been formed prior to reduction. Normally they are difficult to reduce, but when the temperature is higher, they become less stable. With sufficient reducing power, a high reduction extent can still be achieved. In Chapter 4, thermodynamic calculations have shown the same tendency. Therefore, the formation of the high temperature phases does not necessarily decrease the reduction extent. To achieve high reduction extent at high temperature, a reducing gas much richer in reductant is needed, but with higher reduction extents at

Chapter 4, Fig.4.6). Preceding arguments notwithstanding the mineral phase of laterite after calcination still affects the reduction behaviour. To clarify this, two series of experiments were carried out, the results of which are shown in Fig.5.24, and Fig.5.25. In Fig.5.24, two samples were both reduced at 700°C. However, one of them was calcined at 700°C while the other at 740°C. Both of them were calcined below the critical temperature for serpentine-olivine transformation in the hope of not causing much difference in mineral phases prior to reduction. The final reduction extents turned out to be nearly the same.

In Fig.5.25, three samples were all reduced at 740°C, but were calcined at different temperatures. Samples calcined at 850°C and 1000°C, which are both above the critical temperature for serpentine-olivine transformation and thus can be considered have the same mineral phases before reduction, yielded the final reduction extents with little difference between them, but much lower compared to the sample calcined at 740°C, which would be much different in mineral composition compared with the former two.

Calcination experiments showed that for Sample D, even after calcination for 1 hour at some temperatures below 810°C, when the temperature was further increased to above 810 °C, there would be about 0.35% additional weight loss (see Fig.5.26). This may be caused by further removal of crystalline water or by the increase of buoyant force of gas stream when the temperature is higher. This small percentage, however, can not account for the difference in reduction extent between the sample calcined and reduced at 740°C and the samples calcined at 1000°C or 850°C shown in Fig.5.25.

Although different calcination conditions can result in different BET surface areas and hence different reduction rates which, can lead to different final reduction extents, the effect of mineral composition before reduction is still apparent in the above two groups of experiments. In Fig.5.25. the samples calcined at 1000°C and 850°C would be expected have very similar mineral compositions before reduction. Here the mineral phase must have played an important role. This may be considered strong evidence for the deleterious effect of olivine or enstatite on laterite reducibility. Therefore, after decomposition of serpentine and before crystallization of olivine and enstatite, laterite is at its most reducible.

Considering the data plotted in Fig.5.24, there is not much difference in the mineral phases present in the two samples before reduction. The sample calcined at 740°C has a smaller BET surface area, so its reduction rate was lower giving more time for formation of high temperature phases, therefore a lower reduction extent would be expected. However, as can be seen in Fig.5.24, the reduction extent is a little bit higher at 740 °C than at 700°C. This may be because of the incomplete decomposition of serpentine in the latter case.

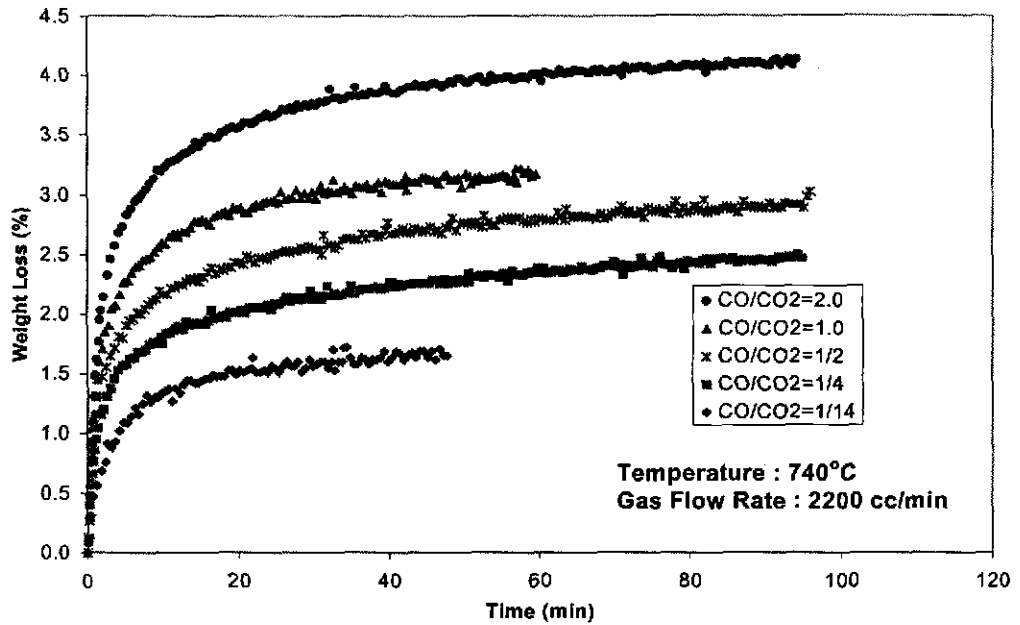


Fig. 5.18 Effect of Reducing Gas Composition at 740°C

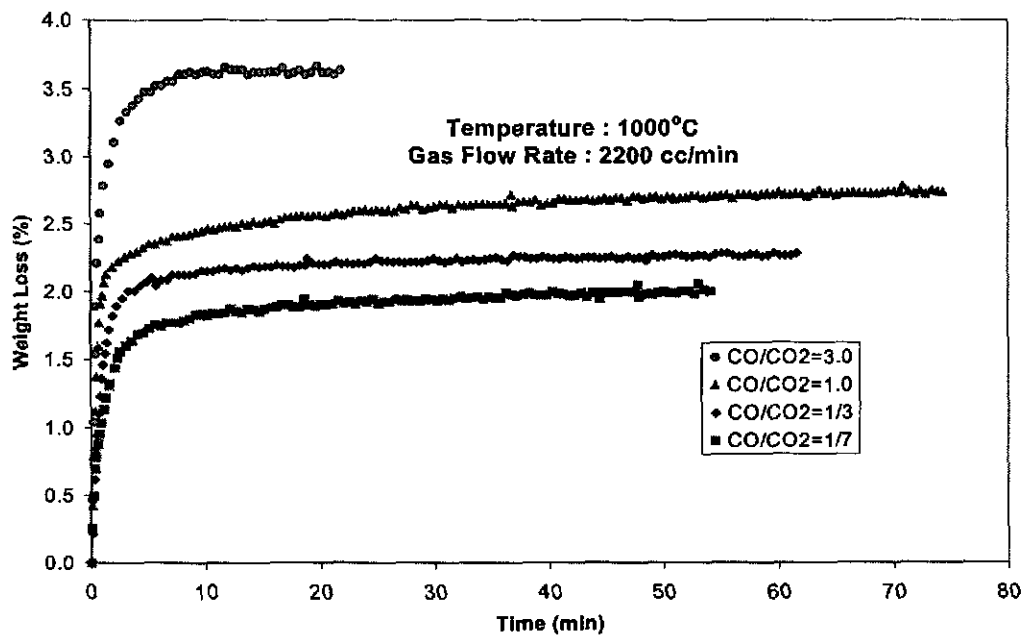


Fig. 5.19 Effect of Reducing Gas Composition at 1000°C

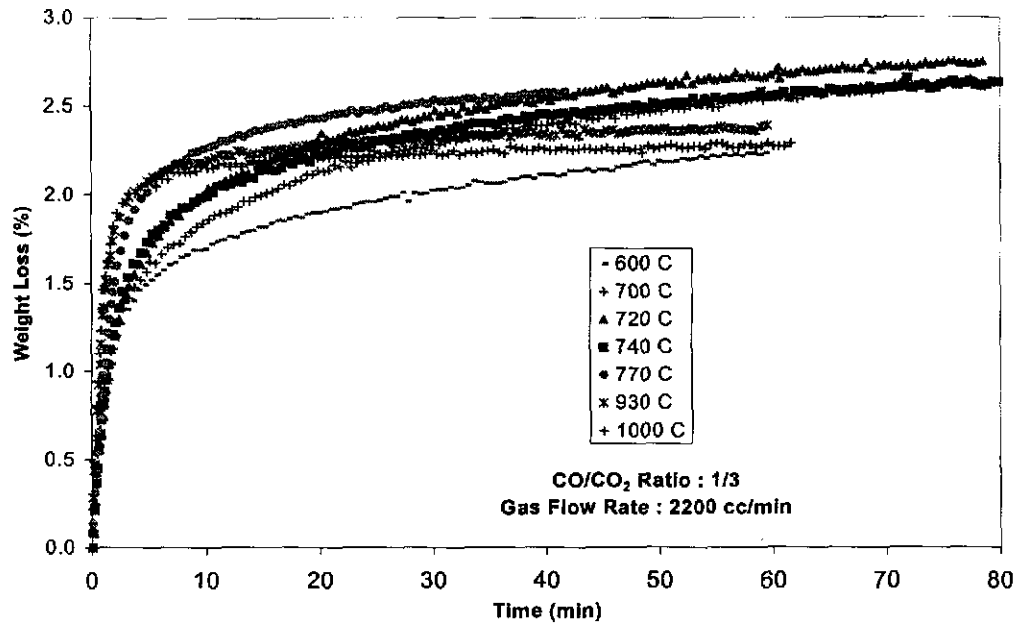


Fig. 5.20 Reduction at Different Temperatures With CO/CO<sub>2</sub>=1/3

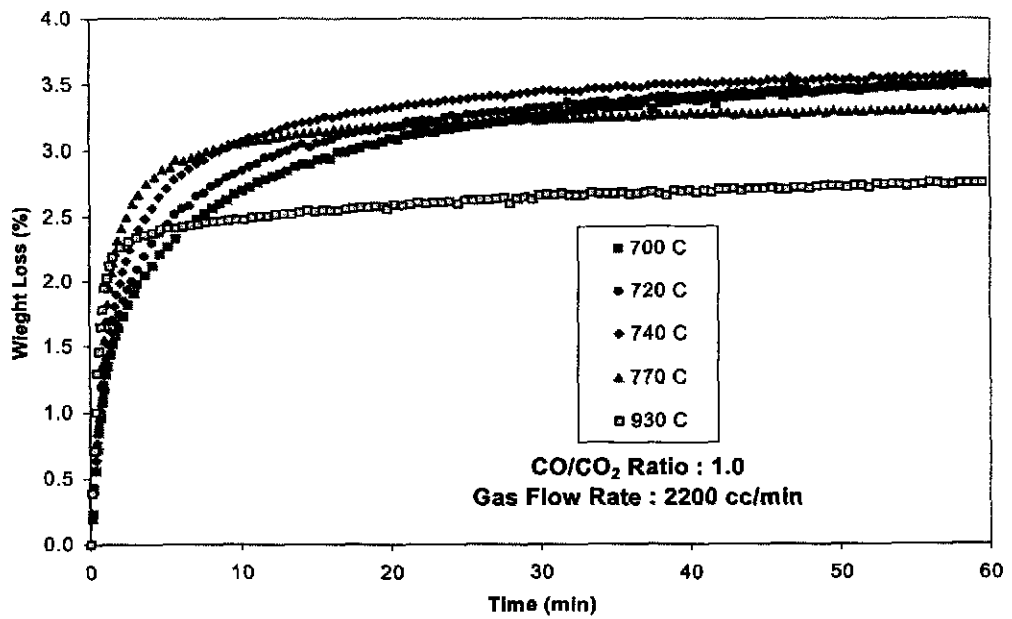


Fig. 5.21 Reduction at Different Temperatures With CO/CO<sub>2</sub>=1.0

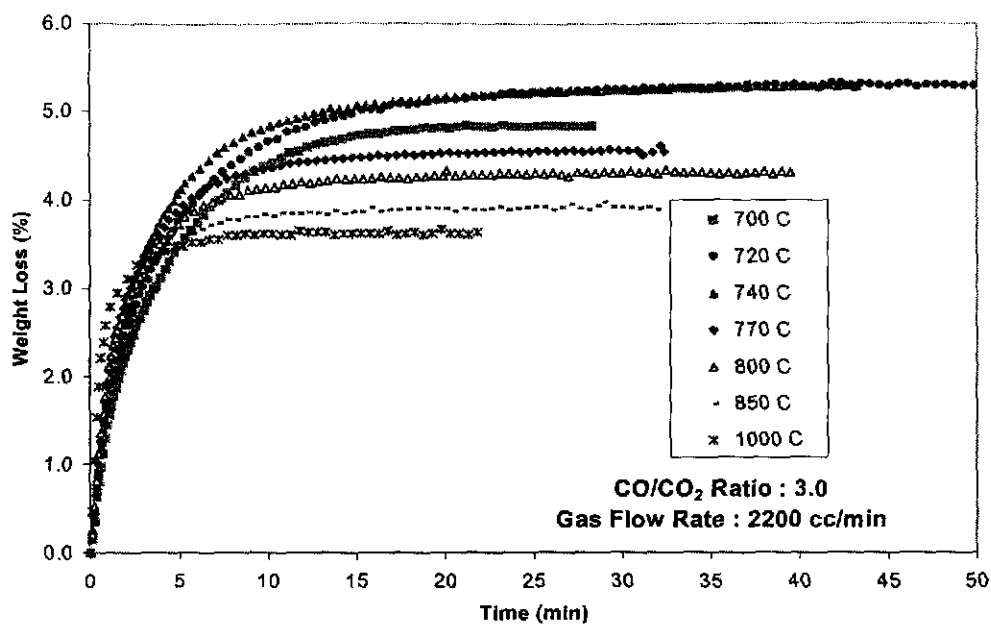


Fig. 5.22 Reduction at Different Temperatures With CO/CO<sub>2</sub>=3.0

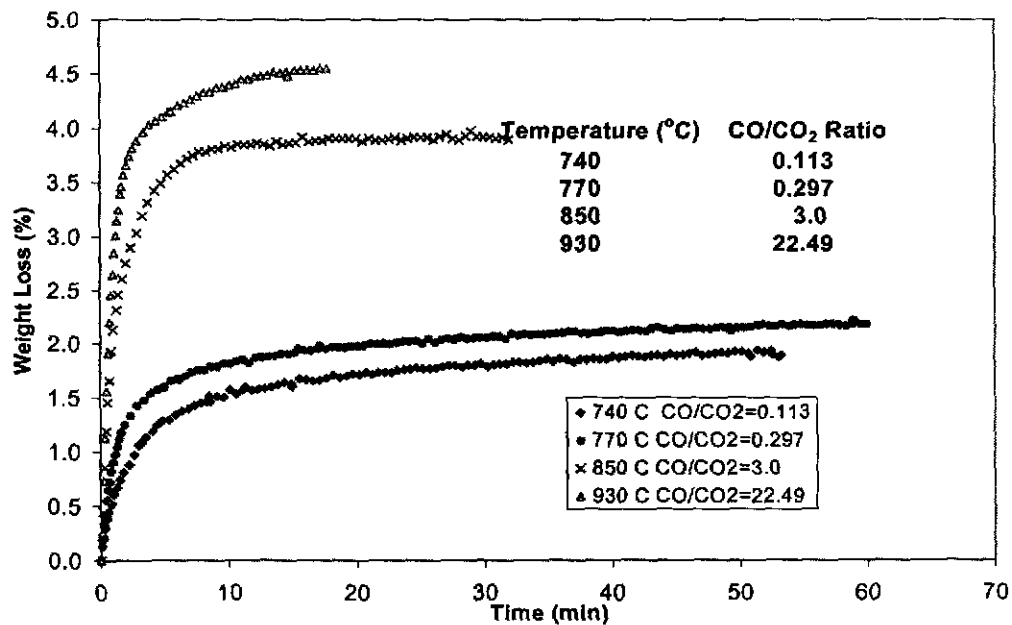
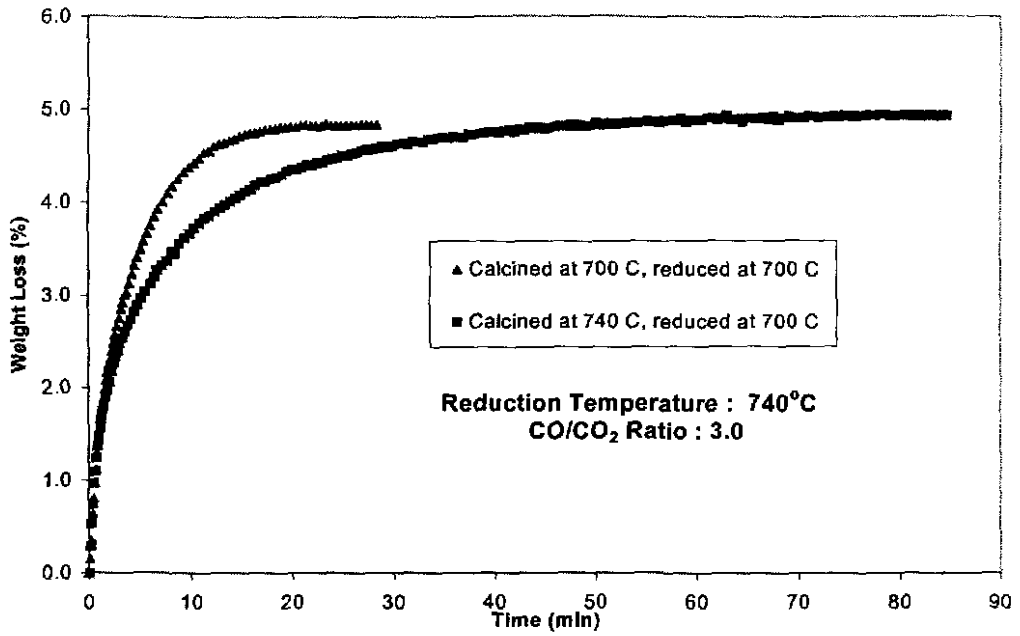
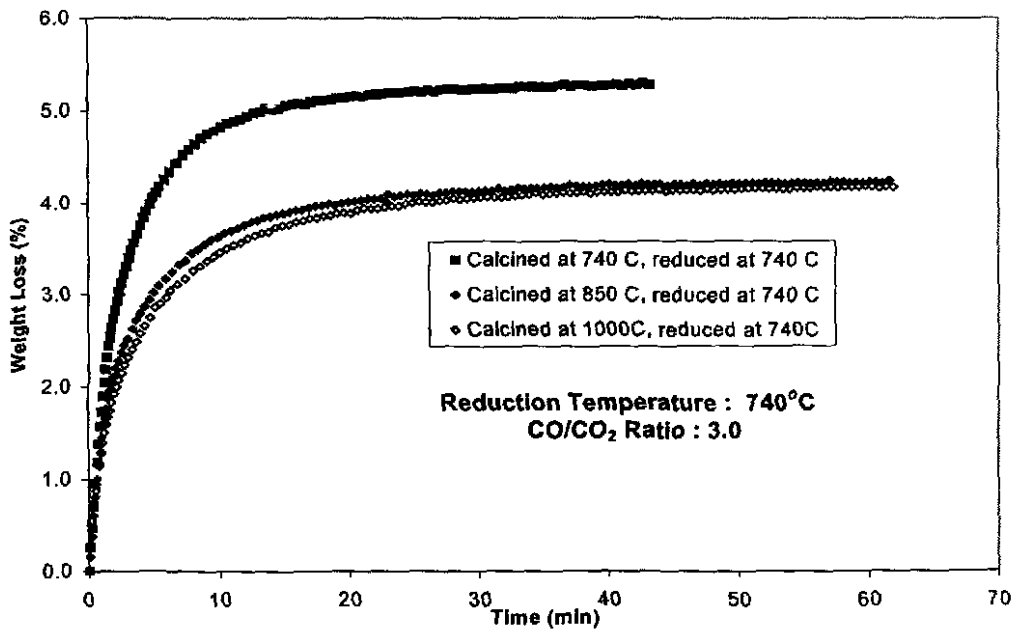


Fig. 5.23 Reduction at Different Temperatures Using CO/CO<sub>2</sub> Mixtures With The Same Oxygen Partial Pressure



**Fig. 5.24 Reduction Under The Same Conditions (CO/CO<sub>2</sub>=3.0, 700°C) After Calcined At Different Temperatures**



**Fig. 5.25 Reduction Under The Same Conditions (CO/CO<sub>2</sub>=3.0, 740°C) After Calcined At Different Temperatures**

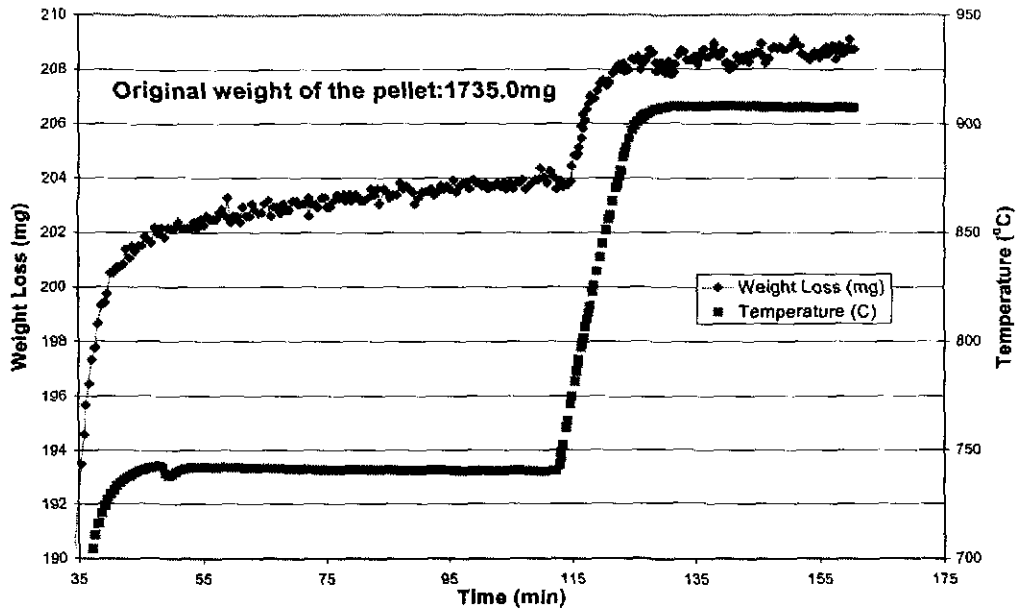


Fig. 5.26 Water Removal Pattern of Sample D

## 5.6 Experiments Using Gases With Composition Varied During Reduction

It is now clear that there are three factors that affect the reduction extent of serpentinic laterite: gas reducing power, temperature, and mineral phases present. Since a reducing atmosphere favours olivine or enstatite formation, there is a competition between the reduction and crystallization processes. If reduction proceeds at a slow rate relative to olivine or enstatite crystallization, more  $\text{Ni}^{2+}$  and to some extent  $\text{Fe}^{2+}$  will be tied up and become unreducible. This will give a lower final reduction extent. In Fig.5.27, three experimental results are compared. In one experiment, the pellet was calcined for 60 minutes at  $740^\circ\text{C}$  and then reduced with gas of  $\text{CO}/\text{CO}_2=3.0$  as has been the normal case in this study. The final reduction extent is 5.28%. Another experiment

was carried out in which the pellet was calcined at 740 °C for 37 min, then was reduced subsequently with gas mixture very lean in CO (ratio of CO/CO<sub>2</sub> is about 1/40) for 13 minutes and then with gas mixture of CO/CO<sub>2</sub> ≈1/10 for 30 minutes, finally the reduction was completed with CO/CO<sub>2</sub> =3.0. This experiment gave a lower reduction extent of 4.53%.

In the latter case, before the reducing gas of CO/CO<sub>2</sub> =3.0 was introduced, the sample had been held at high temperature for nearly 80 minutes totally, which is longer than the first experiment. Therefore the lower reduction extent may be ascribed to the longer calcination time. However, compared with the third experiment, in which the pellet was calcined for 90 minutes before reduction began but a medium final reduction extent was obtained, it is evident that reducing atmosphere helped to accelerate and further the olivine or enstatite crystallization, and if the reduction did not proceed quickly enough in the early stages with weak reducing gas mixtures, more iron and nickel would become unreducible, therefore a low reduction extent would be obtained.

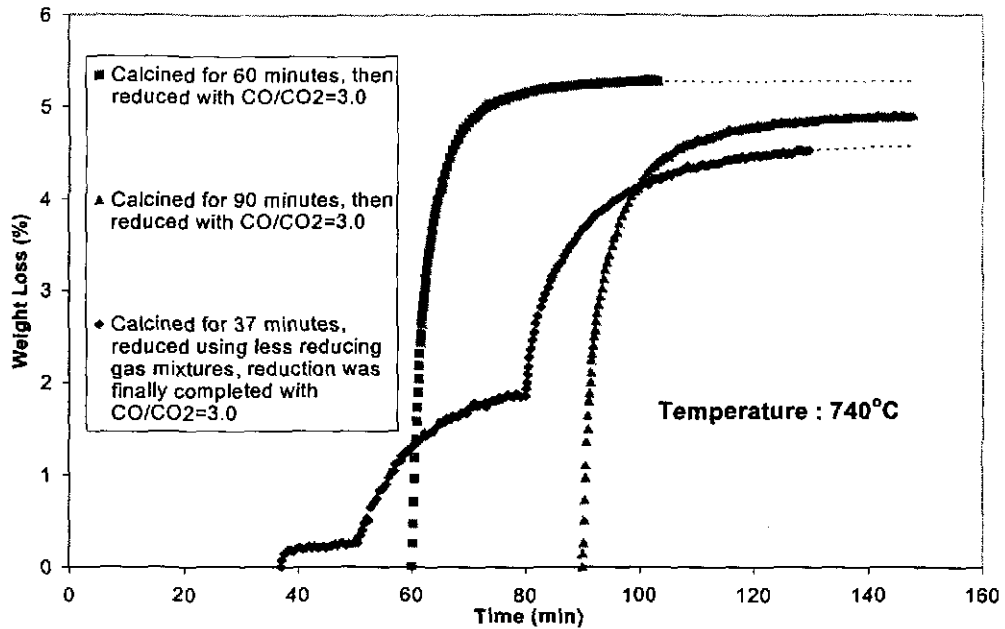


**Fig. 5.27 Reduction with Weak Reducing Gas at Early Stage Gives Low Reduction Extent**

It has been shown that after serpentine dehydration and before olivine or enstatite crystallization, laterite is the most reducible (see Section 5.5). If full advantage can be taken in this period, more metalics may be produced. Fig.5.28 shows the results of an experiment carried out in the following way: a pellet was first calcined at  $700^\circ\text{C}$  for 1 hour, then the temperature was raised to  $850^\circ\text{C}$  progressively. While the temperature was increasing, reducing gas composition was adjusted in steps so as to keep a roughly constant equilibrium oxygen partial pressure. In this way, it was hoped to reduce more laterite at each temperature stage. The major adjustment steps were: At  $700^\circ\text{C}$ ,  $\text{CO}/\text{CO}_2=0.028$ ; At  $740^\circ\text{C}$ ,  $\text{CO}/\text{CO}_2=0.113$ ; At  $770^\circ\text{C}$ ,  $\text{CO}/\text{CO}_2=0.297$ ; At  $800^\circ\text{C}$ ,  $\text{CO}/\text{CO}_2=0.739$ ; and then reduction was completed at  $850^\circ\text{C}$  with  $\text{CO}/\text{CO}_2=3.0$ . This

experiment gave a higher reduction extent compared with the second experiment, which was carried out by calcining the sample for 30 minutes followed by reduction at 850°C with  $\text{CO}/\text{CO}_2=3.0$ . The shorter calcination time in the latter case was intended to minimize the effect of using the different calcination processes.

Had the mineral phases been the same before reduction, a lower reduction extent would have been expected for the first experiment if, at early stage, reduction proceeded more slowly than crystallization. However, in the first experiment, since a strong enough reducing gas was provided, good advantage was taken while temperature was in the range from 700°C to about 790°C where laterite is most reducible, therefore a higher final reduction extent was obtained.

If reducing power is further strengthened while temperature is increased in the range of 700°C to about 790°C, a faster reduction rate and a higher reduction extent will be obtained. In Fig.5.28, the third experiment was done with fixed  $\text{CO}/\text{CO}_2$  ratio of 3.0 but calcination and reduction temperature patterns are the same as for the first experiment. It can be seen that among the three experiments, the third had the fastest reduction rate and reached to the highest reduction extent after about 10 minute reduction. After that, as temperature was increased, reducing power became weaker and metal phase was reoxidized, finally the reduction extent fell to the same level as the first experiment.

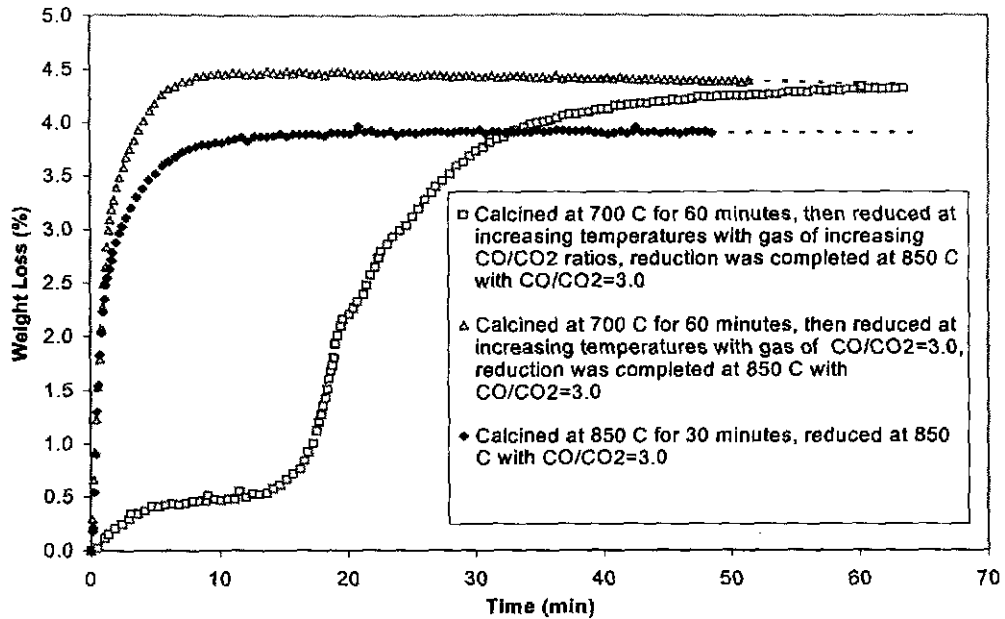


**Fig. 5.28 If More Reduction Takes Place While Some Laterite Minerals Are In Amorphous State, Higher Final Reduction Extent Can Be Achieved**

## 5.7 Summary of Experimental Study

- 1) Sample D in this study is mostly a serpentinic laterite. It contains about 80% serpentine and 20% goethite.
- 2) Upon calcination, laterite will undergo three steps of dehydration: moisture removal, chemically bound water release and crystalline water liberation. Below 600°C, complete dehydration is difficult, and reduction rate and extent are low.
- 3) Upon calcination, goethite will decompose into hematite, and upon reduction hematite will be reduced to magnetite or spinel and then to metallics stepwise.

- 4) Serpentinic samples may contain three kinds of serpentine minerals: chrysotile, lizardite, and antigorite. At elevated temperatures, these minerals will undergo decomposition and crystallization. 810°C is the critical temperature above which most of the serpentine minerals will crystallise to olivine and enstatite. Calcination at higher temperatures and/or for longer times will result in more olivine and enstatite crystallization, even when the temperature is below the critical value. This has been well documented in the literature<sup>[33]</sup>.
- 5) Olivine and enstatite formation will decrease the laterite reduction extent, because once olivine and enstatite are formed, some  $\text{Ni}^{2+}$  and  $\text{Fe}^{2+}$  will be tied up and become unreducible.
- 6) Calcination at higher temperatures and/or for longer time will result in a smaller BET surface area. However, after calcination for more than one hour, especially at high temperature, the BET surface area of the pellet of Sample D does not change much after further treatment.
- 7) Sample D is most easily reduced after serpentine decomposition and before olivine and enstatite crystallization. If full advantage can be taken during this period, a higher reduction extent will be obtained.
- 8) For serpentinic Sample D, at a given temperature, when the  $\text{CO}/\text{CO}_2$  ratio of reducing gas is increased, both reduction rate and extent will be increased. While with a fixed  $\text{CO}/\text{CO}_2$  ratio, when temperature is increased, reduction rate will increase, but reduction extent will generally decrease. With  $\text{CO}/\text{CO}_2$  ratios in the range of 1/3 to

3.0, reduction extent has a maximum value when the temperature is around 720°C~740°C.

- 9) With gas mixtures of fixed reducing power (equilibrium oxygen partial pressure), higher temperature will give a higher reduction rate and reduction extent regardless of mineral crystallization.
- 10) A reducing atmosphere accelerates the formation of olivine and enstatite. There is a competition between the laterite reduction process and olivine and enstatite crystallization. If reduction proceeds slowly in the early stages, more olivine and enstatite will be formed in advance of complete reduction, therefore more  $\text{Ni}^{2+}$  and to some extent  $\text{Fe}^{2+}$  will be tied up and a low reduction extent will be obtained.
- 11) With the pellet size used in this study, reduction proceeds in two stages. In the first reduction stage, resistance of gas diffusion through pellet and resistance of chemical reaction are both significant, and reduction process follows a shrinking mode with a reaction band of a certain width. In the second stage, reduction takes place uniformly within the pellet, but is not adequately described by the accepted model for uniform internal reaction. A more detailed analysis of reduction kinetics will be presented in the following chapter.

# CHAPTER 6

## KINETIC ANALYSIS

### 6.1 Introduction

X-Ray Diffraction analysis and an exploratory SEM study on Sample D at different reduction stages showed that this serpentinic laterite is a complicated mineral mixture. In addition to the nickel and iron oxides and silicates, some other minerals containing a high content of chromium or manganese exist in the laterite (Photo 6.1 and Fig.6.1). However, the two minerals of the most significance are goethite and serpentine or minerals derived from them upon calcination. Therefore it may be the best to determine reduction rate constants for goethite and serpentine or their derivative minerals respectively. The rate constants may then be applied to other types of laterite to predict reduction behaviour based on the proportion of the major mineral phases. Partially reduced samples at different reduction stages were studied by SEM/EDX in an attempt to determine the amount of reduction of each of the derived minerals at each stage. The principle of this method is, if nickel content of metal produced from goethite and serpentine derivative minerals,  $(Ni\%)_G$  and  $(Ni\%)_S$ , are determined by SEM/EDX, and the average metallic nickel grade and the amount of the total metallic phase,  $(Ni\%)_{ave}$  and

$M_{tot}$ , are determined by chemical analysis, then the following two equations can be applied:

$$(Ni\%)_G M_G + (Ni\%)_S M_S = (Ni\%)_{ave} \cdot M_{tot}.$$

$$M_G + M_S = M_{tot}.$$

Solution of these equation will yield the amount of metallic phase produced from goethite and serpentine derived minerals,  $M_G$  and  $M_S$ .  $M_G$  and  $M_S$  can then be correlated with reduction time and used to extract reduction kinetic parameters for each mineral.

However, this method largely failed, since the measured nickel grades (by EDX) in metallic phases produced from both serpentine derivative minerals and goethite derivative minerals are lower than the average nickel grade obtained by chemical analysis. For the sample partially reduced for ~10 minutes at 740°C with CO/CO<sub>2</sub>=3.0, the average nickel grade measured by chemical analysis is around 32%, the SEM and EDX study results are in Table 6.1. These erroneous results may be caused by the easy reoxidation of the newly reduced metallics, or by the different reoxidation rates of the newly reduced nickel and iron. In addition, the metallic phase in reduced samples was very finely distributed (Photo 6.2), therefore it was difficult to obtain accurate analysis by EDX.

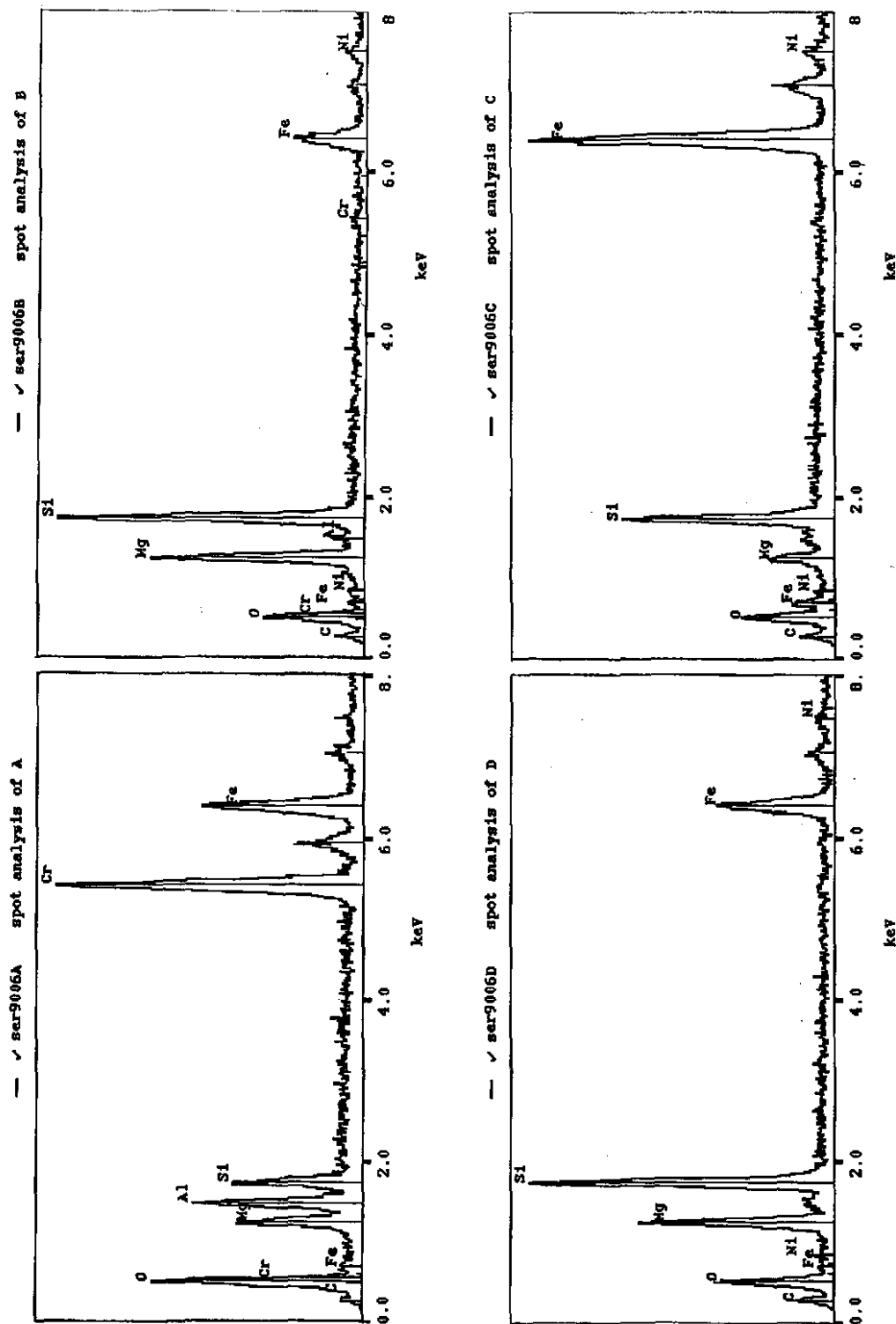
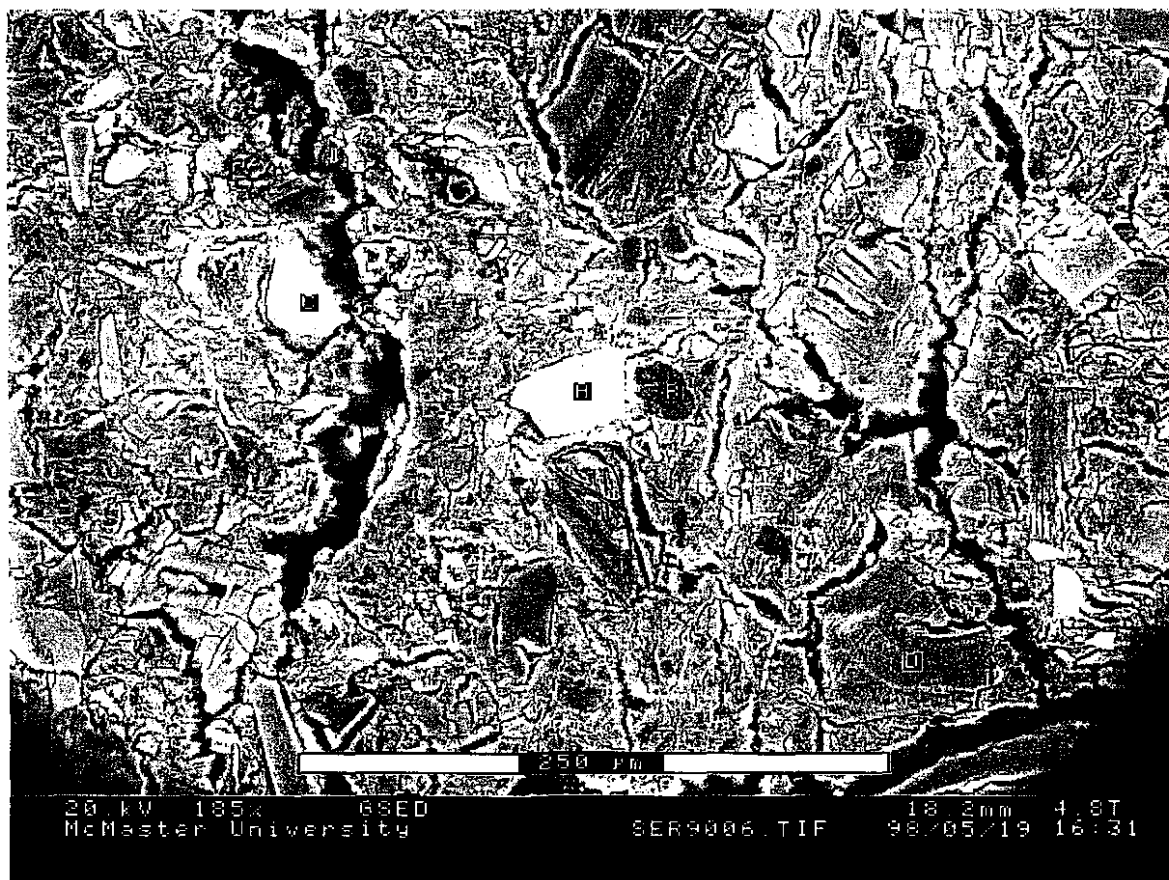
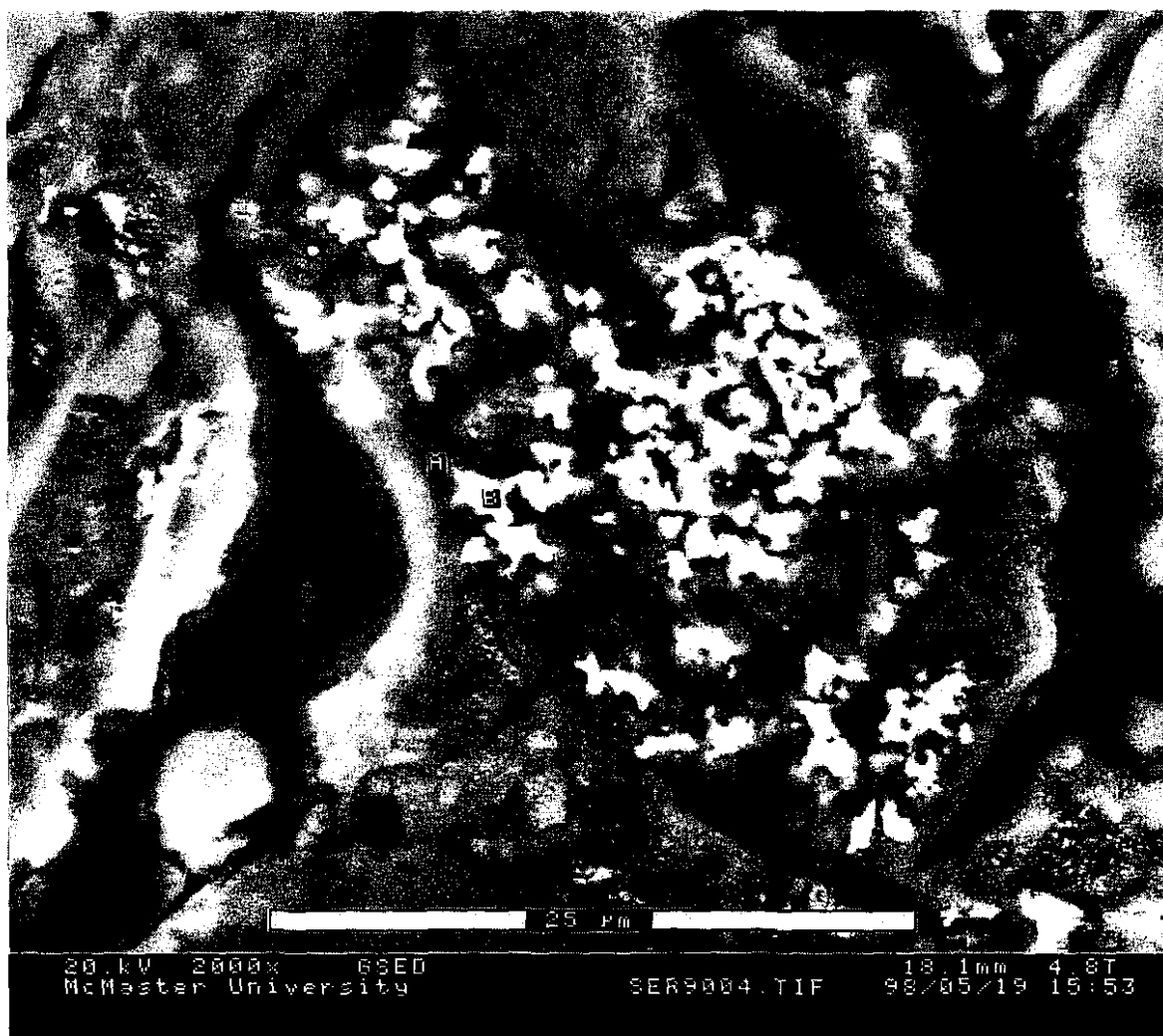


Fig. 6.1 X-Ray Analysis Results Of Spot A, B,C,D In Photo 6.1



**Photo 6.1 Laterite Comprises of Different Minerals**

(A,B,C,D are four spots where the mineral compositions are different)  
(X-Ray analysis results of spot A, B,C,D are in Fig.6.1)



**Photo 6.2 Metallic Phase Is Finely Distributed in The Reduced Pellet**

(A: Laterite, B: Metallic phase)

**Table 6.1 Nickel Grade In Metallics Produced From Goethite And Serpentine Derivative Minerals Measured By SEM/EDX  
(For sample partially reduced at 740°C with CO/CO<sub>2</sub>=3.0 for 9.9 minutes)**

For metallic phase produced by reduction of goethite derivative minerals		For metallic phase produced by reduction of serpentine derivative minerals	
Measured spot	Nickel Grade (%)	Measured spot	Nickel Grade (%)
1	7.55	1	25.01
2	5.88	2	23.62
3	14.56	3	14.39
4	11.91	4	19.19
5	7.02	5	16.02
6	5.32	6	17.10
7	10.82		
8	6.76		
9	5.05		
10	11.31		

Another way to conduct a kinetic study using laterite pellets may be to consider [O] (oxygen dissolved in laterite) as a solid reactant and the chemical reaction takes place in form of



Assuming the laterite pellet is compositionally homogeneous, when oxygen is removed, the minerals can seek a new equilibrium among themselves and metallic phases are produced in this process. The relationship between oxygen removal and nickel and iron reduction can be established experimentally. Kinetic parameter extraction may involve prediction of reducing gas profile within the pellet and calculation of the average reducing gas concentration. However, when subjected to the Grain Model<sup>[44]</sup> or the Uniform Internal Reaction model<sup>[43]</sup>, the experimental data did not fit either sufficiently well. This, at least, indicates that when assuming [O] is the solid reactant and laterite is

homogenous, the established Grain model and Uniform Internal Reaction model are not applicable to the kinetic analysis. This may be because the assumption in these models that the activity of solid reactants remains constant during reaction process, is not an accurate representation of the present case. In this case the activity of [O] is changed as the reduction progresses and oxygen is removed. In addition the assumption that the laterite is homogeneous is not realistic, and it is likely that different minerals in laterite contribute differently to the reduction kinetics.

A detail explanation of the Grain Model will be given in Section 6.3, however, to understand Fig.6.2 we need to know that if chemical reaction control dominates, the conversion function  $g(X)$  will be a linear function of reduction time  $t$ , whilst if diffusion within or among the grains dominates, the conversion functions  $P_{Fg}(X)$  or  $P_{Fp}(X)$  will be a linear function of reduction time  $t$ . If the reduction is under mixed control,  $g(X) + \sigma * P_{Fg}(X)$  or  $g(X) + \sigma * P_{Fp}(X)$  will be linear with respect to reduction time  $t$  ( $\sigma$  is a ratio factor).

As for the uniform internal reaction model, because it is assumed that the pellet is so porous that the gas can permeate freely within it, so the reaction occurs randomly, and the rate is proportional to the fraction of unreacted material. This model is described by the following equation:

$$-\ln(1-X)=kt$$

$X$  is the reaction fraction, and  $k$  is the product of the chemical reaction rate constant and a driving force term. The driving force term is  $P_{co}$  for a simple first order

reaction and will be  $P^n \text{co}$  for  $n^{\text{th}}$  order reactions.  $t$  is reaction time. Therefore, if the reduction occurs uniformly,  $-\ln((1-X))$  will be a linear function of reduction time  $t$ .

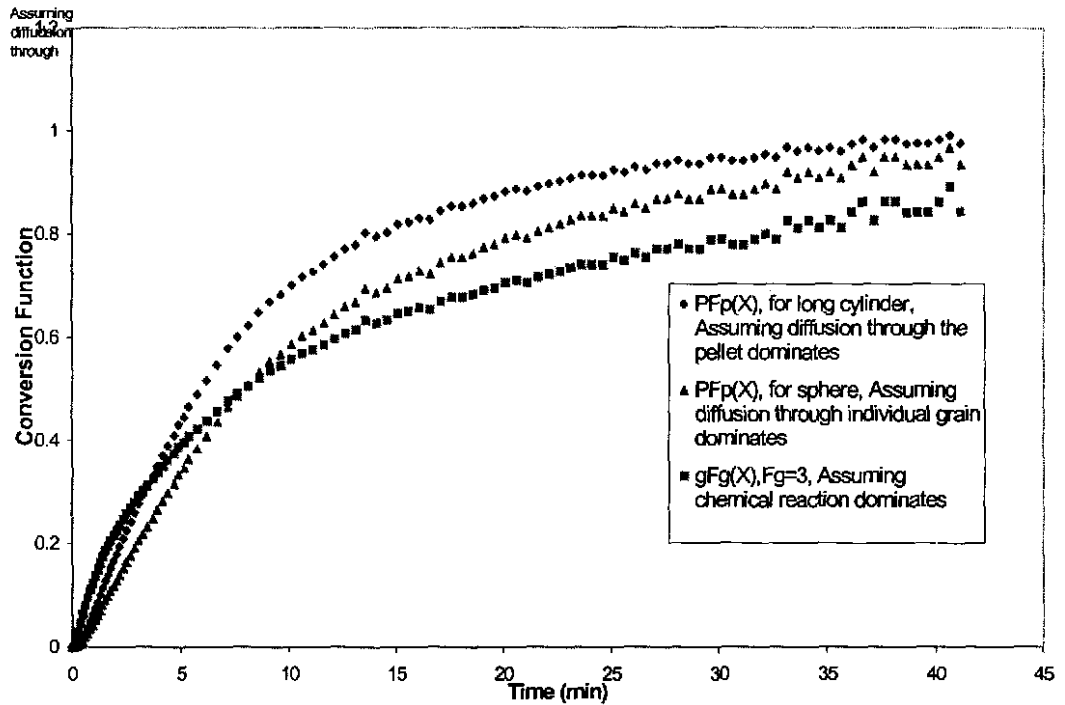


**Fig. 6.2 Experimental Data (Gas flow rate: 2200cc/min, Temperature: 740°C, CO/CO<sub>2</sub> ratio: 3.0) Subjected To The Grain Model**

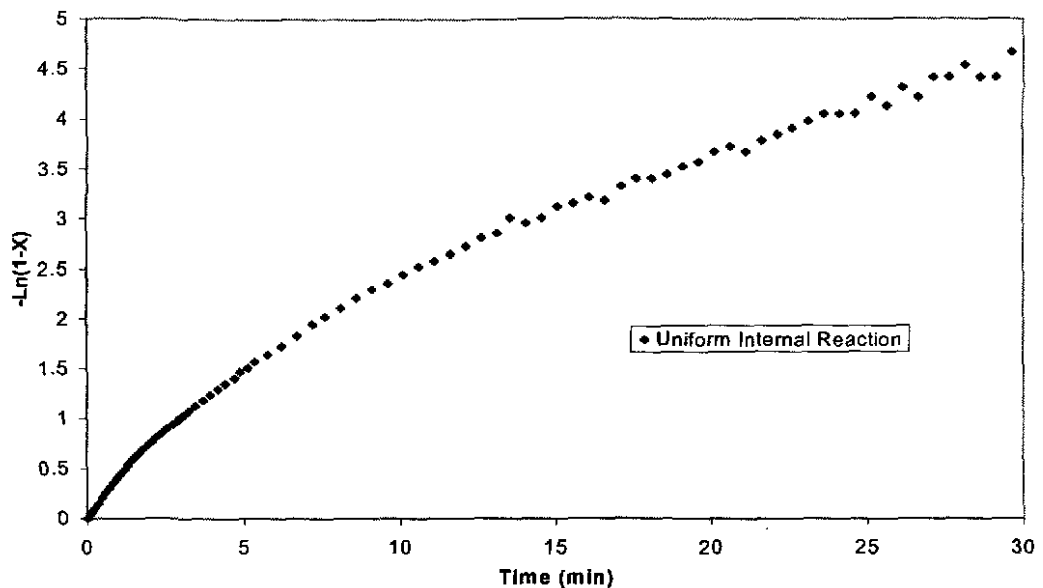


**Fig. 6.3 Experimental Data (Gas flow rate: 2200cc/min, Temperature:740°C, CO/CO<sub>2</sub> ratio:3.0) Subjected To The Uniform Internal Reaction Model**

A third possibility is to assume iron and nickel in calcined laterite exist in form of pure metal oxides, and during reduction process, they are reduced separately. This method has been employed by Nath<sup>[41]</sup> *et al.* Although according to X-ray diffraction data, the reaction of hematite to magnetite occurs in the early stages of laterite reduction, and according to thermodynamic calculations, the reduction from magnetite to wustite and wustite to metallic iron may occur, these reactions are only one contribution to iron reduction in laterite. Furthermore, nickel oxide is not present as a separate mineral. The assumption that iron and nickel in calcined laterite exist in form of pure metal oxides is oversimplified, but it is one feasible way to examine the kinetics considering the time allowance and other limitations on this study. Nath<sup>[41]</sup> had successfully studied Sukinda

laterite reduction kinetics based on this assumption, and a similar approach will be used in this work.

## **6.2 Verification of Experiment Procedure and Chemical Analysis of Partially Reduced Samples**

Partially reduced samples were sectioned axially and studied by optical microscopy. Photo 6.3 shows that although the cylindrical pellet is about 30 mm long and held in the furnace parallel to the furnace tube, the reduction rate was approximately uniform along the length of the pellet, and the reduction at the ends did not show a noticeable difference in reduction compared with the cylindrical surface. This indicates that the sample used in this study can be approximated as an “infinitely long cylinder”.

A series of chemical analyses was carried out for samples partially reduced for different times at different temperatures with  $\text{CO}/\text{CO}_2=3.0$ . The experimental results are shown in Table 6.2.

As described in Chapter 3, the chemical analysis method used is a bromine-methanol leaching followed by ICP (Inductively Coupled Plasma Spectrophotometry). Although this method has been used for many years in determining metallic content, it was found in this study that it is not very effective. Firstly, X-ray diffraction analysis of leach residue showed trace metallic phase (See Fig.6.4). This may be because, as indicated by Anderson<sup>[12]</sup>, the penetrative ability of bromine is not strong enough, or because the reduced calcine was not ground finely enough. It has been found in these experiments that the amount of metallic phase in the leach residue varied with different leaching time and different grinding extent. These two factors, especially the latter, are hard to keep

exactly constant. Secondly, when reduced calcine was transferred from the furnace to the plastic bag, in which it was ground, and when the ground sample was transferred to the leaching liquid, reoxidation may have occurred. Lastly, during ICP analysis, it was found that the measured results sometimes drifted. Although correction methods were employed, since the weight of the analysed sample was small, and the metallic content was not high, the final results show considerable scatter.

Despite the scatter in the analysis, a clear trend can be seen from the data. From Fig.6.5 and Fig.6.6, it can be seen that with  $\text{CO}/\text{CO}_2=3.0$ , when reduction temperature is higher, the equilibrium nickel recovery generally decreases, this is in agreement with the thermodynamic calculation presented in Chapter 4 (Fig.4.3). At 740 °C, the nickel recovery seems to be maximized. However, there is a discrepancy between thermodynamic calculation and chemical analysis with regard to the nickel grade of the metallic product. According to the chemical analysis data, when the reduction temperature is higher, the equilibrium nickel grade in the metallic product is increased. Whereas the thermodynamic calculation showed that when serpentinic ore is reduced with a fixed  $\text{CO}/\text{CO}_2$  ratio of 3.0, the nickel grade of the metallic product would decrease when the reduction temperature is higher (Fig.4.4). This discrepancy might have arisen from experimental error, or, have been caused by inadequate thermodynamic data.

It also can be seen from Fig.6.5 that at certain reduction stages, the nickel grade of the metallic phase in the reduced calcine is higher than the final equilibrium values. This may suggest that if higher nickel grade is of great concern, reduction should not be taken to completion.



**Photo 6.3 Partially Reduced Cylindrical Pellet When Sectioned Along Axis**  
(Reduced At 740 °C With CO/CO<sub>2</sub>=3.0 For 10 Seconds)

**Table 6.2 Chemical Analysis of Partially Reduced Samples**

700°C with CO/CO <sub>2</sub> =3.0			740°C with CO/CO <sub>2</sub> =3.0		
Reduction Time(min)	Recovery of Ni (%)	Recovery of Fe (%)	Reduction Time(min)	Recovery of Ni (%)	Recovery of Fe (%)
0.6	1.76	2.48	0.7	14.08	2.48
1.1	8.08	4.52	0.7	14.54	2.32
1.1	7.49	4.28	2.0	32.99	4.19
1.9	16.48	4.30	2.0	33.39	4.25
2.0	23.01	5.22	2.2	39.54	6.85
2.6	29.97	7.09	3.0	49.80	7.89
3.8	35.22	6.88	4.2	42.64	9.66
4.9	37.11	9.99	4.9	54.15	7.88
5.4	40.09	9.94	4.9	52.31	8.17
6.9	39.77	11.20	6.6	57.30	8.46
8.7	41.83	9.68	7.6	60.26	13.68
10.6	43.72	13.05	7.7	58.17	12.25
15.8	43.52	14.97	9.9	58.35	16.48
20.1	47.45	17.13	15.2	62.57	15.56
30.2	53.02	20.96	15.4	63.71	18.83
35.0	52.97	22.54	15.4	64.87	19.11
114.0	60.79	32.05	20.0	66.03	22.73
			25.7	67.49	24.48
			43.0	70.69	29.48
			53.0	70.59	34.60
770°C with CO/CO <sub>2</sub> =3.0			850°C with CO/CO <sub>2</sub> =3.0		
Reduction Time(min)	Recovery of Ni (%)	Recovery of Fe (%)	Reduction Time(min)	Recovery of Ni (%)	Recovery of Fe (%)
0.6	18.39	3.66	1.0	36.06	9.51
0.6	18.92	3.68	1.8	46.60	10.03
1.3	35.65	6.15	3.5	47.91	13.46
1.9	39.53	8.44	5.1	54.15	14.06
2.9	47.12	8.36	7.7	53.84	15.77
3.0	51.26	10.88	10.1	58.84	14.31
4.7	50.95	14.12	12.4	60.91	15.55
5.0	51.00	12.44	19.8	60.39	16.19
6.8	53.22	17.03	31.0	60.61	17.50
8.3	56.18	16.49			
9.4	59.58	20.59			
14.9	62.03	19.96			
19.8	61.90	20.89			
30.0	59.90	24.69			
32.0	60.75	23.80			
65.0	62.33	26.61			

(Table 6.2 continued )

930°C with CO/CO <sub>2</sub> =3.0			1000°C with CO/CO <sub>2</sub> =3.0		
Reduction Time(min)	Recovery of Ni (%)	Recovery of Fe (%)	Reduction Time(min)	Recovery of Ni (%)	Recovery of Fe (%)
0.7	20.66	6.01	0.7	24.12	7.92
2.3	31.12	8.84	0.7	21.73	6.53
2.8	38.62	9.06	2.3	40.71	9.57
2.9	37.02	11.20	2.3	36.24	8.40
4.9	44.23	12.29	2.8	42.03	11.74
7.1	47.34	11.28	2.9	41.13	9.21
7.9	42.78	14.70	4.0	46.30	14.93
10.1	48.34	13.13	4.0	40.24	13.43
10.1	49.58	12.83	4.8	42.04	10.15
13.6	48.52	13.38	5.0	47.72	11.59
15.1	52.07	12.28	7.2	46.12	11.83
21.0	51.70	14.60	9.8	48.73	13.54
23.6	52.14	15.44	12.7	49.60	12.02
43.0	53.77	14.44	14.7	47.51	12.31
			20.4	47.84	12.15
			20.4	53.95	12.82
			22.0	49.96	14.81
			41.0	48.77	12.29

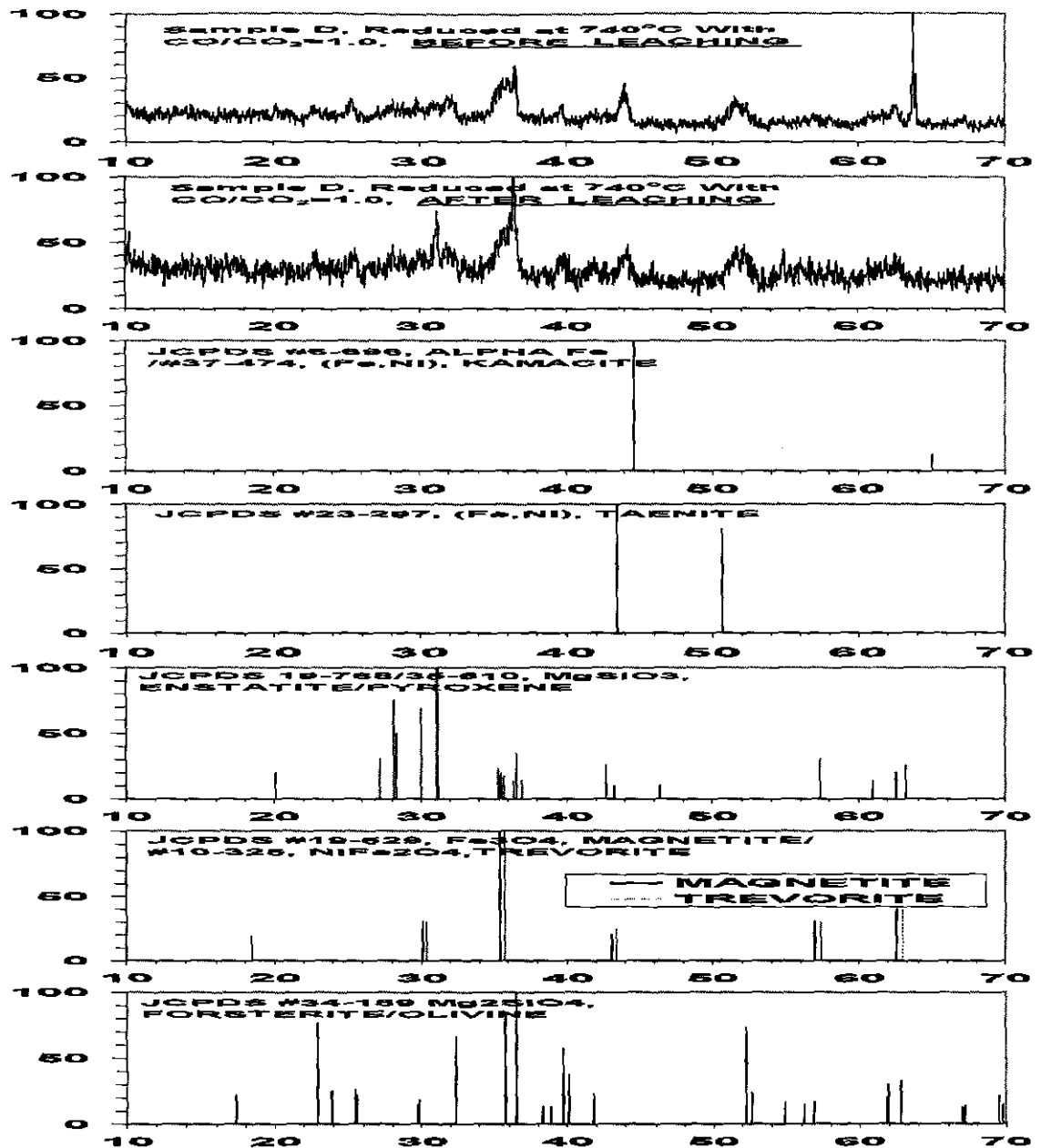
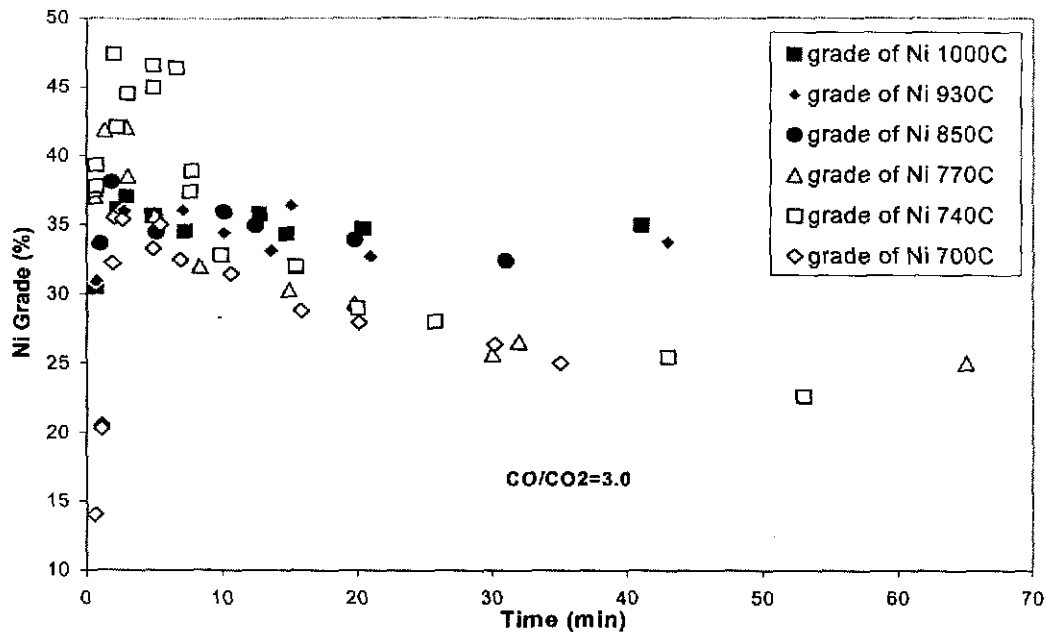
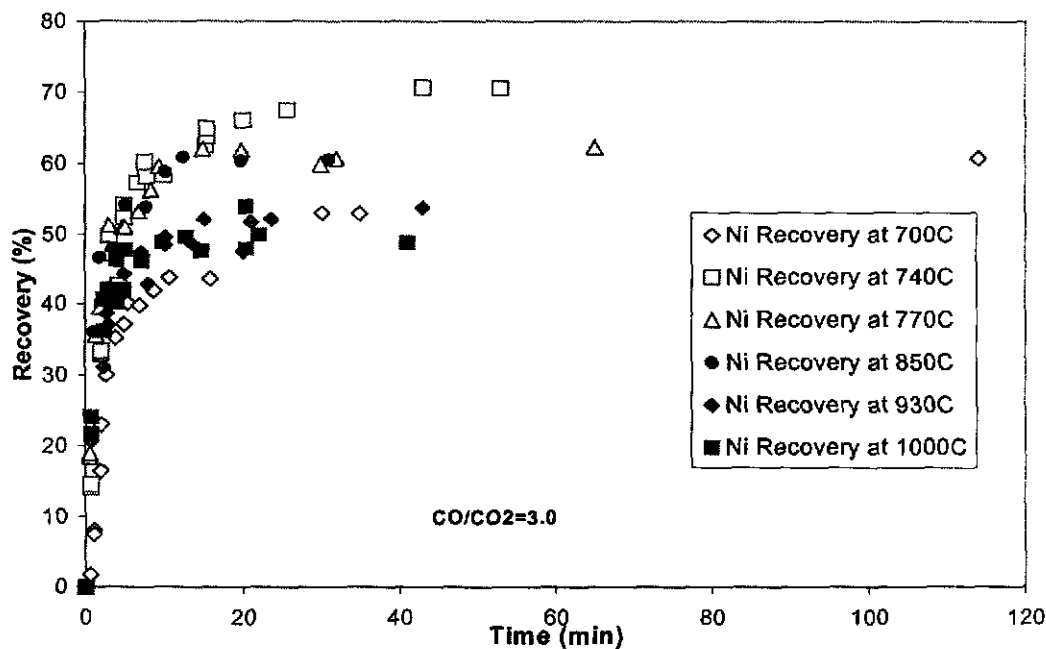


Fig. 6.4 XRD Patterns of Reduced Calcine Before And After Leaching



**Fig. 6.5 Chemically Analysed Nickel Grade of Metallic Product in Partially Reduced Sample D**



**Fig. 6.6 Chemically Analysed Nickel Recovery in Partially Reduced Sample D**

## 6.3 The Grain Model

Developed by Szekely<sup>[44]</sup> *et al.*, the Grain Model is considered to be a significant improvement over some conventional gas-solid reaction models<sup>[41]</sup>.

For solid-gas reactions, two limiting types of model are generally accepted. One is unreacted shrinking core model, also called interface reaction model or topochemical model<sup>[45][46]</sup>, in which chemical reaction is assumed occur only at a very sharp interface between the inner unreacted core and the reacted shell. When the unreacted core is dense, this kind of model is applicable, because gas reactant can not penetrate into the unreacted zone. The other model is called the homogeneous reaction model or uniform reaction model<sup>[47][48]</sup>, in which the porous solid reactant is regarded as a homogeneous medium and the reaction is considered proceed uniformly and randomly throughout the pellet. If the solid reactant is so porous that there is no resistance for gases reactants or products to diffuse in or out the pellet, the latter will come to be realized.

In the real case, however, most solid-gas reactions fall into an intermediate category. As noticed by English<sup>[49]</sup>, when a solid-gas reaction takes place, a reaction zone with a certain width is formed and the reaction interface becomes diffuse. This indicates that intrapellet gas diffusion is as important as chemical reaction. Therefore, to describe the system properly, the structure of pellet, including porosity and grain size, should be considered in the model.

In the Grain Model, the pellet is assumed consist of numerous individual grains, and in the general case, the reaction takes place over a wide range. The grains in the outer

part of the pellet are completely reacted, the grains in the middle part are partially reacted, while the grains in the center remain unreacted. For the solid-gas reaction  $A(g)+bB(s)=cC(g)+dD(s)$ , with the following assumptions :

- 1) The system is isothermal.
- 2) The solid-gas reaction is of the first order in both forward and reverse directions.
- 3) The solid reactant is macroscopically uniform, and this initial physical structure is maintained throughout the reaction.
- 4) Gas concentration within the pellet is of pseudo-steady state approximation.
- 5) Gas transportation within the solid matrix proceeds by equimolar counter diffusion.

The model is given as the following:

$$t^* = g_{Fg}(X) + \sigma_g^2 p_{Fg}(X) + \sigma_p^2 (p_{Fp}(X) + \frac{2X}{N_{sh}^*}) \quad (6-1)$$

$$g_{Fg}(X) \equiv 1 - (1 - X)^{1/Fg} \quad (6-2)$$

$$t^* \equiv \frac{bk}{\rho_{s,mol} r_g} \left( C_{AS} - \frac{C_{CS}}{K_e} \right) t \quad (6-3)$$

$$\sigma_g^2 \equiv \frac{k}{2D_{eg}} \frac{r_g}{F_g} \left( 1 + \frac{1}{K_e} \right) \quad (6-4)$$

$$p(X) \equiv 1 - 3(1 - X)^{2/3} + 2(1 - X) \quad \text{for spheres} \quad (6-5)$$

$$p(X) \equiv X - (1 - X)\ln(1 - X) \quad \text{for long cylinders} \quad (6-6)$$

$$p(X) \equiv X^2 \quad \text{for infinite slabs} \quad (6-7)$$

$$\sigma_p^2 \equiv \frac{k}{2D_{ep}} \frac{r_p^2}{r_g} \frac{1 - \theta}{F_p} \left(1 + \frac{1}{K_e}\right) \quad (6-8)$$

$$N_{sh}^* \equiv r_p \frac{h_D}{D_{ep}} \quad (6-9)$$

In which  $t^*$  is the dimensionless time which is proportional to the reaction time,  $g_{Fg}(X)$  is the conversion function related to chemical reaction,  $p_{Fg}(X)$  is the conversion function related to gas diffusion within individual grains,  $p_{Fp}(X)$  is the conversion function related to gas diffusion within the pellet, and  $\sigma_g^2$  and  $\sigma_p^2$  are moduli which are a measure of the relative importance of chemical reaction and diffusion.  $F_g$  and  $F_p$  are shape factors for the grains and the pellet.

Depending on different conditions, the grain model can take different forms and describe different situations. If the overall rate is controlled by the diffusion of gas through the interstices among the grains, the situation will be identical to the unreacted shrinking core model of a nonporous solid. Then the model will take the following form:

$$t^* = \sigma_p^2 p_{Fp}(X) \quad (6-10)$$

If gas diffusion among the grains presents a negligible resistance to the progress of reaction, all grains will be reduced at the same rate, and the model takes the form:

$$t^* = g_{Fg}(X) \quad (6-11)$$

Since the grain model incorporates structural parameters for the solid reactant, and allows the prediction of the reaction rate in the chemical control, diffusion control, or mixed control regime, it was thought to be attractive by investigators in the solid-gas reaction field. Several successful applications of the grain model can be found in the literature <sup>[19][20][41][50]</sup>.

The grain model is a reasonable description of the situation of the pellets used in this study. Microscopic examination of partially reduced pellets has shown that the reaction interface at certain reduction stages was diffuse, and investigation of the reduction mechanism has found that reduction of laterite pellets did not proceed either in an extreme topochemical manner or uniformly. So the Grain Model is selected to use here.

Previously, Szekeley and Hastaoglu<sup>[19]</sup> used the Grain Model to study the reduction of nickel oxide and hematite mixture by hydrogen. Nasr<sup>[20]</sup> used it in his kinetic study on reduction of hematite doped with NiO. Nath *et al*<sup>[41]</sup> utilized the Grain Model to investigate the selective reduction of Indian nickeliferous ore. They found that the Grain Model, which was developed to study pure oxide-gas reactions, can be easily extended to study laterite reduction.

In this study, the grain model will be used for the two oxide reductions. Parameters such as diffusivity within the pellet  $D_{cp}$ , diffusivity within the individual grain

$D_{eg}$ , initial pellet radius  $r_p$ , initial grain radius  $r_g$ , pellet porosity  $\theta$ , bulk concentration of gas reactant  $C_{AS}$ , bulk concentration of gas product  $C_{CS}$ , shape factor of grain  $F_g$ , shape factor of pellet  $F_p$ , external mass transfer coefficient  $h_D$  are the same in both cases. Other parameters, such as reaction rate constant  $k$ , reaction fraction  $X$  and reaction equilibrium constant  $K_e$ , however, are different for each oxide.

## **6.4 Estimation of Necessary Parameters**

The parameter estimation process was coded into a program using Turbo Pascal. Its calculation procedure will be described in this section.

### **6.4.1 Porosity of Calcined Pellets**

#### **6.4.1.1 Apparent Density of The Pellet Before Reduction**

After being calcined for one hour before reduction, there was no noticeable external dimension change of the pellet, and the weight loss due to moisture removal on average was 13%, which was nearly independent of calcination temperature above 700°C. Since accurate measurement showed the apparent density before calcination was 1.444g/cm<sup>3</sup>, the apparent density after calcination was then approximately set as 1.256 g/cm<sup>3</sup>.

#### **6.4.1.2 True Density of The Pellet Before Reduction**

True density of pellets calcined at different temperatures was measured by

the Archimedes Principle. Calcined pellets were crushed and ground and then, after weighting, placed in a pycnometer. Distilled water was used as penetrating liquid. Trapped or adsorbed air inside or on the surface of the specimen was removed by putting the pycnometer and the specimen, which has already been submerged in the water, into a vacuum chamber for 1 hour.

#### **6.4.1.3 Porosity of Calcined Pellets**

Porosity can have a large effect on reaction rate because it helps to provide a large reaction surface area, and also provides the path through which the gas reactant and gas product diffuse into or out of the solid matrix. When studying iron ore reduction, Joseph<sup>[51]</sup> found that with all other factors constant, the time required to achieve 90 percent reduction of the specimen was inversely proportional to the porosity of the unreacted sample. In this study, the porosity was calculated from the apparent density and true density of the calcined pellet.

$$\theta = 1 - \frac{\rho_{app}}{\rho_{tru}} \quad (6-12)$$

**Table 6.3 True Density of Calcined Pellet.**

Temperature (°C)	700	740	770	850	930	1000
Apparent Density before calcination (g/cm <sup>3</sup> )	1.444					
Apparent Density after calcination (g/cm <sup>3</sup> )	1.256					
True Density after calcination (g/cm <sup>3</sup> )	2.6578	3.3940	3.3942	3.5266	3.5274	3.5275
Porosity	0.5274	0.6299	0.6300	0.6438	0.6439	0.6439

## 6.4.2 Individual Grain Size of The Calcined Pellets

### 6.4.2.1 Specific Surface Area of Pellet Before Reduction

Specific surface area is a determinant factor for solid-gas reaction rate, since it determines how many preferential sites are available for gas-solid reactions. Pellets calcined at different temperatures for different times will undergo different sintering or softening processes and result in different specific surface areas. The BET surface area measurements for the calcined pellets are shown in Table 5.2 and in Table 6.4.

### 6.4.2.2 Individual Grain Size of Calcined Pellets

As has been pointed out in Chapter 5, The measured grain size of the laterite varied according to the measurement methods. Furthermore, after calcination, the physical characters of the grains changed. In dealing with gas-solid reaction kinetics, grain size and shape are actually important as parameters

that define surface to volume ratio. Based on this consideration, the grain size used in this study was converted from BET surface area by assuming the grains in the calcined pellet are spherical and of uniform size. This is clearly not the true grain size as most of the surface area results from pores within the grains. However, it does give an useful “effective grain size”, as has been suggested by Nath *et al*<sup>[41]</sup>.

**Table 6.4 BET Surface Area And Grain Size**

Temperature (°C)	700	740	770	850	930	1000
True Density after calcination (g/cm <sup>3</sup> )	2.6578	3.3940	3.3942	3.5266	3.5274	3.5275
BET surface area(m <sup>2</sup> /g)	113.44	103.16	89.77	42.21	32.15	24.09
Radius of individual grain (µm)	1.00	0.87	0.98	2.02	2.65	3.53

### 6.4.3 Effective Diffusivity of Gas Reactant Within Calcined Pellets

Three mechanisms are possible for gas transport within porous solids, one of them is forced flow which is due to a pressure difference. This situation can arise when the total volume of gas reactant and gaseous product is changed after reaction. However, for most of the porous materials considered here, forced flow, even though it exists, is relatively unimportant compared with diffusion. The reason for this is that the forced flow of the Poiseuille or stream-lined type is proportional to the fourth power of the pore diameter<sup>[52]</sup>, in the present study, the diameter of pores is only 200 Å or so, hence flow of

this type is very slow<sup>[53]</sup>. The second mechanism is two dimensional migration of gases in an adsorbed layer on the pore wall. Although this may be very rapid under some rather special conditions where thick physically adsorbed layers of reactant are formed, there is little necessity to invoke this mechanism to explain solid-gas reaction rates <sup>[53]</sup>. The third mechanism, diffusion is by far the most important. Diffusion is a mass flow caused by random movement of molecules in the absence of total pressure difference. As more molecules will move away from the region of high concentration than will move toward it, a net flow occurs. The flux of gas component A by diffusion is:

$$N_A^{(P)} = -D_A(dC_A/dx) \quad (6-13)$$

In the case where forced flow has to be taken into consideration:

$$N_A^{(P)} = -D_A(dC_A/dx) + y_A(N_A^{(P)} + N_B^{(P)}) \quad (6-14)$$

#### **6.4.3.1 Gas Diffusion Within Fine Pores**

Gas diffusion in the small single pore of a porous solid may be well simulated by a capillary, in which gas diffusion has already been thoroughly studied. Within a capillary, the nature of gas phase diffusion depends upon the magnitude of the mean free path,  $\lambda$ , of the diffusing molecules, relative to the radius of the capillary  $r$ . When the ratio  $r/\lambda$  is less than 0.1, the gas diffusion will be governed only by the collisions of gas molecules with the pore wall, this type of diffusion is usually referred to as Knudsen diffusion, after Knudsen who first investigated this type of behaviour for capillaries. In this regime

$$D_A = D_{KA} \quad (6-15)$$

When  $r/\lambda$  is greater than  $10^{[54]}$ , ordinary diffusion predominates, under this condition, momentum is transferred by intermolecular collision alone. In this case:

$$D_A = D_{AB} \quad (6-16)$$

If  $r/\lambda$  falls between 0.1 and 10, both wall collisions and intermolecular collisions will contribute to the diffusion process.

#### 6.4.3.1.1 Pore Size Of Calcined Pellets

Pore size, in conjunction with the free path of gas molecules, will determine the mechanism of gas diffusion. Direct measurement of pore size proves to be difficult. In this study, the pore size is estimated by BET surface area and the porosity of the calcined pellets. Assuming the pores in the calcined pellet are cylinders with identical radius, and they intercept each other at an average length of  $L_p$ , then pore size is calculated by:

$$r = 2 \frac{V_p}{S_p} = 2 \frac{\theta}{10000 S_{BET} \cdot \rho_{app}} \quad (6-17)$$

This is actually the mean hydraulic radius of the pore <sup>[55]</sup>.

#### 6.4.3.1.2 Mean Free Path of Reactant Gas Molecules

Mean free path is the average distance over which gas molecules move between two instants of collision. Tait calculated the mean free path of gas

molecules in the following way<sup>[56]</sup>:

$$\lambda = \frac{0.667}{\pi n_m \sigma^2} = \frac{0.667 \times 10^{16} RT}{N_o P \pi \sigma^2} = \frac{2.894 \times 10^{-7} T}{P \sigma^2} \quad (6-18)$$

#### 6.4.3.1.3 Knudsen Diffusivity.

As stated above, when the ratio of the pore radius to the mean free path of a gas molecule is less than 0.1, the gas diffusion within the pore will be governed by the collision of gas molecules to the wall of the pore, this kind of gas transportation is referred to as Knudsen diffusion. The Knudsen diffusion coefficient, or Knudsen diffusivity for gas A is given by<sup>[53]</sup>:

$$D_{KA} = 9.7 \times 10^3 r \left( \frac{T}{M_A} \right)^{\frac{1}{2}} \quad (6-19)$$

Since Knudsen diffusion is governed by collisions of molecules with the pore wall, the gas diffusion is independent of the presence of other species and the total pressure gradient.

#### 6.4.3.1.4 Ordinary Binary Diffusivity

For ordinary diffusion, the diffusivity of a binary gas system is usually calculated by the Chapman-Enskog equation<sup>[57]</sup>:

$$D_{AB} = \frac{0.01858T^{3/2} \left( \frac{1}{M_A} + \frac{1}{M_B} \right)^{1/2}}{P\sigma_{AB}^2\Omega_D} \quad (6-20)$$

$$\sigma_{AB} = \frac{\sigma_A + \sigma_B}{2} \quad (6-21)$$

$$\varepsilon_{AB} = (\varepsilon_A \varepsilon_B)^{1/2} \quad (6-22)$$

$$T^* = \frac{\kappa T}{\varepsilon_{AB}} \quad (6-23)$$

$$\Omega_D = \frac{A}{T^{*B}} + \frac{C}{e^{DT^*}} + \frac{E}{e^{FT^*}} + \frac{G}{e^{HT^*}} \quad (6-24)$$

where :

A=1.06036, B=0.15610, C=0.19300, D=0.47635, E=1.03587, F=1.52996,  
G=1.76474, H=3.89411.

Unlike Knudsen diffusion, ordinary diffusion proceeds by intermolecular collisions, therefore not only does the diffusivity depend on the pressure and temperature, but also on the polarity of the gas components. For a binary gas pair containing no polar species, the necessary parameters can be obtained readily from several reference sources<sup>[57][58][59]</sup>. For gas pairs containing polar species,

the Brokaw method is recommended<sup>[57]</sup>, in this case equation (6-20) is still used, but the parameters are determined using equation (6.25) to (6.30).

$$\Omega_D = \Omega_D + \frac{0.19\delta_{AB}^2}{T^*} \quad (6-25)$$

$$\delta = 19400 \frac{\mu_p^2}{V_b T_b} \quad (6-26)$$

$$\frac{\varepsilon}{\kappa} = 1.18(1 + 1.3\delta^2)T_b \quad (6-27)$$

$$\sigma = \left( \frac{1.585V_b}{1 + 1.3\delta^2} \right)^{1/3} \quad (6-28)$$

$$\delta_{AB} = (\delta_A \delta_B)^{1/2} \quad (6-29)$$

$$\sigma_{AB} = (\sigma_A \sigma_B)^{1/2} \quad (6-30)$$

Necessary parameters are available from reference [57].

#### 6.4.3.1.5 Gas Diffusivity in Transition Regime

In the transition region, where both Knudsen and ordinary diffusion is significant, the diffusivity calculation has received considerable attention. An early attempt was made by Wheeler<sup>[53]</sup>, who gave the formula for diffusivity in pores of any size at any pressure as:

$$D_A = D_{AB} (1 - e^{-D_{KA}/D_{AB}}) \quad (6-31)$$

Although this equation can give a correct type of diffusion when  $r/\lambda$  ratio varies and can give a smooth transition between the two extreme types of diffusion, it is, as admitted by the author himself, rather intuitive.

Rothfeld<sup>[60]</sup> and Scott<sup>[61]</sup>, using a momentum balance and Spiegler<sup>[62]</sup>, using a friction factor analysis, derived the theoretical equation for diffusivity in transition region as:

$$\frac{1}{D_A} = \frac{1 - \alpha y_A}{D_{AB}} + \frac{1}{D_{KA}} \quad (6-32)$$

Where:

$$\alpha = 1 + N_B^{(P)} / N_A^{(P)} \quad (6-33)$$

When under the situation of equimolar counter diffusion,  $N_A^{(P)} = -N_B^{(P)}$ ,

$$\frac{1}{D_A} = \frac{1}{D_{AB}} + \frac{1}{D_{KA}} \quad (6-34)$$

This is Bosanquet interpolation formula and it is found to be in agreement with more elaborate calculations and with experimental data<sup>[63]</sup> and therefore is used extensively.

### **6.4.3.2 Effective Diffusivity Within Calcined Pellets**

Within the actual porous solid, gas diffusion is more complicated than in one single capillary, the reasons for this are:

- 1) Within the porous solid, the volume occupied by solid is not available for gas diffusion.
- 2) The actual diffusion path will not follow a straight line as in a straight capillary, but will be quite tortuous. The extent of tortuosity will depend on the structure of the pores and the way in which the pores intersect and connect.

For convenience, the pores are usually still assumed to be capillaries or cylinders, but with some adjustable parameters such as tortuosity to account for their shape, roughness or orientation. Numerous ways and several models have been proposed to describe the diffusion behaviour of gas within porous solids. The Dusty model<sup>[63]</sup>, which was derived from rigorous kinetic theory by visualizing the porous medium as a collection of uniformly distributed dust particles which are constrained to be stationary. The model can be used to predict the gas diffusivity in a porous medium once one gas mixture's diffusivity is measured in the same medium and some characteristics of porous medium are determined. It seems that this model can be well used in the case where the pellet consists of dense grains. However, for the situation under which the particle itself is porous, the dusty model will lose its validity. The Random model<sup>[64]</sup> assumes

that a porous pellet consists of particles that are themselves porous, therefore the pellet contains both micropores (within the particles) and macropores (interstices between the particles). Diffusion occurs through micropores, through macropores and through micropores and macropores in series. Maybe what the random model tries to describe is closest to the real case, and it has been said the random model is one of a few completely predictive models which make it possible to calculate diffusivity using some measurable parameters<sup>[54]</sup>. However, after examining the development process of the model, it appears that there is doubt about its theoretical basis. In the random model, only the area in which the pores on each side of the "rejoined plane" are connected directly are considered to be available for gas diffusion. This is, However, not necessarily true, since the gas may find its way tortuously through the pores which are not connected directly.

Satterfield and Cadle<sup>[65]</sup> had compared the predicted diffusion flux calculated by using the random model with experimental data, and the agreement was not very good. The deviation was generally from 8~40%, sometimes the predicted values are 2 or 3 times higher than those actually found.

Although there are some other models, such as that proposed by Foster and Butt<sup>[66]</sup>, which pay more attention to the shape of pores, after comparing them all, Haynes<sup>[67]</sup> proposed that the parallel model is probably superior to others since it can provide an *a priori* estimation of effective diffusivity which is comparable with experimental data.

The parallel model assumes each pore makes its contribution to the total

diffusion flux independently of the others. When the pore sizes are widely distributed,  $D_A$ , the diffusivity of gas A within a single pore, is not the same for different radii. Assuming tortuosity,  $\tau$ , is the same for all the pores, the effective diffusivity within porous solid is:

$$D_{Ae} = \frac{\theta}{\tau} \int_0^{\infty} D_A f(r) dr \quad (6-35)$$

Where  $f(r)$  is the pore size distribution function:

$$f(r) = \frac{dV_r}{V_p dr} \quad (6-36)$$

Thus,  $f(r)dr$  represents the fraction of pore volume containing pores with radii between  $r$  and  $r+dr$ .

This should be understood easily. Since within the porous solid, the volume occupied by solid is not available for gas diffusion,  $\theta$  is needed to convert the diffusivity from a pore area basis to a solid area basis, and since the pore is not necessarily straight and perpendicular to the external surface of the pellet,  $\tau$  is needed to account for the deviousness of the path.  $\tau$ , by the original definition of Carman<sup>[68]</sup>, is the square of the ratio of the effective average path length in porous medium  $L_e$  to the shortest distance measured along the direction of macroscopic flow  $L$ :

$$\tau = (L_e / L)^2 \quad (6-37)$$

#### 6.4.3.2.1 Tortuosity Of Porous Solid.

Unlike  $\theta$ , which can be determined by BET, mercury porosimetry or other methods, there is no means to determine  $\tau$  for a porous solid directly. By assuming the pores run randomly and on average at  $45^\circ$  angle to the external surface, Wheeler<sup>[53]</sup> showed that  $D_{Ac}=D_A\theta/2$  and hence indicated that for randomly distributed pores, the theoretical value of  $\tau$  is 2. By visualising the porous medium as consisting of three identical bundles of straight cylindrical capillaries, only one of which is oriented in the direction of diffusion, Haynes<sup>[67]</sup> took the theoretical value of  $\tau$  for a isotropic porous medium to be 3. It is noticed here that when Wheeler assumed pores run on average at  $45^\circ$  angle to external surface and when Haynes assumed one third of pores run in diffusion direction, no strict mathematical method was employed.

In the case of pellets consisting of randomly distributed dense grains and pores of uniform size (Fig.6.7), assuming the grains are tiny cubes (this is not necessary, but can make the case more easily understood). If the distance between every two pores is  $a$ , then by random distribution, the average distance between the two nearest pores of the two adjacent layers is  $a/2$ , assuming the pellet has  $n$  layers, then the effective average path length for gas diffusion through the pellet is  $na+(n-1)a/2$ , and the shortest distance along the macroscope flow is  $na$ . By the definition of Carman<sup>[68]</sup>:

$$\tau = ((na+(n-1)a/2)/na)^2 = (1.5-1/2n)^2$$

if  $n$  is large enough,

$$\tau \approx 1.5^2 = 2.25$$

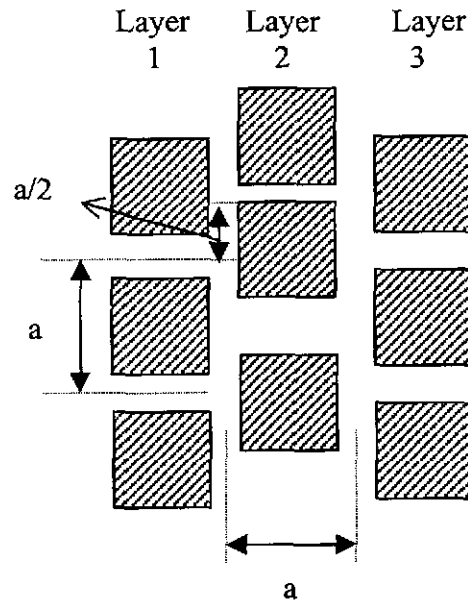


**Fig. 6.7 Schematic Pellet Consists Of Cubic Grains**

Notice that in all the above methods, the pores are assumed to be straight cylinders. This is, however, somewhat oversimplified. Therefore the existence of a definitive value of  $\tau$ , either 2 or 3, or 2.25, is in some doubt.

The complicated actual case is, on one hand the pores are tortuous, this tends to increase the values of  $\tau$  obtained from the above methods, on the other hand, the pores intersect frequently, so when gases are transported within the net of pores, streamline flow may not go parallel to the axis of the pores, instead, it may cut corners making  $\tau$  smaller than the theoretical values derived by the above authors. Therefore  $\tau$  remains largely uncertain.

Furthermore, the pores in reality have a variable cross-sectional area along their length and the part of the narrowest cross-section is more likely control the diffusion process. Also, there are many dead end pores which can not contribute to diffusion process. The measured flux will then be lower than predicted when assuming the pores are ideally constructed. Therefore, the parallel model will predict a higher value for  $\tau$ . If cracks exists in the porous pellet due to reduction or calcination, tortuosity then tends to be lowered. The value of tortuosity given by different researchers in fact varies over a wide range<sup>[67]</sup>.

Nevertheless, by assuming  $\tau=2$  or  $\tau=3$ , a number of researchers<sup>[69][70][71]</sup> seem to have successfully handled the diffusion phenomena of gases within porous solids. According to Satterfield and Cadle<sup>[65]</sup>, in cases where a prediction is needed,  $\tau=2\sim 4$ , may give a sufficient accuracy for most engineering applications. Based on the above review, in this study, tortuosity is selected as 2.25, because when this value was derived, a simple but strict mathematical method was employed.

#### 6.4.3.2.2 Effective Diffusivity Within the Calcined Pellet

In this study, the pore size is assumed to be uniform, then gas diffusivity within each pore is same, in this way the parallel model can be adapted as the following:

(6-38)

$$D_{Ae} = \frac{\theta}{\tau} D_A$$

The calculated effective diffusivities for CO within the calcined pellets when the CO/CO<sub>2</sub> ratio is 3.0 are listed in Table 6.5 for different temperatures used in this study.

**Table 6.5 Effective Diffusivity Of CO Within Calcined Pellet**

Temperature (°C)	700	740	770	850	930	1000
Effective diffusivity (cm <sup>2</sup> /s)	0.0992	0.1588	0.1860	0.3604	0.2398	0.2972

#### 6.4.4 Mass Transfer Coefficient

In the gas stream, a boundary layer will be formed around the pellet. In this layer, gas flow is laminar, and gas molecules next to the pellet are at rest, while those at the other edge of the boundary have the velocity of bulk stream. During reduction, reacting gas and product gas must transport inwards or outwards through this stagnant and laminar flowing layer. Although this boundary layer sometimes may be very thin, if gas mass transfer through it is not sufficiently fast, it may become the controlling step in reduction process.

Assuming that both the thickness of this boundary layer, which depends on temperature, relative gas flow rate and system geometry, and the concentration profile across it remains constant throughout reduction, Fick's first law can be applied.

$$N_A = D_{AB} \frac{\Delta C_A}{\delta_0} \quad (6-39)$$

Due to the difficulty in determining the thickness of the boundary layer, the ratio of  $D_{AB}/\delta_0$  is defined as the mass transfer coefficient  $h_D$ , which is, in general, a function of system geometry and gas and flow properties. This can be estimated using well established correlations between fluid and certain standard shapes. To do this, gas viscosity is required.

#### 6.4.4.1 Viscosity Of Pure Gas

Viscosity of pure gas is estimated by Chapman-Enskog equation<sup>[57]</sup>. For nonpolar gas A:

$$\mu_A = 26.69 \times 10^{-6} \frac{\sqrt{M_A T}}{\sigma_A^2 \Omega_v} \quad (6-40)$$

$$\Omega_v = \frac{A}{T^{*B}} + \frac{C}{e^{DT^*}} + \frac{E}{e^{FT^*}} \quad (6-41)$$

Where:

$$T^* = \frac{\kappa T}{\epsilon_A}, \quad A = 1.16145, \quad B = 0.14874, \quad C = 0.52487, \\ D = 0.77320, \quad E = 2.16178, \quad F = 2.43787$$

While for polar gas A, equation (6-40) still holds, but the collision integral is corrected for polar gases:

$$\Omega_v = \frac{A}{T^{*B}} + \frac{C}{e^{DT^*}} + \frac{E}{e^{FT^*}} + \frac{0.2\delta_A^2}{T^*} \quad (6-42)$$

Necessary parameters and more details may be found in reference [57].

#### 6.4.4.2 Viscosity Of Gas Mixture

To determine the viscosity of gas mixture, the following equation is used, which is extended from Chapman-Enskog theory<sup>[57]</sup>,

$$\mu_{ij} = \frac{\sum_{i=1}^n y_i \mu_i}{\sum_{j=1}^n y_j \Phi_{ij}} \quad (6-43)$$

Here n is number of gas components.

For a gas mixture in which there is no polar component,  $\Phi_{ij}$  is calculated using Wilke's method:

$$\Phi_{ij} = \frac{[1 + (y_i / y_j)^{1/2} (M_j / M_i)^{1/4}]^2}{[8(1 + M_i / M_j)]^{1/2}} \quad (6-44)$$

If any component of a gas mixture is polar,  $\Phi_{ij}$  is calculated using Brokaw's equation:

$$\Phi_{ij} = \left(\frac{\mu_i}{\mu_j}\right)^{1/2} S_{ij} A_{ij} \quad (6-45)$$

Where:

$$A_{ij} = m_{ij} M_{ij}^{-1/2} \left[ 1 + \frac{M_{ij} - M_{ij}^{0.45}}{2(1 + M_{ij}) + \frac{(1 + M_{ij}^{0.45}) m_{ij}^{-1/2}}{1 + m_{ij}}} \right] \quad (6-46)$$

$$m_{ij} = \left[ \frac{4}{(1 + M_{ij}^{-1})(1 + M_{ij})} \right]^{0.25} \quad (6-47)$$

$$M_{ij} = \frac{M_i}{M_j} \quad (6-48)$$

When  $\delta_i > 0.1$  or  $\delta_j > 0.1$  :

$$S_{ij} = S_{ji} = \frac{1 + (T_i^* T_j^*)^{1/2} + (\delta_i \delta_j / 4)}{[1 + T_i^* + (\delta_i^2 / 4)]^{1/2} [1 + T_j^* + (\delta_j^2 / 4)]^{1/2}} \quad (6-49)$$

When both  $\delta_i$  and  $\delta_j$  are less than 0.1:

$$S_{ij} = S_{ji} = 1.0 \quad (6-50)$$

Necessary parameters and more details may be found in reference [57].

#### **6.4.4.3 Mass Transfer Coefficient**

In this study, a cylindrical sample was suspended inside the furnace tube in the direction parallel to the gas flow. According to Sherwood<sup>[72]</sup>, this type of case is considered to be the same as mass transfer to or from a flat plate. Therefore the Reynolds number is:

$$N_{Re} = \frac{L_s U \rho_g}{\mu_g} \quad (6-51)$$

According to the definition of the J factor<sup>[73]</sup>,

$$h_D = j_D U (N_{sc})^{-2/3} \quad (6-52)$$

Where  $J_D$  is estimated by correlations given by Hines<sup>[74]</sup>, that is:

In the laminar flow region, when  $N_{Re}$  is less than 10,000,

$$j_D = \frac{0.664}{\sqrt{N_{Re}}} \quad (6-53)$$

In the turbulent flow region when  $10,000 < N_{Re} < 300,000$ ,

$$j_D = \frac{0.037}{(N_{Re})^{0.2}} \quad (6-54)$$

$$N_{sc} = \frac{\mu_g}{\rho_g D_{AB}} \quad (6-55)$$

The calculated mass transfer coefficients for  $CO/CO_2=3.0$  at the temperatures used in this experimental study are as Table 6.6.

**Table 6.6 Estimated Mass Transfer Coefficients**

Temperature (°C)	700	740	770	850	930	1000
Mass transfer coefficient (cm <sup>2</sup> /s)	0.6979	0.7368	0.7663	0.8464	0.9283	1.0015

### 6.4.5 Equilibrium Constants For Different Reactions

The equilibrium constant is calculated by the Reaction program of F\*A\*C\*T, a software package of physical chemistry, the results for the reactions relevant to this study are in Table 6.7.

**Table 6.7 Equilibrium Constants For Oxide Reductions**

Temperature (°C)	Ke		
	3Fe <sub>2</sub> O <sub>3</sub> +CO= 2Fe <sub>3</sub> O <sub>4</sub> +CO <sub>2</sub>	FeO+CO= Fe+CO <sub>2</sub>	NiO+CO= Ni+CO <sub>2</sub>
700	65034	0.65283	301.96
740	54268	0.59415	239.07
770	47850	0.55753	203.01
850	35214	0.48156	136.96
930	26995	0.42649	97.349
1000	21978	0.38982	74.793

### 6.4.6 Molar Concentration of Solid Reactant

This parameter was calculated based on the maximum reducible solid reactant. Its value varied with the reaction concerned and with the reduction conditions such as temperature and reducing gas composition. To simplify the situation, the removable oxygen was taken as the amount of solid reactant for reaction of hematite to magnetite. For reaction of FeO to Fe or NiO to Ni at different reduction conditions, the amount of

reducible solid reactants was determined by the maximum recovery of Fe or Ni. This was determined by chemical analysis of the reduced calcines. Details are given in Table 6.8.

### 6.4.7 Reaction Fraction of Nickel Oxide And Iron Oxide

The fractional extent of the reaction can be calculated by dividing the metal recovery at time t, see Table 6.2, by the equilibrium metal recovery for a given reduction condition.

**Table 6.8 Molar Concentration of Solid Reactants**

Temperature(°C)	700	740	770	850	930	1000
True density of calcined pellet (g/cm <sup>3</sup> )	2.6578	3.3940	3.3942	3.5266	3.5274	3.5275
$3\text{Fe}_2\text{O}_3 + \text{CO} = 2\text{Fe}_3\text{O}_4 + \text{CO}_2$						
Removable [O] content (%)	0.007743					
Molar density of [O] (10 <sup>-3</sup> mole/cm <sup>3</sup> )	1.2862	1.6425	1.6426	1.7066	1.7070	1.7071
$\text{FeO} + \text{CO} = \text{Fe} + \text{CO}_2$						
Maximum recovery of Fe (%)	32.05	34.60	22.76	15.86	13.85	12.85
Molar density of [FeO] (10 <sup>-3</sup> mole/cm <sup>3</sup> )	2.4733	3.4097	2.2431	1.6240	1.4185	1.3161
$\text{NiO} + \text{CO} = \text{Ni} + \text{CO}_2$						
Maximum recovery of Ni (%)	60.79	70.64	61.38	60.63	52.42	50.12
Molar density of [NiO] (10 <sup>-3</sup> mole/cm <sup>3</sup> )	0.6751	1.0018	0.8705	0.8935	0.7726	0.7388

## 6.5 Kinetic Parameter Extraction

### 6.5.1 Reduction of Hematite To Magnetite

According to X-ray diffraction, after a few seconds reduction, there was no hematite left in the pellet, there was no wustite or metallic phase either (see Fig.5.15 to Fig.5.17), but chemical analysis showed that after nearly ten seconds reduction, noticeable metallic nickel and iron is produced. Wustite and metallic phase were not detected by XRD in lightly reduced pellets, possibly because XRD is not sensitive enough to small quantities, or because of the ease of reoxidation of newly produced metallic phase and the instability of wustite at low temperature ( $<570^{\circ}\text{C}$ ). However, compared with the maximum recovery of the given reduction condition, the amount of metallic phase produced at this early stage is small. Considering the nature of stepwise reduction of hematite, namely from hematite to magnetite, then to wustite and finally to iron, and considering the relative ease of the first step, i.e., reduction from hematite to magnetite, we may say that at the early stage of laterite reduction, the reduction of hematite to magnetite predominates. This may be especially true when reduction time approaches zero.

When  $F_g=3$  (spherical grains) and  $F_p=2$  (cylindrical pellet), differentiating the general form of the grain model with respect to time  $t$  yields:

$$\frac{bk}{\rho_{s,mol}} \frac{1}{r_g} \left( C_{AS} - \frac{C_{CS}}{K_e} \right) = \left[ \frac{\frac{1}{3}(1-X)^{-2/3} + \frac{k}{D_{eg}} \frac{r_g}{F_g} \left(1 + \frac{1}{K_e}\right) \left( (1-X)^{-1/3} - 1 \right) - \frac{k}{2D_{ep}} \frac{r_p^2}{r_g} \frac{1-\theta}{F_p} \left(1 + \frac{1}{K_e}\right) \ln(1-X) + \frac{k}{h_D} \frac{r_p}{r_g} \frac{1-\theta}{F_p} \left(1 + \frac{1}{K_e}\right)} \right] \frac{dX}{dt} \quad (6-56)$$

At the very initial stages,  $t=0$ , and  $X=0$ , then

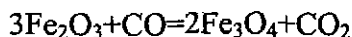
$$\frac{bk}{\rho_{s,mol}} \frac{1}{r_g} \left( C_{AS} - \frac{C_{CS}}{K_e} \right) = \left[ \frac{1}{3} + \frac{k}{h_D} \frac{r_p}{r_g} \frac{1-\theta}{F_p} \left(1 + \frac{1}{K_e}\right) \right] \frac{dX}{dt} \Big|_{t=0} \quad (6-57)$$

Where  $dX/dt$  at  $t=0$  can be converted from the weight loss rate at the initial stage of reduction, which is recorded by the data collection program employed in this study. With other available parameters, the rate constant  $k$  for reduction of hematite to magnetite in laterite at the initial stage can be obtained:

**Table 6.9 Rate Constant For Hematite Reduction To Magnetite In Laterite**

Temperature (°C)	700	740	770	850	930	1000
Initial weight loss rate (mg/g/min)	21.07	24.53	27.06	37.21	46.73	52.70
DX/dt at t=0	0.4535	0.5280	0.5824	0.8010	1.0059	1.1343
Rate constant ( $10^{-6}$ cm/s)	2.06	2.75	3.60	11.28	19.94	35.13

Based on the mechanism analysis in Section 5.4.2, the reduction of hematite to magnetite would occur at the very first stage of laterite reduction, according to the reaction:



Since the  $Fe_2O_3$  content in Sample D is 24.1%, the weight loss percentage contributed by this reaction would be around 0.8%. Comparison between the experimental data and the predicted results using the grain model are shown in Fig.6.8 and Fig.6.9. It can be seen that at this stage the grain model can give an acceptable prediction, but the model calculation would give a higher weight loss, and when the reduction time is longer and the reduction temperature is higher, the deviation will be greater. This is likely to be because gas diffusion played a more significant role as the reduction temperature increased and reduction process progressed.

Since the uncertainty of recorded weight loss data is 1 mg, as stated in Section 3.1, the sample weight is about 1500 mg, the error level of the experimental data is about 0.07%, which is shown in both Fig.6.8 and Fig.6.9.

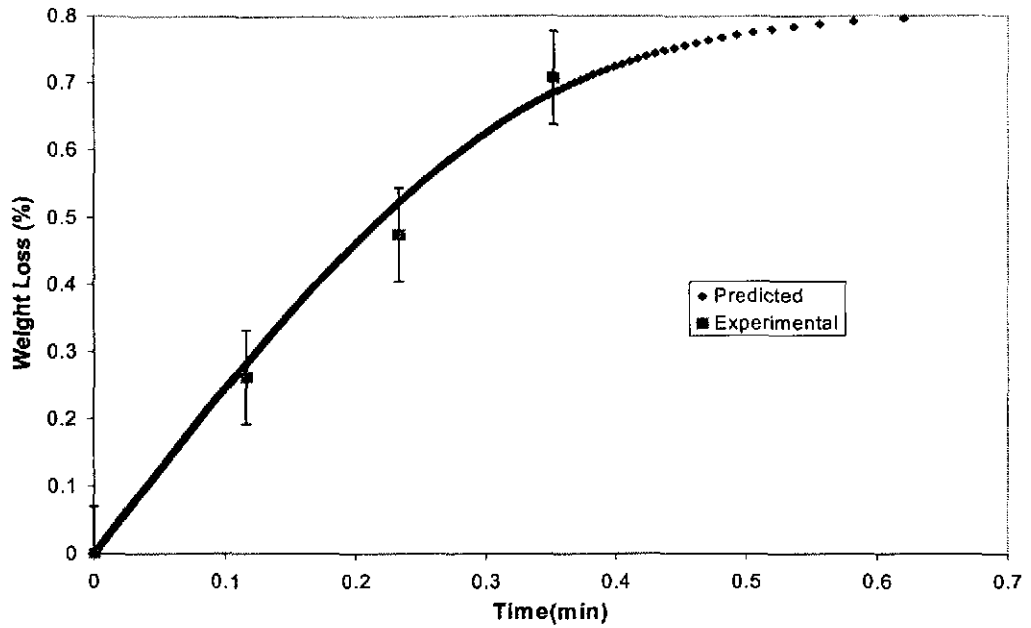


**Fig. 6.8 Comparison Of Predicted And Experimental Weight Loss At 740°C With  $CO/CO_2=3.0$  When Hematite Reduction Is Considered**

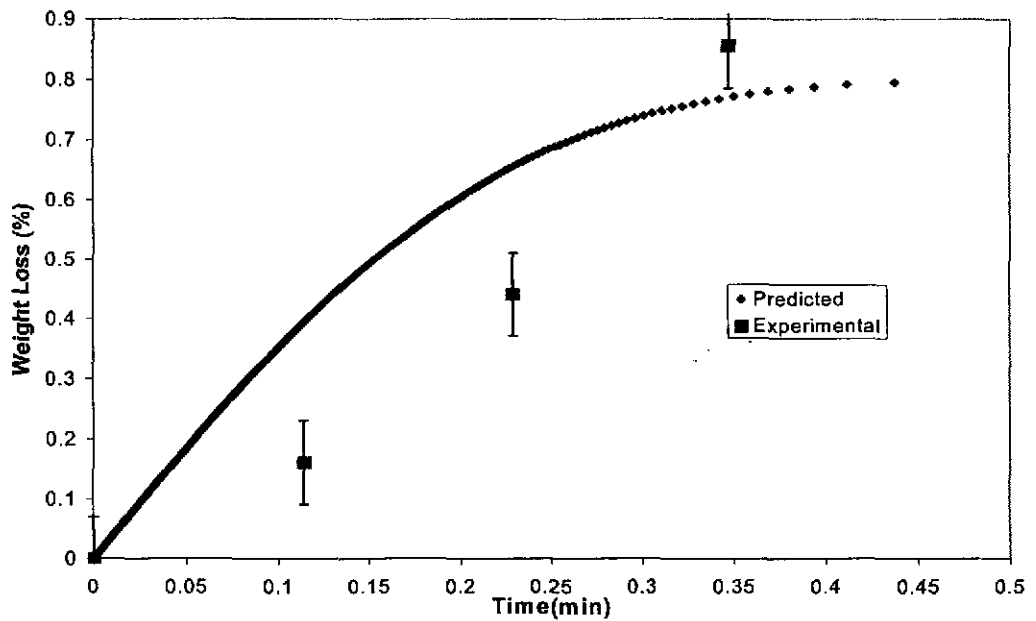


**Fig. 6.9 Comparison Of Predicted And Experimental Weight Loss At 850°C With  $CO/CO_2=3.0$  When Hematite Reduction Is Considered**

## 6.5.2 Reduction Of FeO And NiO

Numerous studies of iron oxide reduction considered that the overall process is controlled by the conversion of FeO to Fe<sup>[75][76]</sup>. Here this assumption is followed. By assuming both reduction of FeO and NiO in the laterite pellet are consistent with the assumptions made for the grain model, and by further assuming that NiO and FeO are present as pure materials, then

$$\begin{aligned} \frac{b}{\rho_{s,mol}} \frac{1}{r_g} (C_{AS} - \frac{C_{CS}}{K_e}) t = & g_{Fg}(X) \frac{1}{k} + \frac{r_g}{2F_g} (1 + \frac{1}{K_e}) p_{Fg}(X) \frac{1}{D_{eg}} \\ & + \frac{1}{2D_{ep}} \frac{r_p^2}{r_g} \frac{1-\theta}{F_p} (1 + \frac{1}{K_e}) p_{Fp}(X) \\ & + \frac{1}{D_{ep}} \frac{r_p^2}{r_g} \frac{1-\theta}{F_p} \frac{1}{N_{sh}} (1 + \frac{1}{K_e}) X \end{aligned} \quad (6-58)$$

In order to make Equation 6-58 more manageable, let:

$$\text{FactorT} = \frac{b}{\rho_{s,mol}} \frac{1}{r_g} (C_{AS} - \frac{C_{CS}}{K_e}) \quad (6-59)$$

$$\text{FactorR} = 1 \quad (6-60)$$

$$\text{FactorDg} = \frac{r_g}{2F_g} (1 + \frac{1}{K_e}) \quad (6-61)$$

$$\text{FactorM} = \frac{1}{D_{ep}} \frac{r_p^2}{r_g} \frac{1-\theta}{F_p} \frac{1}{N_{sh}} \left(1 + \frac{1}{K_e}\right) \quad (6-62)$$

$$\text{FactorDe} = \frac{1}{2D_{ep}} \frac{r_p^2}{r_g} \frac{1-\theta}{F_p} \left(1 + \frac{1}{K_e}\right) \quad (6-63)$$

Equation (6-58) becomes:

$$\begin{aligned} \text{FactorT.t} = & \text{FactorR.g}_{Fg}(X) \frac{1}{k} + \text{FactorDg.p}_{Fg}(X) \frac{1}{D_{eg}} \\ & + \text{FactorDe.p}_{Fp}(X) + \text{FactorM.X} \end{aligned} \quad (6-64)$$

This can be further simplified by defining:

$$\bar{X} = \text{factorT.t} \quad (6-65)$$

$$\bar{Y} = \text{FactorR.g}_{Fg}(X) \quad (6-66)$$

$$\bar{Z} = \text{FactorDg.p}_{Fg}(X) \quad (6-67)$$

$$\bar{C1} = \text{FactorDe.p}_{Fp}(X) \quad (6-68)$$

$$\bar{C2} = \text{FactorM.X} \quad (6-69)$$

Then:

$$\bar{X} = \bar{Y} \frac{1}{k} + \bar{Z} \frac{1}{D_{eg}} + \bar{C1} + \bar{C2} \quad (6-70)$$

With the available data or parameters, reaction rate constant  $k$  for FeO reduction or NiO reduction, and  $D_{eg}$ , effective diffusivity of gas reactant within individual grains, can be obtained by regression.

It is found when  $D_{eg}$  is neglected, i.e., when the gas diffusion within individual grains is assumed to offer negligible resistance to the reduction process, reasonable regression results can be obtained. In this case the rate constants for FeO and NiO reduction are as followings:

**Table 6.10 Rate Constant For FeO Reduction to Fe**

Temperature(°C)	700	740	770	850	930	1000
Rate cons.( $10^{-8}$ cm/s)	8.6418	20.753	61.779	237.56	534.89	1397.02

**Table 6.11 Rate Constant For NiO Reduction to Ni**

Temperature(°C)	700	740	770	850	930	1000
Rate cons.( $10^{-8}$ cm/s)	1.5678	6.2025	12.524	25.270	32.152	70.164

Comparison between the experimental data and the predicted results using the grain model for FeO reduction and NiO reduction are shown in Fig.6.10 to Fig.6.13. It can be seen that the nickel or iron recovery calculated using grain model is in good agreement with the experimental data.

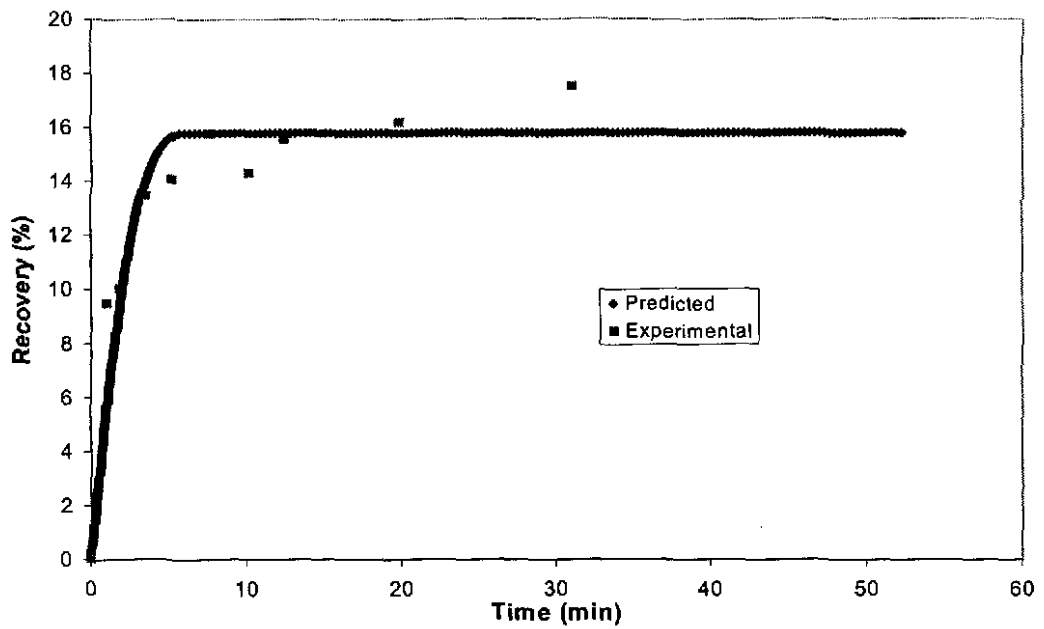


**Fig. 6.10 Comparison Of Predicted And Experimental Iron Recovery When Sample D was Reduced At 850°C With  $CO/CO_2=3.0$  For Different Time**

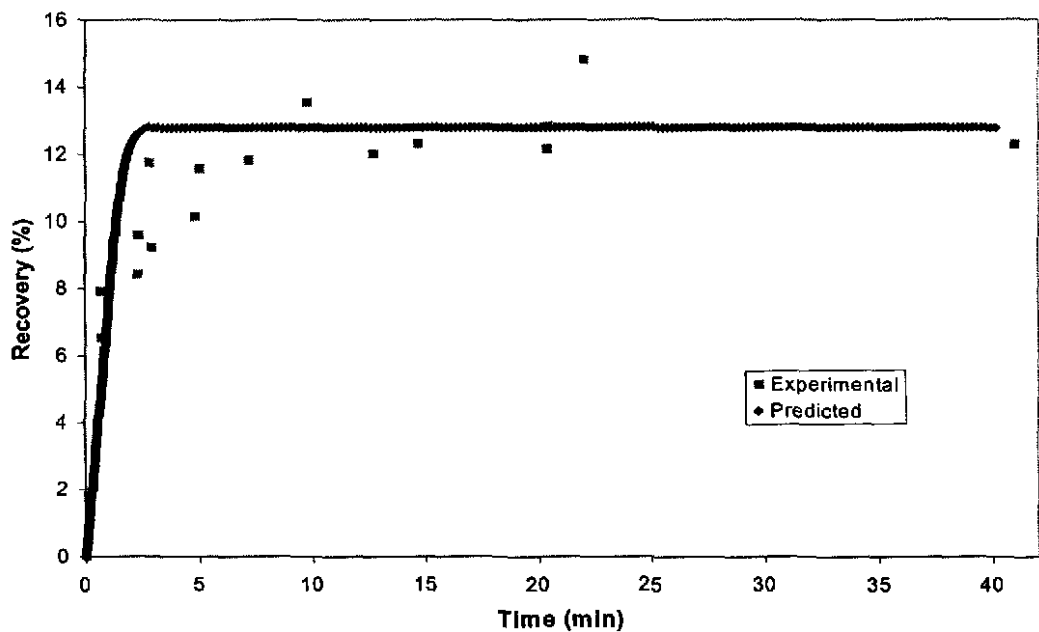


**Fig. 6.11 Comparison Of Predicted And Experimental Iron Recovery When Sample D was Reduced At 1000°C With  $CO/CO_2=3.0$  For Different Time**

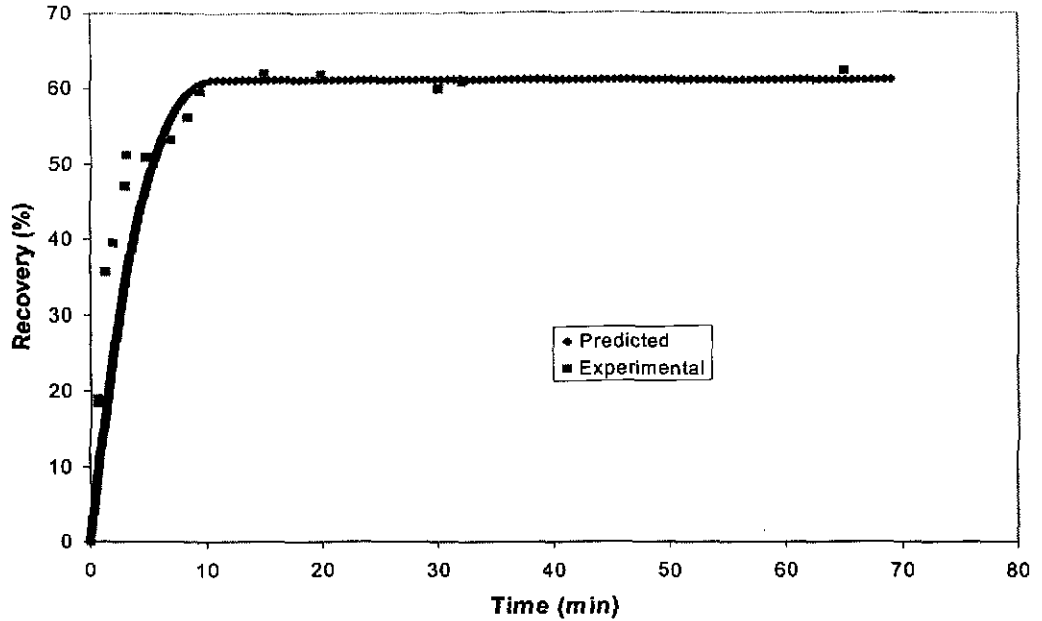


**Fig. 6.12 Comparison Of Predicted And Experimental Nickel Recovery When Sample D was Reduced At 770°C With CO/CO<sub>2</sub>=3.0 For Different Time**

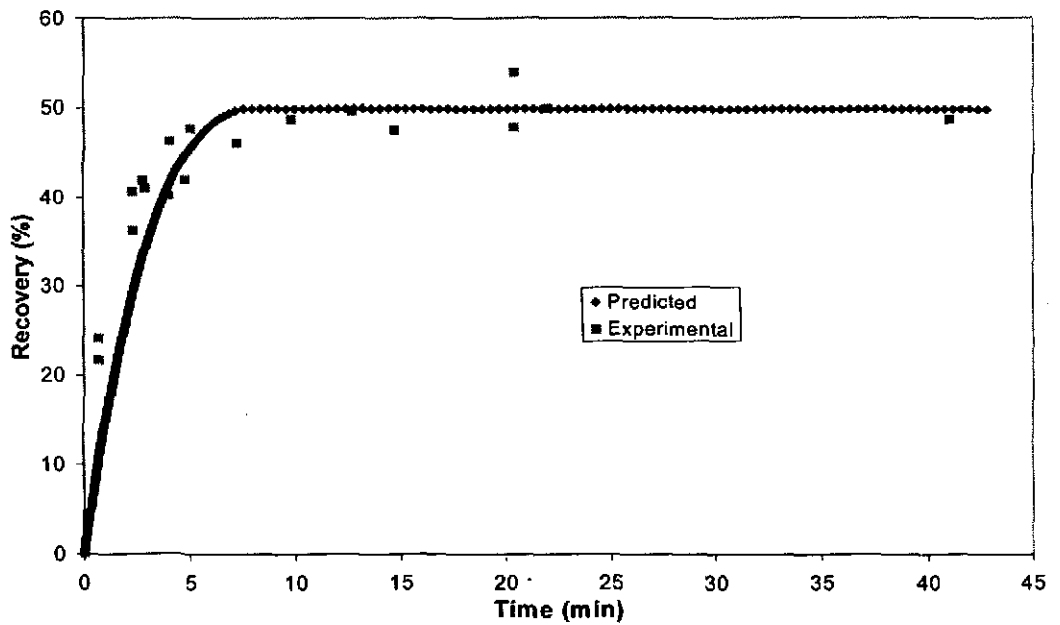


**Fig. 6.13 Comparison Of Predicted And Experimental Nickel Recovery When Sample D was Reduced At 1000°C With CO/CO<sub>2</sub>=3.0 For Different Time**

## 6.6 Discussion

The calculated reduction rate constants (Table 6.9 Table 6.10 and Table 6.11) are plotted in Fig.6.14, Fig.6.15 and Fig.6.16 according to Arrhenius equation. For FeO reduction and NiO reduction, it is found the plotted data can not be regressed into a single line within the temperature range from 700°C to 1000°C, instead, the data can be regressed into two linear sections, one is below and one is above ~800°C. This may be an indication of the effect of the serpentine-olivine transformation on Ni and Fe reduction. Because the difference between the slopes of the two linear sections for NiO reduction is larger, it can be concluded that the mineral crystallization has a stronger effect on nickel reduction.

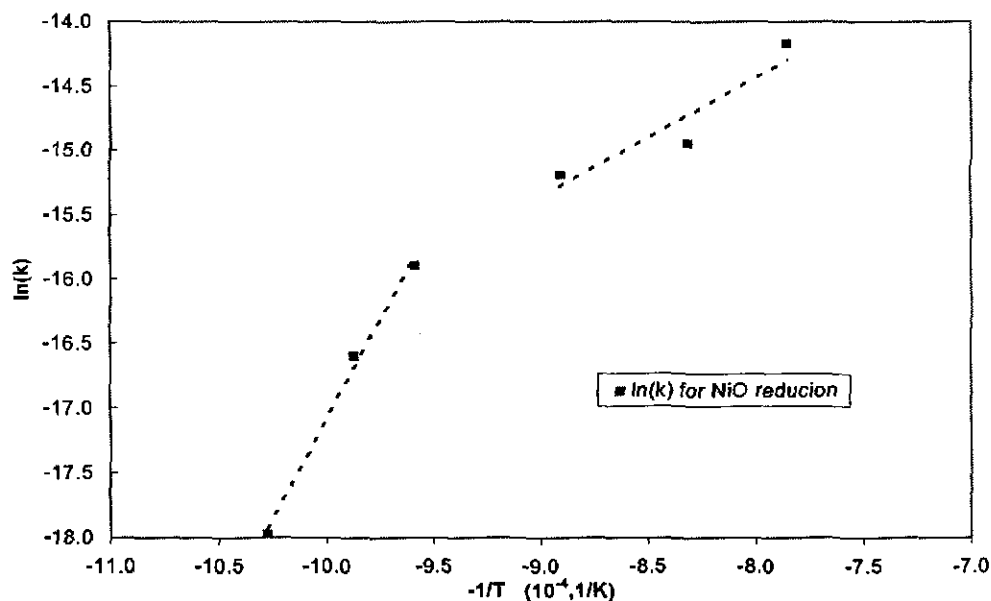
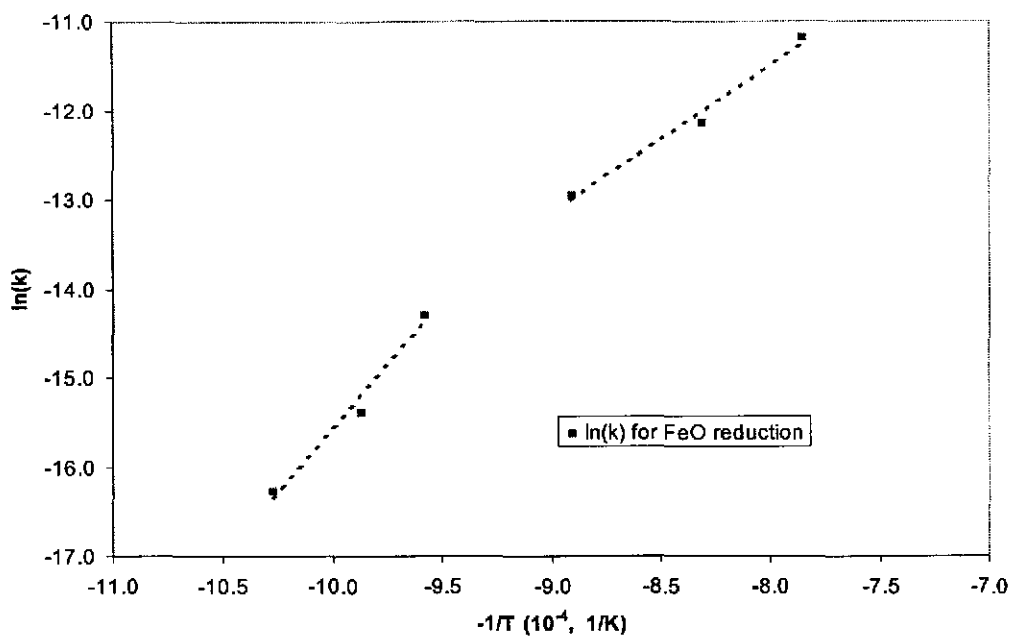
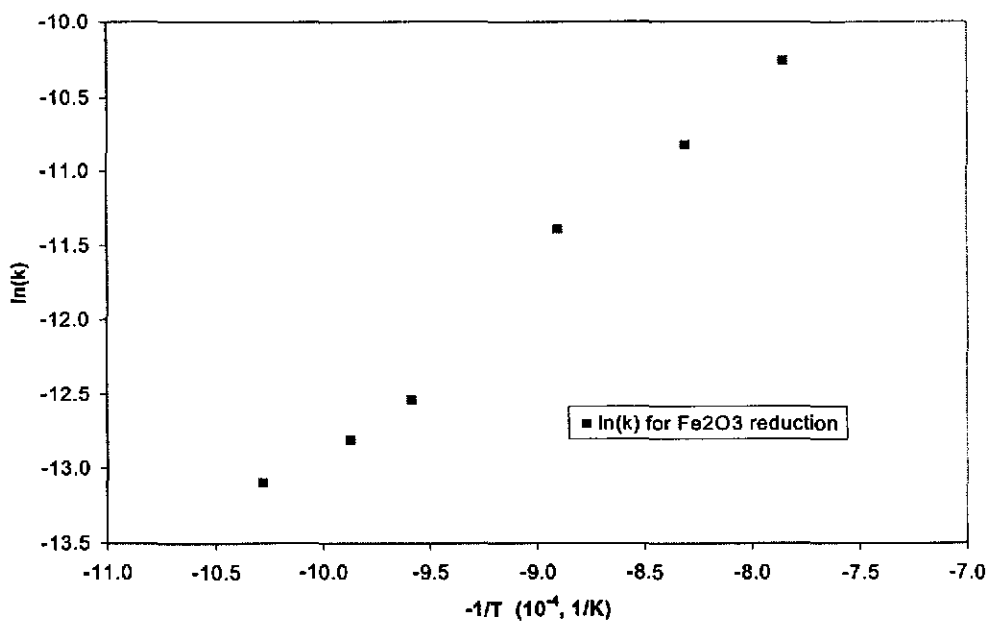


Fig. 6.14 Arrhenius Plot for Reduction of NiO



**Fig. 6.15 Arrhenius Plot for Reduction of FeO**



**Fig. 6.16 Arrhenius Plot for Reduction of Hematite**

## 6.6 Summary of Kinetic Analysis

- 1) With the pellet length used in this study, the cylinder sample can be approximated as infinitely long cylinder.
- 2) The theoretical value of tortuosity for porous solid is 2.25. Although many factors in the real case make it uncertain, this theoretical value seems more reasonable than others quoted in the literature<sup>[53][67]</sup> (2 or 3).
- 3) The grain model can be extended to study laterite reduction. However, the assumption that the iron and nickel exist in laterite in the form of pure oxides is oversimplified and not physically justified, and the chemical analysis result of partially reduced samples, as discussed in Section 6.2, are not very reliable, therefore the kinetic analysis in this study is rather qualitative. However, physical examination of reduction products supports the assessment of the reduction mechanism.
- 4) The crystallization of olivine and enstatite has a stronger effect on nickel reduction than on iron reduction.

## 6.7 NOMENCLATURE

b:	Stoichiometric coefficient.
$C_{AS}$ :	Concentration of gas reactant, mole/cm <sup>3</sup> .
$C_{CS}$ :	Concentration of gas product, mole/cm <sup>3</sup> .
$\Delta C_A$ :	Concentration difference of gas A (across the boundary layer), mole/cm <sup>3</sup> .

$D_A$ :	Diffusion coefficient (diffusivity) of gas A, $\text{cm}^2/\text{s}$ .
$D_{AB}$ :	Ordinary binary diffusivity, $\text{cm}^2/\text{s}$ .
$D_{Ae}$ :	Effective diffusivity of gas A, $\text{cm}^2/\text{s}$ .
$D_{eg}$ :	Effective diffusivity of gas reactant within individual grains, $\text{cm}^2/\text{s}$ .
$D_{ep}$ :	Effective diffusivity of gas reactant within pellet, $\text{cm}^2/\text{s}$ .
$D_{KA}$ :	Knudsen diffusivity of gas A, $\text{cm}^2/\text{s}$ .
$F_g$ :	Shape factor of individual grain.
$F_p$ :	Shape factor of pellet.
$g_{FG}(X)$ :	Conversion function related to chemical reaction, defined by eq. (6-2).
$h_D$ :	Mass transfer coefficient, $\text{mole}/\text{s}/\text{cm}^2$
$j_D$ :	Mass transfer J factor, dimensionless.
$K_e$ :	Chemical reaction equilibrium constant.
$k$ :	Reaction rate constant, $\text{cm}/\text{s}$ .
$L$ :	The shortest distance measured along the direction of macroscopic flow, $\text{cm}$ .
$L_e$ :	Effective average path length of gas flow, $\text{cm}$ .
$L_s$ :	Pellet length, $\text{cm}$ .
$M_A, M_B, M_i, M_j$ :	Molecule weight of gas A, gas B, gas i and gas j.
$M_G, M_S, M_{tot}$ :	The amount of metallic phase produced from goethite derived minerals, from serpentine derived minerals and the total amount of metallic phase in the reduced sample.

$n_m$ :	Number of molecules per unit volume, $\text{cm}^{-3}$ .
$N_A$ :	Molar flux of gas A, $\text{mole/s/cm}^2$ .
$N_A^{(P)}, N_B^{(P)}$ :	Molar flux of gas A, gas B in pores, $\text{mole/cm}^2/\text{s}$ .
$(\text{Ni}\%)_G, (\text{Ni}\%)_S$ :	Nickel content of metal produced from goethite or serpentine derivative minerals.
$(\text{Ni}\%)_{\text{ave}}$ :	The average nickel content of metal in reduced samples.
$N_o$ :	Avogadro's number, $6.023 \times 10^{23}$ .
$N_{Re}$ :	Reynolds number, dimensionless.
$N_{Sc}$ :	Schmidt number, dimensionless.
$N_{sh}^*$ :	Modified Sherwood number, defined by eq. (6-9).
$P$ :	Pressure, atm.
$p_{Fg}(X)$ :	Conversion function related to diffusion within individual grains, defined by eq. (6-5 or 6-6 or 6-7).
$p_{Fp}(X)$ :	Conversion function related to diffusion within pellet, defined by eq. (6-5 or 6-6 or 6-7).
$R$ :	Gas constant, $82.06 \text{ atm}\cdot\text{cm}^3/(\text{mol}\cdot\text{K})$ .
$r$ :	Pore radius, cm.
$r_g$ :	Original radius of individual grains, cm.
$r_p$ :	Original radius of pellet, cm.
$S_{BET}$ :	BET surface area, $\text{m}^2/\text{g}$ .
$S_p$ :	Total surface area of pores, $\text{cm}^2/\text{g}$ .
$T$ :	Temperature, K.

$T^*$	Defined by eq. (6-23).
$t$ :	Time, s.
$t^*$ :	Dimensionless time defined by eq. (6-3).
$T_b$ :	Normal boiling point, K.
$U$ :	Bulk gas velocity, cm/s.
$V_r$ :	Volume of pores with radius between $r$ to $r+dr$ , cm <sup>3</sup> /g.
$V_b$ :	Liquid molar volume at boiling point, cm <sup>3</sup> /mole.
$V_P$ :	Total pore volume, cm <sup>3</sup> /g.
$X$ :	Fractional conversion of solid reactant.
$x$ :	Length co-ordinate, cm.
$y_A, y_i, y_j$ :	Mole fraction of gas A, gas i and gas j.
$\alpha$ :	Quantity defined by eq. (6-33).
$\delta_0$ :	Thickness of boundary layer, cm.
$\delta_A, \delta_B, \delta_{AB}$ :	Polar parameters for gas A, gas B and gas mixture of A and B.
$\epsilon_{AB}, \epsilon_A, \epsilon_B$ :	Energy potential parameters for gas A, gas B and gas mixture of A and B.
$\kappa$ :	Boltzmann's constant.
$\lambda$ :	Mean free path of gas molecules, cm.
$\mu_A, \mu_i, \mu_j, \mu_{ij}$ :	Viscosity of gas A, i, j, and gas mixture of i and j, poise or g/s/cm.
$\mu_g$ :	Viscosity of gas mixture, g/s/cm.

$\mu_p$ :	Dipole moment, debyes.
$\theta$ :	Porosity of pellet.
$\rho_{app}$ :	Apparent density, $g/cm^3$ .
$\rho_{tru}$ :	True density, $g/cm^3$ .
$\rho_{s.mol}$ :	Molar concentration of solid reactant, $mol/cm^3$ .
$\rho_g$ :	Bulk gas density, $g/cm^3$ .
$\sigma$ :	Diameter of molecule, Å.
$\sigma_{AB}$ , $\sigma_A$ , $\sigma_B$ :	Characteristic length, Å.
$\sigma_g^2$ :	Modulus defined by eq. (6-4)
$\sigma_p^2$ :	Modulus defined by eq. (6-8)
$\tau$ :	Tortuosity.
$\Omega_D$ :	Diffusion collision integral, dimensionless.
$\Omega_v$ :	Collision integral for viscosity, dimensionless.

## SUMMARY AND CONCLUSIONS

1) The four major components of laterites, i.e.  $\text{Fe}_2\text{O}_3$ ,  $\text{NiO}$ ,  $\text{MgO}$ ,  $\text{SiO}_2$  were taken into consideration when the thermodynamic study of laterite reduction was carried out.

The major conclusions of the thermodynamic study are:

- (1) No pure metal will be produced after laterite reduction.
- (2) By comparison, limonitic ore reduction will give a higher nickel recovery and lower nickel grade in the metallic product than serpentinitic ore reduction.
- (3) Higher temperatures will result in more olivine formation, therefore more nickel and iron will be tied into it and will be difficult to reduce.
- (4) After serpentine decomposition and before olivine/enstatite crystallization, laterite is most reducible, but the equilibrium metallic product will have a poor nickel grade.
- (5) If the equilibrium oxygen partial pressure in the gas phase is fixed, both nickel and iron recovery will increase with increase in temperature. Since the amount of metallic iron increases at a greater rate, the nickel grade in the metallic phase will decrease with increasing temperature.
- (6) For serpentinitic ore, at  $710\sim 740^\circ\text{C}$  when the  $\text{CO}/\text{CO}_2$  ratio is 2.0~3.0, nickel recovery has a maximum value.

- 2) Calcination decreases the BET surface area of the pellet made of Sample D. The longer the calcination time and the higher the calcination temperature, the smaller the pellet BET surface area. When calcining for more than 60 minutes, especially at high temperature, calcination time has little effect on surface area.
- 3) Upon calcination, goethite will decompose into hematite, and upon reduction hematite will be reduced to magnetite or spinel and then to wustite, followed stepwise by to metallics.
- 4) At elevated temperatures, serpentinic minerals will undergo dehydration and will decompose into an amorphous material, which subsequently crystallise to olivine and enstatite. 810°C is the critical temperature above which most of the decomposed serpentine will crystallise. However, longer calcination times and higher calcination temperatures will result in more olivine and enstatite formation. This is true even when the temperature is below the critical value. However, the crystallization is very slow below this temperature, except when a reducing atmosphere is used.
- 5) Olivine and enstatite formation is detrimental to laterite reduction. After serpentine decomposition and before olivine and enstatite crystallization, laterite is the most reducible. If full advantage can be taken during this period, a higher reduction extent will be obtained. However, according to thermodynamic calculations, the nickel grade in the product will decrease.
- 6) With a fixed CO/CO<sub>2</sub> ratio in range of 1/3 to 3.0, reduction extent has a maximum value when the temperature is around 720°C~740°C. With gas mixtures of fixed

reducing potential (equilibrium oxygen partial pressure), higher temperatures will give higher reduction rates and reduction extent.

- 7) A reducing atmosphere helps to accelerate and further the formation of olivine and enstatite. There is a competition between the olivine and enstatite formation process and reduction process. If reduction proceeds too slowly in the early stages, more olivine and enstatite will be formed in advance of complete reduction, more  $\text{Ni}^{2+}$  and to some extent  $\text{Fe}^{2+}$  will be tied up, and a low reduction extent will be obtained. This competition depends on the reducing power of the gas. A mildly reducing atmosphere will increase olivine crystallization, but will have only a small influence on reduction, while more strongly reducing conditions will not increase the crystallization appreciably over mildly reducing conditions, but will have a great effect on the extent and rate of reduction.
- 8) With the pellet size used in this study, reduction proceeds in two stages. In the first reduction stage, resistance of gas diffusion through pellet and resistance of chemical reaction are both significant, the reduction shows a shrinking core mode. In the second stage, reduction takes place uniformly within the pellet, but does not proceed in the way described by the generally accepted uniform internal reaction model.
- 9) The Grain Model was used to carry out kinetic analysis of laterite reduction. However, because the chemical analysis results are not so reliable and the assumption for the Grain Model is somewhat oversimplified, the kinetic analysis result is rather qualitative.

- 10) Kinetic analysis showed that the mineral crystallization in Sample D affects nickel reduction more than iron reduction.

## REFERENCE

- [1] Schade, J. P. and Pearce, M. O., "The Role of Nickel in Modern Technology", in Extractive Metallurgy of Nickel and Cobalt, ed. by Tyroler, G. P. and Landolt, C. A., ( Phoenix, Arizona: 1988), p.53-63.
- [2] Alcock, R. A., "The Character and Occurrence of Primary Resources Available to the Nickel Industry", in Extractive Metallurgy of Nickel and Cobalt, ed. by Tyroler, G. P. and Landolt, C. A., (Phoenix, Arizona: 1988), p.67-89.
- [3] Diaz, C. M. *et al.*, "A Review of Nickel Pyrometallurgical Operation", in Extractive Metallurgy of Nickel and Cobalt, ed. by Tyroler, G. P. and Landolt, C. A., (Phoenix, Arizona: 1988), p.211-239.
- [4] Pearce, M. O., "Nickel Economy", in International Seminar On Laterite, MMIJ, (Japan:1985), p. K1-K12.
- [5] Rankama, Kalervo, and Sahama, TH. G., Geochemistry, (Chicago: The University Of Chicago Press, 1950), p.682
- [6] Van Vlack, L. H., Elements Of Materials Science And Engineering, (Addison-Wesley Publishing Company, 1985), Appendix B.
- [7] Boldt, Joseph R., Queneau, Paul(Technical Editor): The Winning Of Nickel, (Princeton, New Jersey: D. Van Nostrand Company, Inc, 1967).

- [8] Crawford, G. A., "Segregation Of Nickel In Laterite—The Falconbridge Experience", in Nickel Segregation, AIME, Edited by A.A.Dor, (San Francisco: 1972), p.219-240.
- [9] Simons, C. S., "The Production of Nickel: Extractive Metallurgy ---Past, Present and Future", in Extractive Metallurgy of Nickel and Cobalt, ed. by Tyroler, G. P. and Landolt, C. A., (Phoenix, Arizona: 1988), p91-134.
- [10] Extractive Metallurgy Of Nickel, ed. by Burkin, A. R. , (New York: John Wiley & Sons, 1987).
- [11] Weir, D. R., and Sefton, V. B., "Development Of Sherritt's Commercial Nickel Refining Process For Low And High Iron Laterites", in International Laterite Symposium, AIME, (New Orleans: 1979), p.325-345.
- [12] Anderson, William T., Reduction Studies On Low Iron Laterite Nickel Ores, M. Sc. Thesis, (University of Toronto, 1995).
- [13] Tzeferis, P.G., "Leaching Of A Low Grade Hematitic Laterite Ore Using Fungi And Biologically Produced Acid Metabolites", International Journal Of Mineral Processing, **42**, Dec., (1994), p.267-283.
- [14] Sukla, L. B., *et al.*, " Bioleaching Of Sukinda Laterite Using Ultrasonics", Hydrometallurgy, **37**, April, (1995), p.387-391.
- [15] Mehrotra, S. P., *et al.*, "Extraction Of Nickel From An Indian Laterite By Segregation Roasting", Transactions Of The Institution Of Mining And Metallurgy, Section C –Mineral Processing And Extractive Metallurgy, **103**, (1994), p. C97-C104.

- [16] Jena, P. K., Tokuda, M., "Extraction Of Nickel From Lean Ores", in proceedings of International Conference On Mining And Metallurgy Of Complex Nickel Ores, (Jinchang, China: 1993), p.339-345.
- [17] Taylor, A., "Laterites—Has The Time Finally Come?", Mining Magazine, **172**, March, (1995), p167-170.
- [18] Telewiak, Robert G., "State Of The International Nickel Industry—A Canadian Perspective", in Extractive Metallurgy of Nickel and Cobalt, ed. by Tyroler, G. P. and Landolt, C. A., (Phoenix, Arizona: 1988), p.33-40.
- [19] Szekely, J. and Hastagolu, A., "Reduction Of Nickel Oxide-Hematite Mixtures With Hydrogen", Transactions Of The Institution Of Mining And Metallurgy, Section C –Mineral Processing And Extractive Metallurgy, **85** (1976), p.C78-C87.
- [20] Nasr, M. I., *et al.*, "Effect Of Nickel Oxide Doping On The Kinetics And Mechanism Of Iron Oxide Reduction", ISIJ International, **35** (1995), No.9, p.1043-1049.
- [21] Ajarov, V. I., *et al.*, Dokl. Akad. Nauk SSSR, **87** (1952), No.1, p.49-52.
- [22] Cores, A., *et al.*, "Technical Note, Kinetic Regularities In Joint Reduction Of Nickel And Iron Oxides Under Non-Isothermal Conditions", Ironmaking and steelmaking, **16** (1989), No.6, p.446-449.
- [23] Konchakovskaya, L. D., Poroshk. Metall, **90** (1970), No.6, p.1.
- [24] Sarkisyan, L .E., Sov. Powder Metall. Met. Ceram., **25** (1986), No.10, p.832-837.

- [25] Shirane, Y., *et al.* "Activities Of NiO In Solid Solutions Of Ternary System MgO-NiO-SiO<sub>2</sub>", in Australia Japan Extractive Metallurgy Symposium, (Sydney, Australia: 1980), p.409-418.
- [26] Hallett, C.J., "A Thermodynamic Analysis Of The Solid State Reduction Of Nickel From Laterite Minerals", in Proceedings Of The Nickel-Cobalt 97 International Symposium—Volume II. Pyrometallurgical Fundamentals And Process Development, ed. by Levac. C. A. and Berryman, R. A., (Sudbury, Canada:1997), p.299-312.
- [27] Caron, M. H., "Fundamental And Practical Factors In Ammonia Leaching Of Nickel And Cobalt Ores", Transactions AIME, Journal Of Metals **188** (1950), Jan., p.67-90.
- [28] De Graaf, J. E., "The Treatment Of Lateritic Nickel Ores—A Further Study Of The Caron Process And Other Possible Improvements, Part I. Effect Of Reduction Conditions", Hydrometallurgy, **5**, (1979), p.47-65.
- [29] Utigard, T. And Bergman, R. A., "Gaseous Reduction Of Laterite Ores", Metallurgical Transaction B, **24B** (1992), Apr., p.271-275.
- [30] Kawahara, M., Toguri, J. M. and Bergman, R. A., "Reducibility Of Laterite Ores", Metallurgical Transaction B, **19B** (1988), Apr., p.181-186.
- [31] Mohanty, J. N., *et al.*, "Reduction Of Nickel-And Cobalt-Bearing Oxide Ores In Fluidized Bed", in Proceedings Of The Nickel -Cobalt 97 International Symposium—Volume II. Pyrometallurgical Fundamentals And Process

- Development, ed. by Levac. C. A. and Berryman, R. A., (Sudbury, Canada:1997), p.113-123.
- [32] Queneau, P. E., Cobalt And The Nickeliferrous Limonites, Ph. D. Thesis, (Delft University: 1971).
- [33] Hayashi, M., Effect Of Phase Transition On Reductive Roasting Of Nickel Bearing Serpentine, M.A. Thesis, (University of Utah: 1961).
- [34] Fisher, R. B. and Dressel, W. M., "The Nicaro (Cuba) Nickel Ores Basic Studies", in U.S Bureau of Mines, Report of investigation, n5496, (1959).
- [35] Saha, A.K., *et al.*, "Extraction Of Nickel From Indian Low-Grade Siliceous Ore", Trans. Instn. Min. Metall. (Sec.C: Mineral Process. Extr. Metall.), **101** (1992), April, p.C52-C56.
- [36] Lopez-Rendon, J. E., Geology, Mineralogy, And Geochemistry Of The Cerro Matoso Nickeliferrous Laterite, Cordoba, Colombia, M. Sc. Thesis, (Colorado State University, Spring: 1986)
- [37] Kukura, M. E., Stevens, L.G. and Auck, Y. T., "Development Of The UOP Process For Oxide Silicate Ores Of Nickel And Cobalt", in International Laterite Symposium, New Orleans, 1979, (New York: AIME, 1979), p.527-552.
- [38] De Graaf, J. E., "The Treatment Of Lateritic Nickel Ores—A Further Study Of The Caron Process And Other Possible Improvements, Part II. Leaching Studies", Hydrometallurgy, **5**, (1980), p.255-271.
- [39] Jha, A., Grieveson, P., and Jeffes, J. H. E., "An Investigation On The Carbothermic Reduction Of Copper Sulphide Minerals: Kinetic And

- Thermodynamic Considerations”, Scandinavian Journal of Metallurgy, **21** (1989), p.50-62.
- [40] Machingawata, N., Jha, A. and Grieveson, P., “Mechanism Of Carbothermic Reduction Of Nickel Sulphide Minerals In The Presence Of Lime”, Scandinavian Journal of Metallurgy, **18** (1989), p.81-88.
- [41] Nath, N.K. Chakraborti, N. and Shekhar, R.: “ Selective Reduction Of Indian Nickeliferrous Ore: Single Pellet Experiments”, Scandinavian Journal of Metallurgy, **24**, June, (1995), p121-138.
- [42A] Bergman, R.A. , private communication, CCMP, 1998.
- [42] Valix, M., *et al.*, “Thermodynamic Analysis Of The Reduction Of Nickel Laterite Ores”, in 23<sup>rd</sup> Australasian Chemical Engineering Conference Proceeding, 1995, p142-146.
- [43] Ray, H.S., Kinetics of Metallurgical Reactions, (New York: International Science Publisher, 1993).
- [44] Szekely, J., Evans, J. W. and Sohn, Hong Yong: Gas-Solid Reactions, (Academic Press, 1976).
- [45] Spitzer, R.H., Manning, F.S. and Philbrook, W.O.: “ Generalized Model For The Gaseous, Topochemical Reduction of Porous Hematite ”, Transactions of The Metallurgical Society of AIME, **236**, (1966), p1715.
- [46] Lu, W-K. and Bitsianes, G.: “ The General Rate Equation for Gas-Solid Reactions in Metallurgical Processes. II-With The Restrictions of Reversibility of Chemical Reaction and Gaseous Equimolar Counterdiffusion”, Transactions of The

- Metallurgical Society of AIME, **236**, (1966), p531.
- [47] Ishida, M. and Wen, C.Y.: "Comparison of Kinetic and Diffusional Models for Solid-Gas Reactions", AICHE Journal., **14**, (1968), p311.
- [48] Lahiri, A.K. and Seshadri, V.: "Kinetics of Reaction of Porous Solid With Gas", Journal of The Iron Steel Institute, **206**, (1968), p1118.
- [49] English, B.L., and Roberts, D.A., "Kinetics of Hydrogen Reduction of Porous Magnetite Disks Between 1173 And 1573K", Transactions Mineral Processing And Extractive Metallurgy, Section C of The Transactions of The Institution of Mining And Metallurgy, **87**, (1978), pC113.
- [50] Srinivasan, N.S. and Staffansson, L.-I.: "Reduction Kinetics Of Dicalcium Ferrite By Hydrogen: Application Of The Grain Model", Scandinavian Journal of Metallurgy, **17**, (1988), p281-284.
- [51] Joseph, T.L., "Porosity, Reducibility and Size Preparation of Iron Ore", Transactions of the American Institute of Mining and Metallurgical Engineers, Iron and Steel Division, **120**, (1936), p72 .
- [52] Geiger, G. H. and Poirier, D. R., Transport Phenomena In Metallurgy, (Addison-Wesley Publishing Company, 1973), p.45.
- [53] Wheeler, Ahlborn, " Reaction Rates And Selectivity In Catalyst Pores", in Catalysis, ed. by Emmett, Paul H., (New York: Book Division, Reinhold Publishing Corporation: 1955), Vol.2 ,p.105-165.

- [54] Youngquist, Gordon R., "Diffusion And Flow Of Gases In Porous Solids", in Flow Through Porous Media, (Washington, D.C.: American Chemical Society, 1970), p.58-69.
- [55] Dullien, F.A.L., Porous Media, Fluid Transport And Pore Structure, (Academic Press, 1979), p95.
- [56] Jeans, J.H. Sir, The Dynamical Theory Of Gases, (New York Dover Publications, 1959), p15.
- [57] Reid, Robert C., Prausnitz, John M. and Sherwood, Thomas K., The Properties of Gases and Liquids, third edition, (McGraw-Hill Book Company, 1977).
- [58] Bird, R.B., Stewart, W.E. and Lightfoot, E.N., Transport Phenomena, (New York: John Wiley & Sons, Inc., 1960).
- [59] Hirschfelder, J.O., Curtiss, C.F. and Bird, R.B., Molecular Theory of Gases and Liquids, (New York: John Wiley & Sons, Inc., 1954).
- [60] Rothfeld, Leonard B., "Gaseous Counterdiffusion In Catalyst Pellets", AICHE Journal, **9**, No.1, (1963), p.19-24.
- [61] Scott, D.S. and Dullien, F.A.L., "Diffusion Of Ideal Gases In Capillaries And Porous Solids", AICHE Journal, **8**, No.1, (1962), p.113-117.
- [62] Spiegler, K.S., "Diffusion Of Gases Across Porous Media", Industrial and Engineering Chemistry Fundamentals, **5**, (1966), p.529-532.
- [63] Evans, R.B., Watson, G. M. and Mason, E.A., "Gaseous Diffusion In Porous Media At Uniform Pressure", The Journal of Chemical Physics, **35**, No.6.(1961), p.2076-2083.

- [64] Wakao, N., and Smith, J. M., "Diffusion In Catalyst Pellets", Chemical Engineering Science, 17, (1962), p.825-834.
- [65] Satterfield, Charles N., and Cadle, P. John, "Diffusion In Commercially Manufactured Pelleted Catalysts", Industrial And Engineering Chemistry, Process Design And Development, 7, No2, April, (1968), p.256-260.
- [66] Foster, Richard N., and Butt, John B., "A Computational Model For The Structure Of Porous Materials Employed In Catalysis", AIChE Journal, 12, No.1, (1966), p.180-185.
- [67] Haynes, H. W., "Diffusion And Reaction In Porous Media-I", AIChE Modular Instruction, Series E: Kinetics, Volume 3: Heterogeneous Catalysis, (American Institute Of Chemical Engineers, 1982), p.1-7.
- [68] Carman, P.C., "Fluid Flow Through Granular Beds", Transactions Of The Institution Of Chemical Engineers, 15, (1937), p.150-166.
- [69] Johnson, M. F. L. and Stewart, W. E., "Pore Structure And Gaseous Diffusion In Solid Catalysts", Journal of Catalysis, 4, (1965), p.248-252.
- [70] Spitzer, R. H., Manning, F. S. and Philbrook, W. O., "Mixed-Control Reaction Kinetics In The Gaseous Reduction Of Hematite", Transactions of The Metallurgical Society of AIME, 236, May, (1966), p.726-742.
- [71] Turkdogon, E. T., Olsson, R. G. and Vinters, J. V., "Gaseous Reduction Of Iron Oxides: Part II. Pore Characteristics Of Iron Reduced From Hematite In Hydrogen", Metallurgical Transactions, 2, Nov., (1971), p.3189-3196.

- [72] Sherwood, T. K., Pigford, R.L. and Wilke, C.R., Mass Transfer, (McGraw-Hill Inc., 1975), p201.
- [73] Geankoplis, C.J., Mass Transport Phenomena , (Holt, Rinehart and Winston, Inc., 1972).
- [74] Hines, A.L. and Maddox, R.N., Mass Transfer, Fundamentals and Applications, (New Jersey: Prentice-Hall, Inc., 1985).
- [75] El-Geassy, A. A. and Rajakumar, V., “gaseous Reduction of Wustite With H<sub>2</sub>, CO and H<sub>2</sub>-CO Mixtures”, Transactions ISIJ, **25** (1985), p449.
- [76] Turkdogan, E.T. and Vinters, J.V., “Gaseous Reduction of Iron Oxides: Part I. Reduction of Hematite in Hydrogen”, Metallurgical Transactions, **2**, November, (1971), p3175.

